Electrochemical Behavior and Application of Phosphorus Modified Zeolite Carbon Paste Electrode

BY

ADAMU AMINU IDRIS

A Thesis Presented to the
DEANSHIP OF GRADUATE STUDIES

KING FAHD UNIVERSITY OF PETROLEUM & MINERALS

DHAHRAN, SAUDI ARABIA

In Partial Fulfillment of the
Requirements for the Degree of

MASTER OF SCIENCE

In

CHEMISTRY

MAY 2015

KING FAHD UNIVERSITY OF PETROLEUM & MINERALS

DHAHRAN- 31261, SAUDI ARABIA

DEANSHIP OF GRADUATE STUDIES

This thesis, written by **Adamu Aminu Idris** under the direction of his thesis advisor and approved by his thesis committee, has been presented to and accepted by the Dean of Graduate Studies, in partial fulfillment of the requirements for the degree of **MASTER OF SCIENCE in CHEMISTRY**

Thesis committee

Dr. A. Al-Betar (Advisor)

Dr. Tawfik Saleh (Co-Advisor)

Dr. Abdulaziz Al-Saadi

Department Chairman

Dr. Oki Muraza (Member)

Dr. Salam A. Zummo

Dean of Graduate Studies

20/5/15

Date

Dr. A Kawde (Member)

Dr. Nisar Ullah (Member)

Dedication

I dedicate this piece of work to Almighty Allah "SUBHAANAHU WA TA'ALAA"

Acknowledgement

I must begin by glorifying Almighty Allah the all-knowing, the omnipotent and the merciful for everything. Everlasting peace and blessings of Allah be upon his most beloved messenger prophet Muhammad (S.A.W).

It is my pleasure to thank the kingdom of Saudi Arabia and King Fahd University of petroleum and minerals for this privilege of scholarship to study a master degree. My also goes gratitude to the chemistry department and its entire community. Specifically, I acknowledge the support, help and encouragement given to me by my advisor Dr. Abdul Rahman Al-Betar throughout the thesis. I am grateful to my committee members, Dr. Tawfik Saleh, Dr. Oki Muraza, Dr. Nisar Ullah and Dr. Abdel-Nseer Kawde for the immense contribution to the achievement of the research objectives.

I also thank the chairman of the chemistry department. I appreciate the help of Mr. Muhammad Arab, Mansur Al-Zaki for their assistant in NMR session I thank Mr. Nadeem Baig and Mr. Azeem Akbar for their support. I appreciated the mutual and rigorous discussion we had with Ismail Abdul Aziz which contribute immensely to the success of the wok. I also extend my profound gratitude to CENT and its members particularly, Dr. Abbas, Mr. Ibrar, Saheed Ganiyyu, Idrees bakare.

At end I wish to thank my family for their continuous and tireless support, encouragement and prayers.

Table of Content

List of Table

List of Figures

List of equations

List of Schemes

List of Abbreviation

Ag/AgCl	:	Silver, silver chloride
CV	:	Cyclic voltammetry
DME	:	Dimethyl ether
EDX	:	Energy Dispersion X-ray Spectrophotometer
FE-SEM	:	Field Emission Scanning Microscope
FT-iR	:	Fourier Transform Infrared
HMDA	:	Hexamethylenediamine
HMI	:	Hexamethyleneimine
H-MOR	:	Proton mordenite
KCl	:	Potassium chloride
LDH	:	Layered Double Hydroxide
MOR	:	Mordenite
Na/Si	:	Sodium to Silicon ratio
NMR	:	Nuclear Magnetic Resonance
$NO2^-$	:	Nitrite ion
OFAl	:	Octahedral Framework Aluminium
OPDA	:	o-phenylenediamine
OSDA	:	Organic Structure Directing Agent
P/Al	:	Phosphorous to Aluminium ratio
P-MCPE	:	Phosphate Mordenite Carbon Paste Electrode
P-MOR	:	Phosphate Mordenite
P-ZSM-5	:	Phosphate ZSM-5
SCN^-	:	Thiocyanate
Si/Al	:	Silica to Alumina ratio
SWV	:	Square wave voltammetry
TEABr	:	Tetraethyl Ammonium Bromide

TEAOH	:	Tetraethyl Ammonium Hydroxide
XRD	:	X-ray diffraction
ZCPE	:	Zeolite Carbon Paste Electrode
ZME	:	Zeolite Modified Electrode

Thesis Abstract (English)

Name: **Adamu Aminu Idris**

Thesis Title: **Electrochemical Behavior and Application of Phosphorous Modified Zeolite Carbon Paste Electrode**

Major Field: **Chemistry**

Date: **May, 2015**

We report the synthesis and phosphate modification of pure mordenite crystal with Si/Al molar ratios 15, 20 and 25 in the absence of organic structure directing agent and without seed addition. Both parent and modified zeolite were characterized using XRD, SEM, FT-iR, NMR, and XRF. The phosphate mordenite was used as a modifier in carbon paste electrode and its electrochemical behavior was investigated in the cyclic voltammetry of potassium ferrocyanide ($K_4Fe(CN)_6$). The composite electrode containing 5% phosphate mordenite (Si/Al = 20), showed good linearity within thiocyanate concentration range of 10 µM to 150 µM (R^2 = 0.997) in phosphate buffer (pH 8). While the composite electrode containing 15 % phosphate mordenite (Si/Al = 25), showed strong linearity between nitrite concentration range of 10 µM to 250 µM (R^2 = 1) in phosphate buffer (pH 7). Both composite electrodes showed excellent reproducibility with RSD values of 2.3 % and 3.3 % in the detection of thiocyanate and nitrite respectively. Hence, the composite electrodes showed a promising application for real sample analysis.

Master of Science Degree

King Fahd University of Petroleum and Minerals

Dhahran, Saudi Arabia

Thesis Abstract (Arabic)
خلاصة الرسالة

الاســـــــــم أدم إدريس

عنوان الرسالة التصرف الالكتروكيميائي و التطبيقات للقطب الكهربائي المكون من زيولايت الموردنايت معدل بالفوسفورس وعجينة الكربون

التخصـــــص كيمياء

التاريـــــــخ مايو 2015

لقد قومنا بتصنيع بلورات المردينايت من الزيوليت الصافي و إدخال الفوسفورس عليه في غياب المعامل العضوي الموجه وبدون إضافة اية بذور. وقد كانت نسب السيليكون الى الالمونيوم هي: 15، 20، 25. وتمت التشخيصات بواسطة كلا من الاجهزة XRD, SEM, FT-iR, NMR . الموردينايت المعدل بالفوسفورس استخدم في تحسين اداء عجينة الكربون. وقد تم اختبار هذا القطب من الخليط بواسطة الفولتميتري الدائري (cyclic voltammetry) مع البوتاسيوم فيروسينايت ($K_4Fe(CN)_6$). القطب الكهربائي المكون من الخليط يحتوي على 5% من الفوسفورس ونسبة السيليكون الى الالومونيوم = 20، اظهر تجاوب خطي جيدا لتراكيز منخفضة (150 µM -10 µM) من الثيوسينايت (SCN) في محلول الفوسفيت ثابت الحامضية (pH 8).

بينما أظهر القطب الكهربائي الذي يحتوي على 15% فوسفيت موردنايت تجاوبا لقياس اكسدة النيتريت في التراكيز (250 µM -10 µM) في محلول الفوسفيت ثابت الحامضية (pH 7). كلى القطبين اظهرا تجاوبا ممتازا عند اعادة القياس لعدة مرات بثابت انحراف 2.3 % و 3.3 % في قياس كلا من الثيوسينايت والنيتريت. وبهذا أصبح القطب الكهربائي المعدل ذو تطبيقات واعدة في تحليل عينات الحقيقية.

درجة الماجستير في العلوم

جامعة الملك فهد للبترول والمعادن

الظهران- المملكة العربية السعودي

Chapter One

General Introduction

1.1 Zeolites

Zeolites are a well-established materials used in a range of processes in different industries. The occurrence of zeolites in nature as aluminosilicates can be dated back to 250 years ago [1]. The name "zeolite" which has the Greek interpretation (*zein,* ''to boil''; *lithos,* ''a stone'') was given to them by the Swedish mineralogist Axel Friedrich Cronstedt in 1756 after he discovered that upon rapid heating they produced huge amount of steam from adsorbed water [2]. The implicit properties of zeolites were believed to be a consequence of this phenomenon. They occur as natural aluminosilicates with characteristic microporous crystal structure [3]. To name but few include faujasite, mordenite, offretite, ferrierite erionite and chabazite. Zeolite structures play important role as catalysts with limited applications attached to the naturally occurring ones. The exploitation the porous materials in catalysis began during 1945 to 1955, after the advent of their synthetic form by the work of Barrer and Milton [1]. The replacement of amorphous aluminosilicates as cracking catalyst outbreaks the application of zeolites in the 1960s [4].

Structurally, zeolites contain tetrahedral silicon and aluminum atoms, linked together through oxygen atom forming a framework of tetrahedral TO_4 (T = Si or Al). Therefore, zeolites, comprise SiO_2 and AlO_2 units that are chemically combined together [5]. The unbalance negative charges in zeolites resulting from the substitution of silion with aluminium is usually compensated by extra-framework cations normally alkali or alkaline earth metals [3]. The characteristic windows and cages of zeolites rings were the

consequence of the tetrahedral linkages [6]. The number of rings is a factor of the tetrahedral atoms which grouped to form pores of sizes ranging from 8-, 10- and 12-membered rings [7].

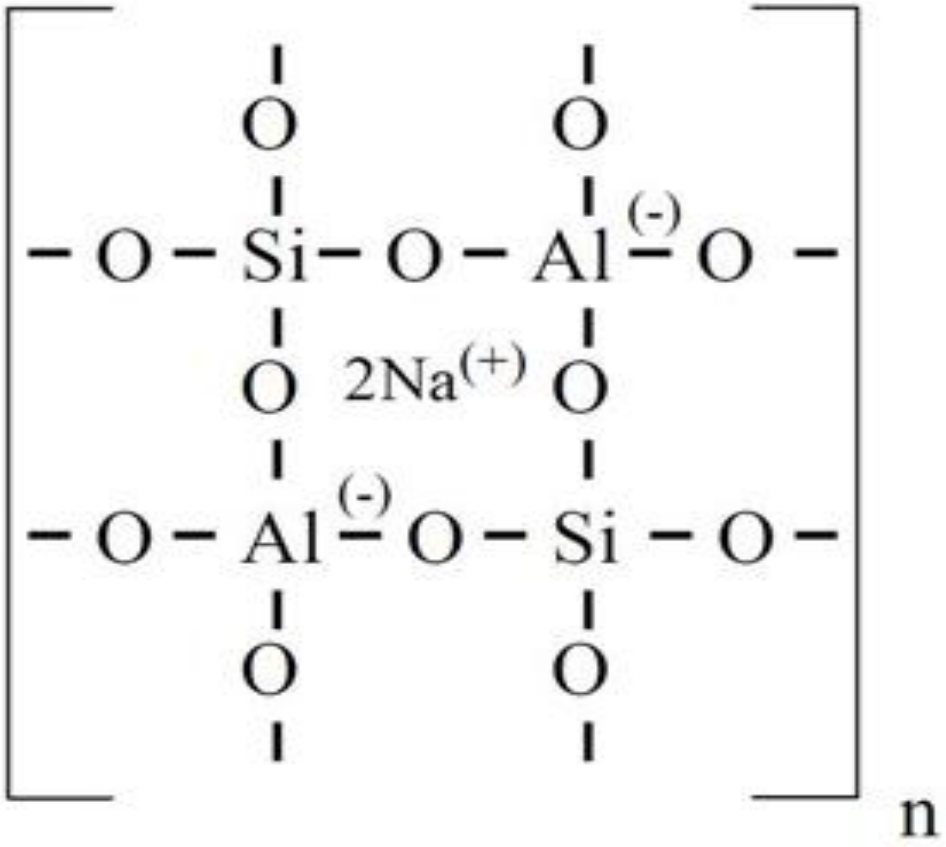

Fig. 1. 1 Chemical structure of zeolite[8]

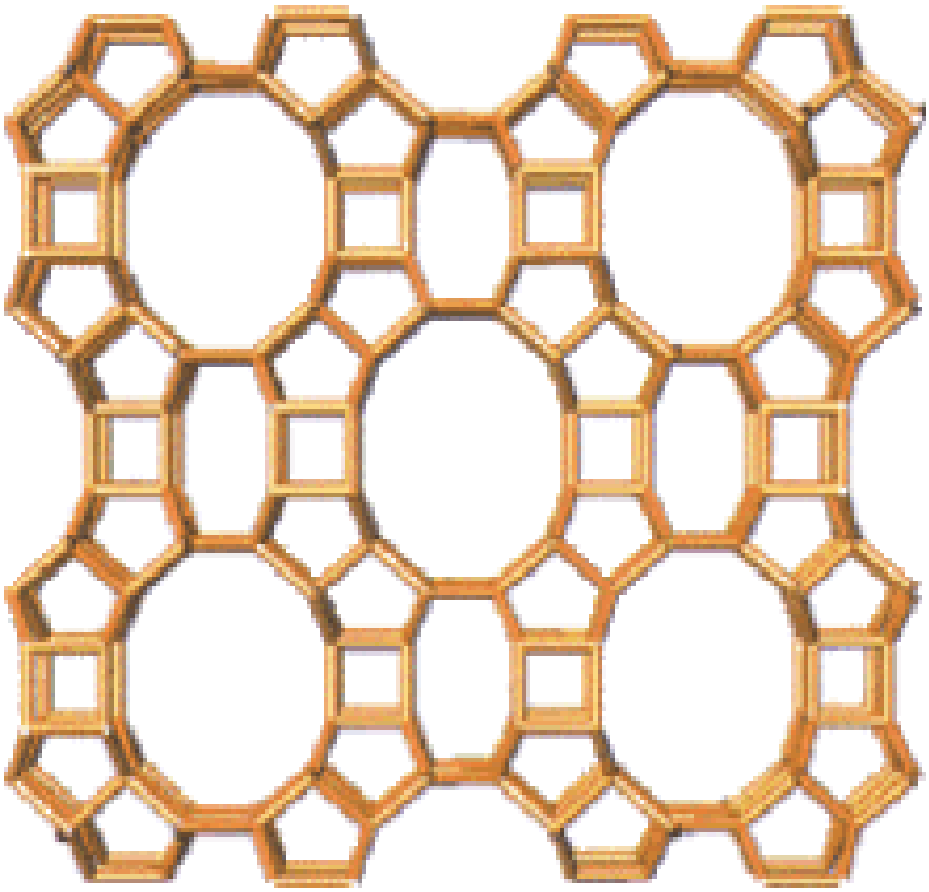

Fig. 1. 2 3D structure of MOR type zeolite [9]

The catalytic activity and stability of zeolites are requisite to the distribution of aluminium atom in the framework [10]. This is because the acidity of zeolites is a functional property of the location of aluminium. The distribution of bronsted acid sites in zeolites, their categorization and their accessibility have been shown to essentially depend on the number of aluminium atoms [5]. Hydrothermal treatment in hot water lead to the partial loss of crystallinity due to the hydrolysis of Si-O-Al bonds and the subsequent removal of octerhedrally coordinated Al-framework. Thus, forming amorphous extra-Al cationic specie at the surface of the zeolites [11].

1.2 Application of zeolites

Zeolites are important group of heterogeneous catalyst existing mainly as crystalline solids. The molecular sieves [12] allow their easy separation from reaction fluids making them more applicable in industry than liquid catalyst [13]. Adaptability to either batch or flow reactors, ease of recovery and low cost, are reason for their excessive demand in heterogeneous catalysis [12].

Possession of micropores with active acidic sites and large surface area have made zeolites suitable for application in gas separation, adsorption, ion-exchange and catalytic reactions [14]. Due to their thermal and chemical stability, zeolites have shown a remarkable stability and functionalities in the so-called zeolite imidazole framework ZIF [15]. The presence of cages and windows of different sizes in zeolites allow them to host different functional material that can manifest an unusual property [6]. Consequently, chemical and physical treatment to modify zeolite structure, porosity, acidity, reactivity and selectivity emerged as advanced technology in zeolites [16, 17]. This has broaden the applications of zeolite from not only being a catalyst but also for chemical and gas sensing applications [18]. Some major applications of the material include the following:

1.2.1 Catalysis

Zeolite acidity with different pore dimension is key feature responsible for their catalytic property. The intracrystalline holes of zeolites contain exchangeable cations that can be exchange with cations of specific catalytic activity such as proton, phosphates organosilanes. The possession of bronsted acid sites and Lewis acid sites has also make them good acid catalyst in many variety of industrial processes

1.2.2 Gas separation

This is due to the ability of zeolite to partially and discriminatingly adsorb one molecule from a mixture of gases. The property can be attributed to the sieving property provided by the pore sizes of the material, which allow only molecule of specific size to pass through. Thus, offering a molecular sieving property. The property gave zeolites ability to be used as desiccants and drying agents

1.2.3 Ion Exchange

The cations that compensate the framework negative charge are loosely bound. Hence when zeolites are introduced to an aqueous solution containing other cations, an equilibrium condition is established at which the cations in the framework are exchange with those in the solution. This property allow for the incorporation of different metals with catalytic property both in electrochemical process and cracking reactions

1.3 Synthesis of zeolites

Hydrothermal crystallization of reactive alkali metal aluminosilicates gels at high pH and typically above 100 ^{o}C and ambient pressure was the original method for the chemical preparation of zeolites. Alkali cations direct the formation of structured crystalline material, although materials with low to intermediate silica to alumina ratio are formed. The pioneering work of Barrer opens the door to the use of Organic Structure Directing Agent (OSDA) commonly known as template to obtain high silica zeolites. The cost of its procurement and environmental pollution render the OSDA process unfavorable [3]. Several organic compounds since then have been in use for zeolites synthesis adding a necessary post synthesis calcination process to remove the organic-template. The OSDA-free hydrothermal synthesis of zeolite remains a green route to

zeolite. Recently, a group of researchers are working on solvent-free and OSDA-free synthesis of zeolites [19, 20]. Although, pure zeolites were possible through this process, the size of the zeolite is uncontrollable. Therefore the addition of solvent during the gel preparation is important.

1.4 Voltammetry

1.4.1 Cyclic Voltammetry

Although it was only proposed in the 1950s, cyclic voltammetry has today become a powerful tool for rationalizing the chemical reactivity of species. The three-electrode system has the dynamic nature that allows the use of different working electrode. When the working electrode is dipped in a solution containing electrolyte compound, the movement of charged species and products is suppressed. Consequently, the electrode process is limited to diffusion [21].

The defined characteristics of cyclic voltammetry for a reversible electrochemical reactions as reported in [22] are; (i) current peaks interval , (ii) scan rate is independent of peak position, (iii) forward peak current is proportional to reverse (iv) scan rate is proportional to the square of peak currents. These are demonstrated in Equation 1.1 and Equation 1.2 and the waveforms are shown in Fig. 1.3 and 1.4

$$\Delta E = E_p^a - E_P^c = \frac{59}{n}\,\text{mV} \qquad \textit{Eqn. 1. 1}$$

$$\frac{I_p^a}{I_p^c} = 1 \qquad \textit{Eqn. 1. 2}$$

In voltammetric studies, zeolites are used in the fabrication of composite electrodes, which facilitate mass transport of analyte and affect the electrode total surface coverage. Thus, the current limitation will be determined by the added zeolites [23]. In

electrochemical studies current is produce as a measure of rate, which depend on the mass transport of analyte species govern by either convection as in stirred cells, migration as in charged electrode or diffusion where a concentration gradient led to the formation of a diffused layer across which analyte move [24].

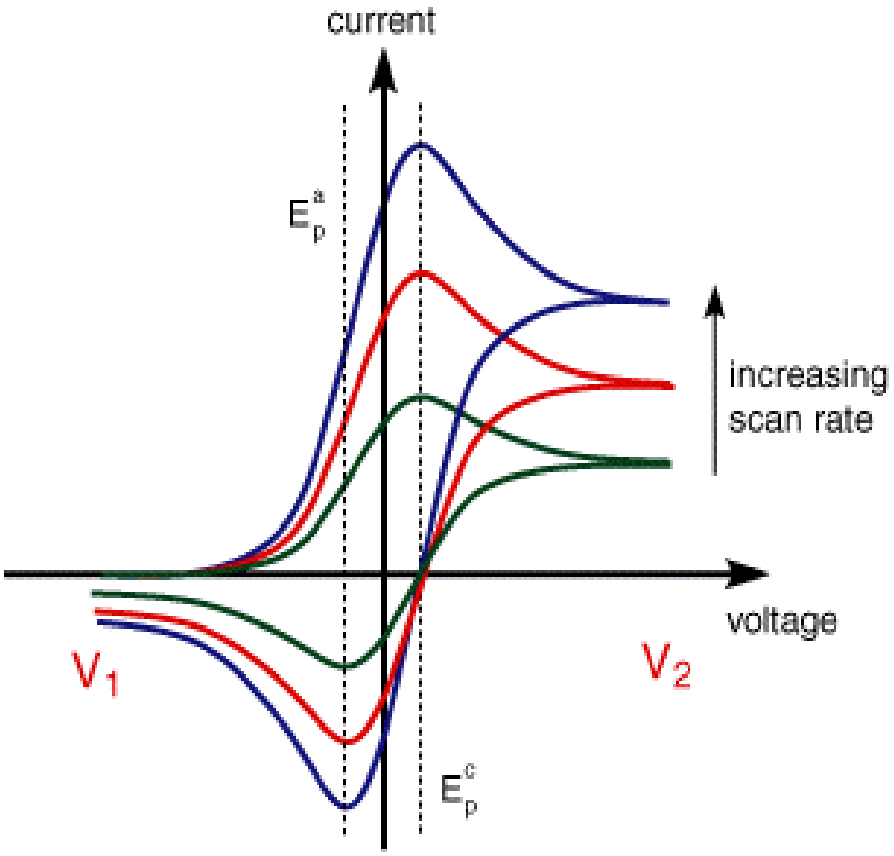

Fig. 1. 3 Peak current against scan rate [22]

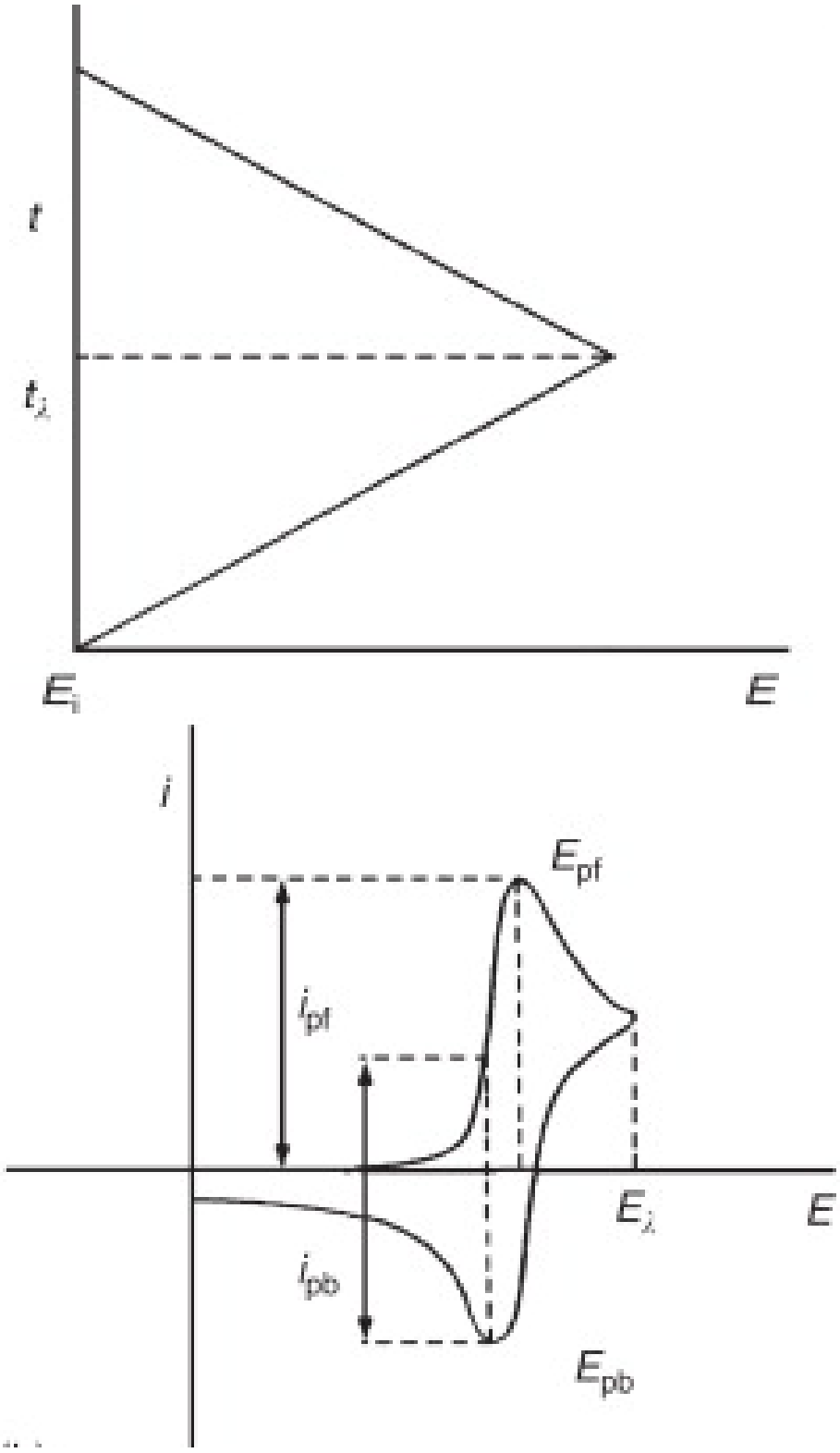

Fig. 1. 4 Potential waveforms for cyclic voltammetry and the resulting voltammograms [22]

1.4.2 Square Wave Voltammetry

In 1957 Baker reported Square wave voltammetry. However, the technique has not become feasibly practicable until the recent advancement achieved in electronics [25]. Square wave differs from differential pulse technique in the sense that it can be run at much higher scan rate of up to 1 V. Thus, a run, which will take 3 min in differential pulse, can be done in 3 seconds using square wave. Practically, it involves induction period; the working electrode is held at an initial potential, then shifting it to a forward and reverse potential and finally relaxation period. For instance, in a reaction involving reduction of specie O, the working electrode is held at an initial potential higher than that for reduction potential O, in the forward pulse while more positive potential should be applied in the reverse step. The peak height is calculated using Equation 1.4.2.2

$$\mathbf{O^- + e \rightarrow R} \qquad \textit{Eqn. 1. 3}$$

$$\Delta i_p = \frac{nFAD_o^{1/2}C_o^*}{\pi^{1/2}t_p^{1/2}}\Delta\Psi_p \qquad \textit{Eqn. 1. 4}$$

Where n = number of electrons,

F = Faraday constant (96500 C/mol)

A = Electrode Area in cm^2

D_O = Diffusion coefficient for O (cm^2/s)

C_O = Specie O concentration (mol/cm^3)

t_p = time of pulse and $\Delta\psi_p$ = Unit less.

1.5 Literature review

The crystallinity and crystal size of zeolites particularly mordenite type zeolite have been proofed to depend not only on gel composition but also on the gel preparation mode, crystallization time and temperature [26]. Hincapie and co-workers claimed to obtained small and highly crystalline mordenite in a shorter crystallization time and at lower temperature with 389 $m^{-2}g^{-1}$ BET (Brunauer Emmett And Teller) surface area by dissolving the silica source rather than dispersing it to mixed with the alumina source [26].

The addition of template Organic Structure Directing Agent (OSDA) to the gel in mordenite synthesis had successfully led to nanocrystalline material at relatively lower temperatures [27-31]. The BET area of mordenite was also improved by Dual templating system [32]. However, inclusion of organic template in hydrothermal process requires a longer synthesis time and a necessary post synthesis calcination step to remove template matrix, which also course environmental pollution.

Mordenite of high BET area at shorter crystallization time has been achieved from direct synthesis of mordenite without organic template [33]. Mordenite framework possessing high Si/Al was successfully synthesized in template-free process [34]. The presence of alkali metal cations in the gel assist crystal growth and the formation of the specific structure in direct synthesis [35]. Very recently, Wu Q et al [19] reported the catalytic activity of Beta and ZSM-5 zeolites obtained from solvent-free and template-free synthesis. They found that there are great similarities in the catalytic properties with the conventional ones. It has also been shown elsewhere that zeolite product yield dramatically increased in a solvent-free process, which is true of the fact that some

silicate and alumina are not transported during the crystal growth in the solvent synthesis [20]. Table 1.1 and 1.2 summarize some synthesis parameters and physico-chemical properties of mordenite zeolites obtained from OSDA and OSDA-free processes, respectively. Mordenite large crystal was obtained in row 7 of Table 1.1 although the gel silica to alumina ratio was low (6.2), uniform crystal with accessible micropore volume of 0.17 cm^3/g was obtained, which has great interest for application in functional devices. In the last row of Table 1.2 Wang J *et al* achieved high silica mordenite in template-free and fluoride free process with lower crystallization time of less than one day at 160 ^oC [34].

Table 1. 1 Gel parameters for Mordenite Synthesis using different OSDA

MOR-Zeolite	Composition	Template	Temp °C	Time h	Si/Al	BET m^2g^{-1}	Ref.
NaMOR	7.4 H_2O/Si, 20 Si/Al, 0.23Q/Si,4 OH/Al	TEAOH	170	72	18.1	434	[27]
MFI/MOR Overgrowth	6Na2O:0.84 Al2O3:16.8 SiO2:8TEABr: 1000H2O	TEABr	170	48	19.4	480	[36]
NaMOR	38 Si/Al, 0.5 Na_2O/Si, 0.0299 Q/Si, 16 H_2O/Si	OPDA	160	144	38	324	[30]
HMOR	--	TEABr	150	72	20	390	[37]
DMOR	$(TEA)_2O$:Na_2O:$A1_2OSiO_2$:H_20	TEABr	170	120	86.9		[38]
NaMOR	NH_4^+/Si=0.05, Na^+/Al=18, Si/Al=60, TEA/Si=0.12, HMI=0.17	TEAOH & HMI	170	72	37.1	518	[32]
NaMOR	10SiO_2:Al_2O_3:3Na_2O:500 H_2O:4.0$C_6H_6O_2$	Benzene-1,2-diol	140	264	32.2	-	[39]
NaMOR	10SiO_2:Al_2O_3:3Na_2O:500 H_2O	Benzene-1,2-diol	140	48	10.8	-	[39]
MOR	SAR=32	HMDA	150	90	22	544	[40]

Table 1. 2 Mordenite Gel parameters from different Template-free processes

MOR-Zeolite	Composition	Temp. (^oC)	Time h	Si/Al	BET m^2g^{-1}	Ref.
NaMOR	$6Na_2O:Al_2O_3:30SiO_2:780H_2O$	150	24	15	389	[26]
PMOR	$16.6SiO_2:Al_2O_3:7.5Na_2O:900 H_2O$	170	24	8.3	419	[41]
PMOR	$20SiO_2:Al_2O_3:7.5Na_2O:900H_2 O$	170	24	10.2	485	[41]
HMOR	$6Na_2O:Al_2O_3:30SiO_2:780H_2O$	180	24	15		[42]
NaMOR	$12Na_2O:2Al_2O_3:100SiO_2:500 H_2O$	180	120	16	52.14	[43]
NaMOR	$1.0Na_2O:0.56Al_2O_3:10SiO_2:22 5H_2O$	164	60	15.7	429	[44]
NaMOR	$1.0SiO_2:0.052Al_2O_3:0.23Na_2O 15.2H_2O$	170	96	6.20	480	[45]
HMOR	$6Na_2O:Al_2O_3:30SiO_2:780H_2O$	170	36	64	389	[46]
NaMOR	$6Na_2O:Al_2O_3:30SiO_2:780H_2O$	170	24	20.9	331	[47]
NaMOR	SAR 80, $NaOH:SiO_2$= 0.50, $H_2O:SiO_2$	433	20	31.0	378	[34]

The early application of Phosphorus is seen in the selectivity to p-xylene during disproportionation toluene pioneered by kaeding [48]. Phosphate zeolite later emerged as steam resistant functional catalyst during steam-assisted catalytic cracking reactions [49]. The stabilizing effect of phosphorous on ZSM-5 in steam has been investigated [50]. Although cations of the rare earth element were first used for stabilizing zeolite Y framework [50]. In the case ZSM-5, steam treatment after P-impregnation not only stabilizes the aluminium framework but also preserves enormous Bronsted acid sites, increase catalytic activity and selectivity to lighter olefins in cracking of n-decane [50]

The mechanism of interaction of Phosphorus added to zeolite Y by impregnation has been reported by Pannervelsam *et al* [51]. Zaiku *el al* reported the different models of phosphorus interaction with the bronsted acidity of ZSM-5 [52]. The computational model of Hung *et al* however, favors the kaeding model in which he concluded that strong Hydrogen bonding interaction occur between the framework tetrahedral oxygen atom and a hydrogen atom from the phosphoric acid [53]. The schemes of these proposed mechanisms were shown below

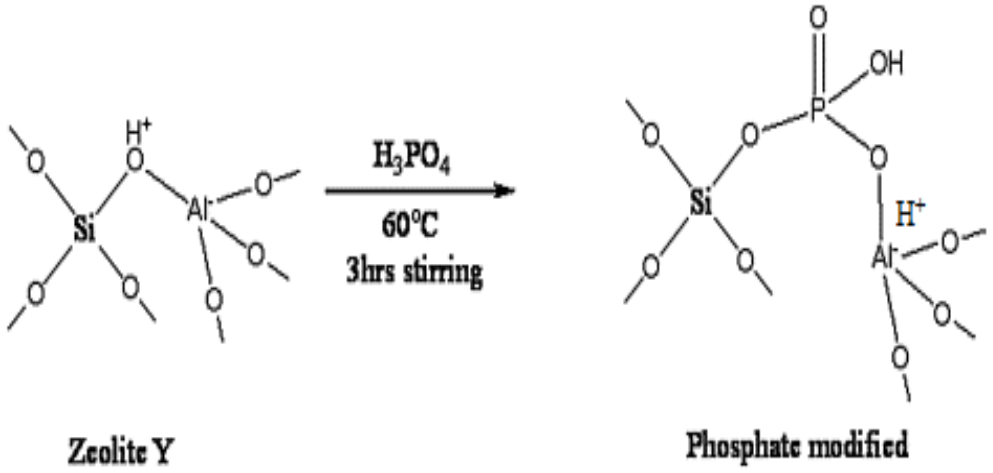

Scheme 1. 1 Proposed model of phosphoric acid interaction with zeolite Y Pannervelsam et al [51]

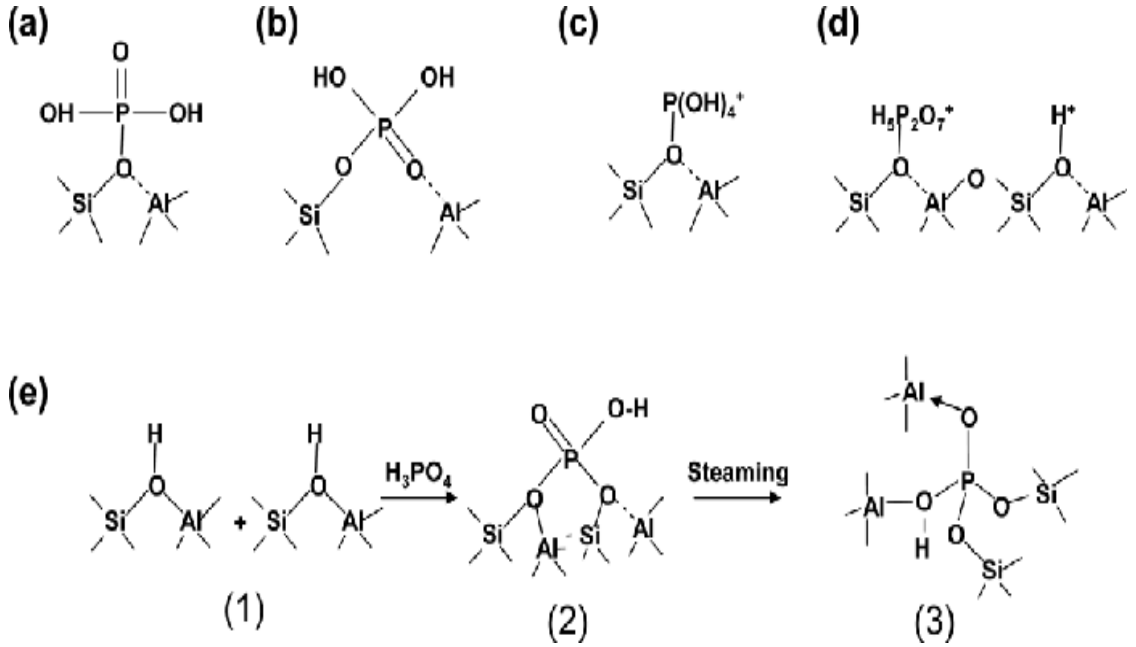

Scheme 1. 2 Proposed interaction models of phosphate with ZSM-5 framework **(a)** Kaeding *et al* [54] and Vedrine *et al.* [55] **(b)** Lercher *et al* [56] **(c)** and **(d)** Corma *et al* [57]; **(e)** Zaiku *et al* [52]

The ^{1}H NMR self-diffusion experiment conducted by Caro et al [58] on ZSM-5 shown that the phosphoric acid entered the channel system of the zeolite. The removal of octahedral extra-aluminium framework by oxalic acid treatment has also showed some decrease in silanol groups while nitric acid treatment led to creation of mesopores by leaching silica [59]. The proposal of Zhuang et al [60] showed that phosphorous can take silicon position in the framework after hydrothermal treatment of P-ZSM-5. The study of Van der et al [61] reveals that agglomeration of zeolites was caused by direct phosphate modification in ZSM-5 type zeolite. Van et al [62] reported that the difficulty in accessing the micropore in mordenite is caused by the presence of extra-framework aluminium in the micropore. They found that mild oxalic acid treatment greatly improved the adsorption capacity of n-hexane as the model compound.

The shape selectivity and stability of phosphate zeolites in catalytic reactions is available in literature [63-66]. Corma et al. [63] reported the optimum phosphorous loading based on the framework Si/Al of ZSM-5. Table 1.3 and 1.4 respectively present a survey of optimum p-loading, catalytic activity and selectivity of P-zeolites in some selected reactions.

Table 1. 3 Optimum P-loading for different zeolites from literature

Zeolite	P-loading	Si/Al	Feed	Con.(%)	Olefin selectivity (%)	Ref.
P-HZSM-5St.	0.5 wt.% $NH_4H_2PO_4$	25	naphtha	100	97 **(80.4) propylene**	[67]
P-ZSM-St.	1.0 wt.% $NH_4H_2PO_4$	25	naphtha	88	**(74.2) propylene**	[67]
P-ZSM-5St.	1.0 wt.% H_3PO_4	25	n-decane	@40	**7.60 $C_3^=$**	[57]
P-ZSM-5	0.1wt.% H_3PO_4	220	methanol TOS 100hrs	70	70 **(70) propylene**	[68]
P-ZSM-5/ZSM-11	4 wt.% H_3PO_4	103	methanol	99.9	85 **(51) propylene**	[69]
P-ZSM-5	2.1 wt.% H_3PO_4		C_4-olefins	64	57.5 **(45) propylene**	[70]
SAPO-34	30%		1-hexene	42.35	92.88 **(72.79) propylene**	[71]
P-MCM-22	3 wt.% $(NH_4)_2HPO_4$	15	methanol	100	70 **(50) propylene**	[72]
P-ZSM-5	5 wt.% $NH_4H_2PO_4$	21.3	methanol	100	80	[66]

Table 1. 4 Different phosphorus zeolites applied in production of olefins Values in bracket represent selectivity to propylene.

Catalyst	P-loading	Reaction Condition	Con. %	Feed Stock	Olefins Selectivity	Ref.
P-ZSM-5	1.5 wt.% H_3PO_4	600 ^oC , 1ATM, in N_2 WHSV of 3.2h^{-1}, 2.0g of cat, after 50hr TOS	71	C-4 olefins	57.5 **(42.5)**	[70]
P-ZSM-5	2.1 wt.% H_3PO_4	600 ^oC 1ATM, N_2, WHSV of 3.2h^{-1}, 2.0g of cat, after 50hr TOS	64	C-4 olefins	57.5% **(45)**	[70]
P-ZSM-5 Si/Al=55	4 wt.% H_3PO_4	500 ^oC 1atm, N_2, cat. Loading 60mg WHSV=2h^{-1}	96%	methanol	70% **(42.5)**	[69]
P-ZSM-5/ZSM-11intergrowth Si/Al=103	4 wt.% H_3PO_4	500 ^oC 1atm, N_2, Loading 60mg WHSV=2h^{-1}	99.9 %	methanol	85% **(51)**	[69]
PHAPTMS-MOR Si/Al=8.3	9 mol% PHAPTMS	420 ^oC, 2hrs, 0.15g catalyst 1atm	56.6 %	7.5 g LDPE (pellets)	45% of C1-C5	[41]
PHAPTMS-MOR Si/Al=10.2	22 mol% PHAPTMS	420 ^oC, 2hrs, 0.15g catalyst 1atm	57.1 %	7.5 g LDPE (pellets)	28% of C1-C5	[41]
P-HZSM-5 Si/Al=25	0.1% wt. $(NH_4)_2HPO_4$	650 ^oC, 1atm, N_2, 300mg cat	99%	C_4 alkanes (n-butane and i-butane)	48.7% **(17.1)**	[73]
P-HZSM-5 Si/Al=25	0.5 wt.% $(NH_4)_2HPO_4$	650 ^oC, 1atm, N_2, 300mg cat	99.3 %	C_4 alkanes (n-butane and i-butane)	55.7% **(19.0)**	[73]
P-HZSM-5 Si/Al=25	1.0 wt.% $(NH_4)_2HPO_4$	650 ^oC, 1atm, N_2, 300mg cat	96.1 %	C_4 alkanes (n-butane and i-butane)	53.0% **(26.6)**	[73]

Table 1. 4 (cont'd)

Catalyst	P-loading	Reaction Condition	Con. %	Feed Stock	Olefins Selectivity	Ref.
P-HZSM-5 Si/Al=25	0.5 wt.% $NH_4H_2PO_4$	923K, 1atm He carrier gas,	100 %	naphtha C_5-C_{12}	97% **(80.4)**	[67]
P-HZSM-5 Si/Al=25	1.0 wt.% $NH_4H_2PO_4$	923K, 1atm He carrier gas	100 %	Naphtha C_5-C_{12}	88% **(74.2)**	[67]
P-ZSM-5	3.48 wt.% $P(OCH_3)_3$ in n-octane	600 ^oC, 1ATM, WHSV=2.3$h^{—1}$	100 %	DME	74.6% **(38.7)**	[74]
ZSM-5 Si/Al=9.3	1.1 wt.% $P(OCH_3)_3$ in n-octane	470 ^oC, 0.1g cat. WHSV 11.2 h^{-1}	93%	3 mol% DME 5%mol methanol	70% **(40)**	[75]
P-ZSM-5 Si/Al=12.6	1.1 wt.% $P(OCH_3)_3$ in n-octane	470 ^oC, 0.1g cat. N_2 carrier gas WHSV 12.1 h^{-1}	83%	11 mol% DME 6%mol methanol	71% **(40)**	[75]
W-P/HZSM-5 Si/Al=35	$(NH_4)_2HPO_4$, & $((NH_4)_6H_2W_{12}O_{40})$	803K, 0.1 MPa, N_2 20 $mlmin^{-1}$, WHSV of 13h^{-1}, cat. loading 10mg	75%	1-butene N_2/1-Butene=3	60.6 **(47.8)**	[76]
W-P/HZSM-5-ST Si/Al=35	2wt.% Each of $(NH_4)_2HPO_4$, $((NH_4)_6H_2W_{12}O_{40})$	803K, 0.1 MPa, N_2 20 $mlmin^{-1}$, WHSV of 13h^{-1}, cat. loading 10mg	57.4 %	1-butene N_2/1-Butene=3	56.8% **(50)**	[76]
P-ZSM-5 Si/Al=35	2 wt.% $(NH_4)_2HPO_4$,	803K, 0.1 MPa, N_2 20 $mlmin^{-1}$, WHSV of 13h^{-1}, cat. loading 10mg	69%	1-butene N_2/C_4=3	55.1% **(46.5)**	[76]
P-ZSM-5-ST Si/Al=35	1.54wt%. $(NH_4)_2HPO_4$	803K, 101KPa, WHSV=10h^{-1},	75.5	84 vol. % butane 16vol% butane N_2/C_4=3	55.9 **(43.1)**	[77]

Table 1. 4 (cont'd)

Catalyst	P-loading	Reaction Condition	Con. %	Feed Stock	Olefins Selectivity	Ref.
P-ZSM-5 Si/Al=220	0.1 wt.% H_3PO_4	733 K weightily hour velocity 0.75 h^{-1} atm MeOH: H2O = 1:5, cat. Loading 0.5g 3hrs TOS	100 %	methanol	72.2% **(46.4)**	[68]
P-ZSM-5 Si/Al=220	0.1 wt.% H_3PO_4	460 ^oC; LHSV 0.75 h^{-1} atm MeOH: H2O = 1:5, cat. Loading 0.5g 100hrs TOS	70%	methanol	**70% (55.6)**	[68]
MCM-22 Si/Al=15	0.5 wt.% $(NH_4)_2HPO_4$	723K, WHSV=1h^{-1}, 40hrs TOS, 0.4g cat. In N_2	100 %	methanol	50% **(38)**	[78]
P-MCM-22 Si/Al=15	1wt.% $(NH_4)_2HPO_4$	723K, WHSV=1h^{-1}, 40hrs, 0.4g cat. In N_2	100 %	methanol	65% **(40)**	[78]
P-MCM-22 Si/Al=15	2 wt.% $(NH_4)_2HPO_4$	723K, WHSV=1h^{-1}, 40hrs, 0.4g cat. In N_2	100 %	methanol	68% **(47)**	[78]
P-MCM-22 Si/Al=15	3 wt.% $(NH_4)_2HPO_4$	723K, WHSV=1h^{-1}, 40hrs, 0.4g cat. In N_2	100 %	methanol	70% **(50)**	[78]
P-MCM-22 Si/Al=15	4 wt.% $(NH_4)_2HPO_4$	723K, WHSV=1h^{-1}, 40hrs, 0.4g cat. In N_2	100 %	methanol	57% **(42)**	[78]
30% SAPO-34	H_3PO_4	500 ^oC, 0.12MPa, WHSV=2h^{-1}, TOS, 1.5 min	42.35%	hexane	92.88% **(72.79)**	[79]
30% SAPO-34	H_3PO_4	550 ^oC, 0.02MPa, WHSV=1.98h^{-1}, TOS, 1.5 min	60%	hexane	95% **(67)**	[79]

Table 1. 4 (cont'd)

Catalyst	P-loading	Reaction Condition	Con. %	Feed Stock	Olefins Selectivity	Ref.
P-ZSM-5 Si/Al=21.3	5 wt.% $NH_4H_2PO_4$	723K. WHSV=4 h^{-1}	100	methanol	80	[66]
Ni-P-ZSM-5 Si/Al=25	5 wt.% $(NH4)_2HPO4$ and 2wt. % $Ni(NO_3)_2$	550 ^oC under N_2 at 1 atm. 20-40 mesh of cat. Steam/feed 0.5g/g WHSV=5 h^{-1}	42.41	1-butene	87.84 **(55.66)**	[80]
Ni-P-ZSM-5 Si/Al=25	2 wt.% $(NH4)_2HPO4$ and 2wt. % $Ni(NO_3)_2$	550 ^oC under N_2 at 1 atm. 20-40 mesh of cat. Steam/feed 0.5g/g WHSV=5 h^{-1}	79.93	1-butene	74.08 **(43.54)**	[80]
Ni-P-ZSM-5 Si/Al=25	1 wt.% $(NH4)_2HPO4$ and 2wt. % $Ni(NO_3)_2$	550 ^oC under N_2 at 1 atm. 20-40 mesh of cat. Steam/feed 0.5g/g WHSV=5 h^{-1}	82.56	1-butene	69.5 **(41.07)**	[80]
Ni-ZSM-5 Si/Al=25	0wt% P 2 wt. % $Ni(NO_3)_2$	550 ^oC under N_2 at 1 atm. 20-40 mesh of cat. Steam/feed 0.5g/g WHSV=5 h^{-1}	88.01	1-butene	52.84 **(25.0)**	[80]
P/C-ZSM-5 Si/Al=33	0.3 wt.% H_3PO_4	600 ^oC, 12 hrs.	96	c_5-reffinate	59 E&P	[81]
La-P/C-ZSM-5 Si/Al=33	0.3 wt.% H_3PO_4 0.7 La/Al $La(NO_3)_3.6H_2O$	600 ^oC, 12 hrs.	95	c_5-reffinate	63 E&P	[81]
P-ZSM-5 Si/Al=280	1 wt.% H_3PO_4	500 ^oC 5g cat. 1.35 bar	70.1	1-butene	52.7 **(46.9)**	[82]
PITQ Si/Al=100	0.5 wt.% $NH_4H_2PO_4$	0.3 cat. 500 ^oC WHSV=3.5 h^{-1}, 101.325kpa TOS 5min	95.6	1-butene	57.3 **(41.6)**	[83]

From Patwardhan's report, it was observed that ion-exchange ability of zeolites can be increased by decreasing framework Si/Al ratio [35]. Thus, zeolites with low to intermediate Si/Al ratios are better in ion exchange voltammetry [84]. This property together with the availability of adsorption sites provided by their porosity, have made zeolites very important component of composite electrodes [85]. The framework negative charge of zeolite A was successfully reversed by surfactant ion which showed excellent selectivity to nitrate in potentiometric determination [86]. The fact that solid materials including zeolites, clays and other non-conducting oxides such as alumina and LDH, affect the rate of electron transfer has been established long time ago by Shaw et al [87]. Shaw *et. al.* reported that carbon paste composite electrodes have the advantage of surface renewability and reproducibility by polishing. Zeolites, in carbon paste electrode affects the total surface coverage which affects the mode of current limitation, kinetic of electron movement to and from the supporting graphite and stability of the fabricated sensor [23]. The observed Improved sensitivity was a consequence of the pore size of 3, 4 and 5 Å, of zeolite A which facilitated the chemical deposition of the cobalt ions [88]. Table 1.5.5 show review of application of some ZCPEs

Table 1. 5 Review of different zeolite modified electrodes in electroanalytical applications

SN	Zeolite Modified Electrodes (ZMEs)	Characterization technique	Application	Comments	Ref.
1	Mordenite MOR/ZCPE	Amperometry	Determination of ascorbic acid	Ease of preparation and high sensitivity	[90]
2	Nickel Phosphate VSB-5.- ZME	Cyclic voltammetry	Electrocatalytic oxidation of methanol	Improve activity	[91]
3	Fe-Y Zeolite ZME	Square wave voltammetry	Electrocatalytic oxidation of ascorbic acid	Enhancement o f anodic peak current with lowering e ffect on overpotential	[92]
4	NH_4-Y-ZME	Voltammetry	Detection of lead and cadmium	Excellent reproducibility	[93]
5	ZSM-5	Cyclic voltammetry	Electrocatalytic oxidation of methanol	Reduced overvoltage in diffusion control process Improved efficiency	[94]
6	Ag-zeolite	Cyclic voltammetry cyclic voltammetry MPA	Simultaneous determination of nitrates and nitrites	Reproducibility and strong dynamic range against nitrates concentration of 1-10 mM and nitrites concentration	[95]
7	Ni-zeolite Y Carbon electrode	Cyclic voltammetry	Oxidation of methanol	Stabile surface and strong dynamic range	[96]

Although enough data was gathered from the study of P-zeolites, there is disagreement between results documented. Thus, study on the exact zeolite-phosphate interaction is still an open field of discussion. Phosphate mordenite has seldom been reported or not at all available. The electrochemical characterization and electrocatalytic behavior of phosphate mordenite have never been attempted.

This current work aimed to obtain mordenite from direct hydrothermal synthesis without seed and organic template. Phosphorous impregnation was carried out to modify the diffusivity and acidity of the mordenite. The electrocatalytic performance of the phosphate mordenite was investigate in detection of some toxic anionic species was investigated and reported in this document.

Chapter Two

Synthesis zone of OSDA-free and seed-free Mordenite

Abstract

Direct hydrothermal synthesis of mordenite without the addition of both seed and organic template is reports in this work. The role of inorganic cations in crystal purity and directing the mordenite structure was actualized. It was observed that higher Si/Al ratio requires higher alkalinity ratio of the gel. Pure mordenite was obtained using silica gel, colloidal silica and fumed silica, while TEOS and water could not produce mordenite phase due to the difficulty in silica dissolution and transportation. Smaller crystals were achieved at 160 ^{o}C. Framework Si/Al ratio can be raised to as high as 50 using silica gel in template-free process. At fixed Na/Si ratio of 0.52 pure mordenite Si/Al molar ratios of only 15 and 20 can be obtained. The FE-SEM revealed the formation long flat prism crystals in 48 h using silica gel. While much shorter small prismatic crystal was obtained in 24 h using the fumed silica.

2.1 Background

The suitability of zeolites as catalyst in many important industrial processes can be said to be due to their porosity, interconnected channels and acidic sites [97]. Important features of zeolites that made them unique include surface area, microporous, sieving ability, exchangeable cations, internal surface area with acidic sites, ability to resist hash temperature in the presence of water and their attraction to charge species. They are inorganic polymeric materials [98].

The structural chemistry of zeolites is based on two functional units constituting silicon or aluminium atom (or some other elements) bonded to four oxygen atoms forming a tetrahedral, with the oxygen liked to two tetrahedral atoms normally bent (ca 145 ^{o}) which are link together to form a ring containing commonly 4, 5, 6, 8, 10 and 12 [3].

Mordenite is an industrially important zeolite with ideal composition $Na_8[(AlO_2)_{400}].24H_2O$. Its framework is built on 5-membered rings arranged in columns parallel to the [001] axis. Hence, the framework includes elliptical micropore (6.7 x 7.0 Å) channels parallel to the c-axis and (2.6 x 5.7 Å) channels parallel to the b-axis [43, 99]. Difficulty in accessing the smaller aperture, led to its characterization as 1-D zeolite [100]. Owing to its high thermal and acid stabilities, mordenite is used in several applications such as in the adsorptive separation of gas or liquid mixtures and in catalysis such as hydrocracking, hydro-isomerization, alkylation, reforming, dewaxing and in the synthesis of dimethyl amines [27, 101]. More recently, it has been considered as host for use in semiconductors, chemical sensors and non-linear optical materials [43].

The crystallization parameters that might affect the morphology of zeolites synthesized using aluminium sulfate as aluminum source were reported recently [102]. Various parameters determine the crystallinity and the crystal size in the hydrothermal synthesis of zeolites [30]. For instance, different cations; NH^{4+}, Ca^{2+}, Li^{+}, H^{+} and Ni^{+} were used to understand the effect of ion-exchange on crystallinity and morphology of EU-1 zeolite [103].

Hincapie et. al. obtained a 62 nm mordenite crystal from low Si/Al gel in a seed assisted template-free synthesis, the group claimed to obtained small and highly crystalline mordenite in a shorter crystallization time and lower temperature with a good BET surface area. by dissolving the silica source rather than dispersing to mixed with the alumina source [26]. Zhang et al in [44] and [45]obtained mordenites with high BET area of respectively 429 and 480 in a template-free hydrothermal process.

Although, Hincapie et al [26] reported the synthesis of mordenite without seed addition. However, other factors affecting the formation of pure mordenite phase were limited in the literature. In this work, direct hydrothermal synthesis of mordenite type zeolite crystals is reported. The factors that affect mordenite crystal growth and crystal purity, especially inorganic cations content and alkali ion concentration in seed-free and template-free synthesis were studied. The morphology of mordenite crystals obtained from different silica source were revealed using FE-SEM.

2.2 Experimental

2.2.1 Materials

PTFE-lined stainless steel autoclaves with a volume of 100 ml were used throughout the synthesis. No OSDA used in this research. Colloidal silica (40 wt. % suspension in water, Ludox AS-40 Sigma Aldrich), Silica gel (Sigma Aldrich grade 7734 pore size 60Å, 70-230 mesh), water glass (sodium orthosilicate reagent grade) and fumed silica were utilized as silica sources. Sodium Aluminate 13404 Sigma Aldrich was used as Aluminium sources. Sodium hydroxide (NaOH) pellets PRS-CODEX 98% was used to control alkalinity.

2.2.2 Procedure

Mordenite synthesis was started according to the gel dispersion procedure reported by Hincapie *et. al.* [26]. Adding extra Silica sources stated above did modification of synthesis procedure; also in contrast, seed was not used in our procedure. The initial sol-gel mixture was prepared by dissolving 2.097 g of NaOH in 54.13 g of deionized (DI) water, followed by the addition of 0.632 g of sodium Aluminate under stirring condition at room temperature. After a clear solution was obtained the silica source (silica gel in the first case) in then added. The gel composition $6Na_2O:Al_2O_3:30SiO_2:780H_2O$ obtained was continuously stirred at room temperature for one hour before transferring to Teflon-lined stainless steel autoclave. The crystallization was initially performed at 180 ^oC for 48hrs in the absence of both seed and organic template. To study the effect of Si/Al ratio, the gel composition was conditioned to Si/Al of 15, 20, 25 and 30. When different silica source or aluminium source were used the appropriate amount of silica or aluminium required were calculate from stoichiometric

equations. Moreover morphology at fix Si/Al ratio was also studied by changing silica source (water glass, TEOS, Colloidal silica, silica gel). All products were washed by deionized water until the pH of the product was 7 using a centrifuge. The products were dried in air circulating fume hood for 24 h. All zeolite synthesis experiments were carried out under static condition.

Ion exchange was performed under microwave irradiation. 2 M Ammonium nitrate ($NH_4(NO_3)$ was prepared by adding 16 g of ammonium nitrate in 100 ml of DI water. Then 20 g of this solution was used against each 1 g of the zeolite. The temperature of the microwave was ramped to 85 C in 2 min. Then, it was dwelled at 85 C for 10 min. After two sequential ion-exchange steps, the products were washed once by DI time each and finally the products were washed three times by the DI water using centrifuge. The products were dried in fume hood for 24 h, thereafter, calcination done under airflow for 15 h. The temperature was ramped from ambient temperature to 550 C in 3 h. Then the temperature was dwelled at 550 C for 12 h. Finally the sample was obtained in the H-MOR formed.

2.2.3 Characterization

Mordenite peak patterns were confirmed using a diffractometer (Miniflex, Rigaku) equipped with Cu Kα radiation (1.5405 Å). XRD patterns were recorded at 2θ from 5° to 50° using a scan of 0.03° per step and a counting time of 3 s for each step. The morphology of the synthesized mordenite were revealed by Field-emission scanning electron microscopy (FE-SEM) LYRA 3 Dual Beam (Tescan) equipped with energy dispersive X-ray spectrometry (EDX, Oxford Instruments) to give the elemental

composition, operated at an acceleration voltage of 30 kV. The elemental composition of the samples was obtained from the EDX.

2.3 Result and discussion

2.3.1 Effect of alkalinity ratio Na/Si ratio

To understand the effect of the alkalinity ratio, the Na/Si ratio was varied for each the gels with Si/Al molar ratios of 20, 25 and 50. For the sample prepared from gel of Si/Al 20 it was observed that the crystallinity was improved by increasing the Na/Si ratio from 0.52 to 0.54 (corresponding to $^{-}OH/Si$ = 0.49). It was also observed that the morphology of the product is becoming richer in the prism-like crystals with disappearance of the sphere-like crystals compared to the sample prepared at 0.52 Na/Si ratios. This showed that the alkali acts as seed or structure directing agent. Seronu et al. [104] reported the spheres present in the samples with less Na/Si ratio as Analcime which accounted for the decreased crystallinity of former sample. From the diffractogram in Fig 2.1, it is seen that the broadening of the peaks decrease with increasing Na/Si concentration as a result of the disappearance of the spheres. Fig. 2.2 shows the FE-SEM images of the samples at Na/Si ratios of 0.52 and 0.54. It can be further justified that, there are no much sphere like crystals in the sample with higher alkalinity ratio. Although the morphology of the materials are similar but the variation in the parameter has led to increased purity and size. Nucleation was the first stage in Mordenite synthesis followed by a crystal growth in a continuous nucleation stage [7] which led to larger crystal. Thus, in the presence of higher alkali and metals cations concentrations, the rate of nucleation increase continuously even in crystal growth forming a bigger crystal.

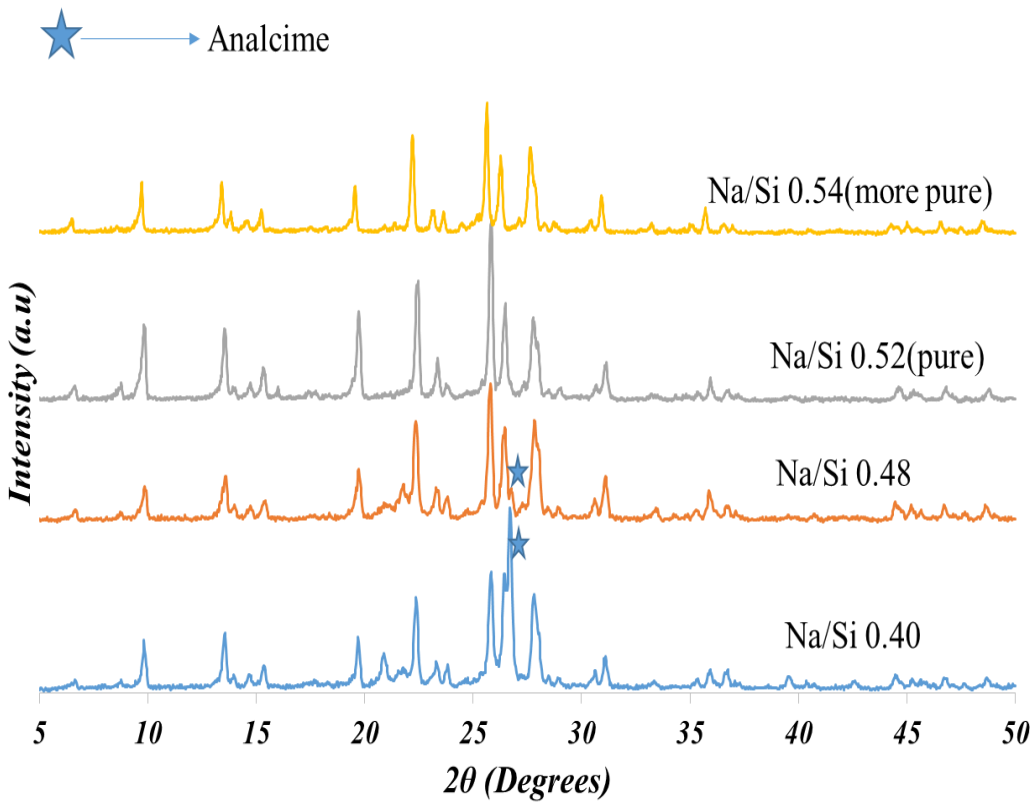

Fig. 2. 1 XRD patterns of mordenite zeolites synthesized with different Na/Si ratios at fixed Si/Al of 20 at 180 ^{o}C for 48 h using silica gel and sodium aluminate

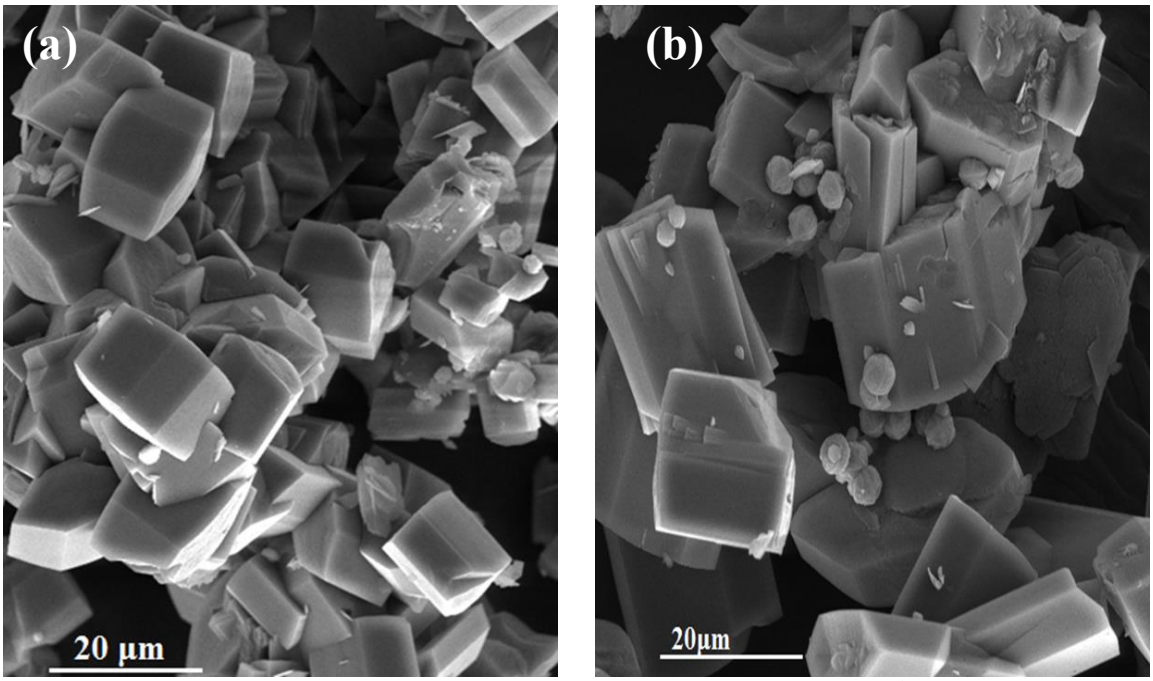

Fig. 2. 2 SEM of MOR samples at Si/Al ratio 20 synthesized at 180 ^{o}C in 48 h from gel with Na/Si of; (a) 0.52 (b) 0.54

Fig 2.3 and Fig 2.4 present the differactograms of the variation of Na/Si from 0.40 to 0.56 at Si/Al ratio of 25 and from 0.60 to 0.70 at Si/Al ratio of 50. The same argument discussed above is enough to justify the trend. The broadening of the peaks in both cases decrease due to the increase in purity and crystallinity corresponding to the effect of high alkali concentration. At lower aluminium content the silica requires higher alkali concentration to be incorporated in to the framework as discussed earlier.

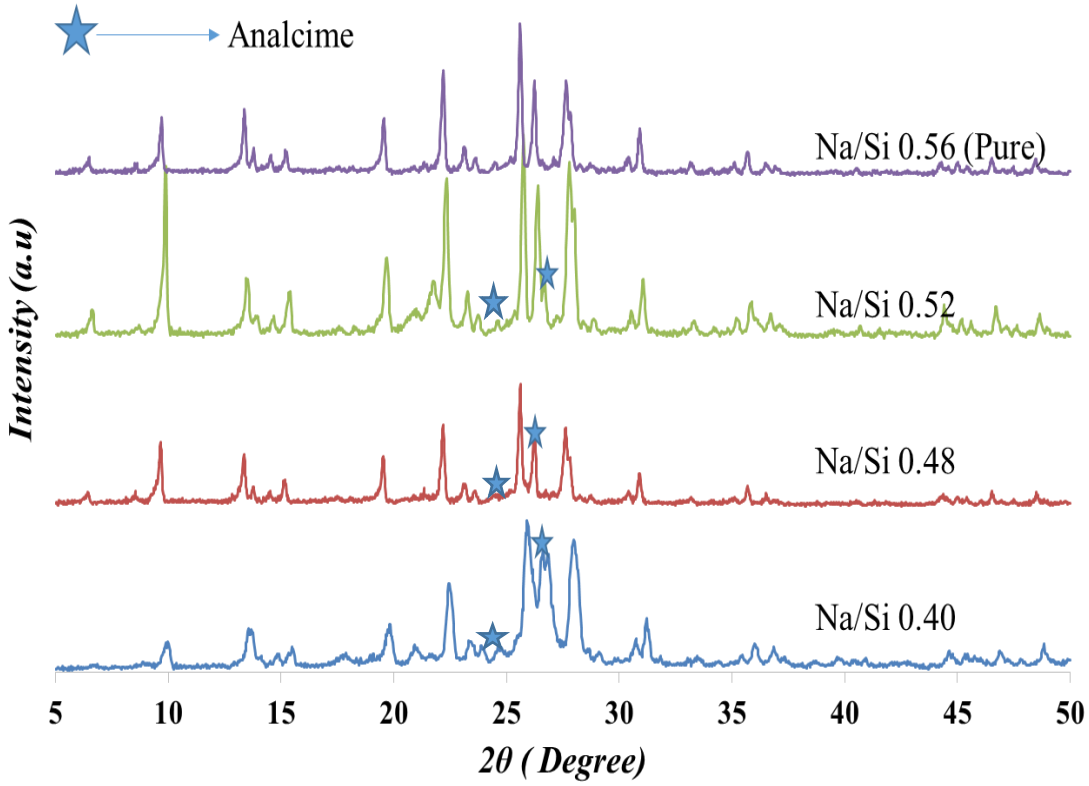

Fig. 2. 3 XRD patterns of mordenite zeolites synthesized with different Na/Si ratios at fixed Si/Al of 25 at 180 ^{o}C for 48 h using silica gel and sodium aluminate

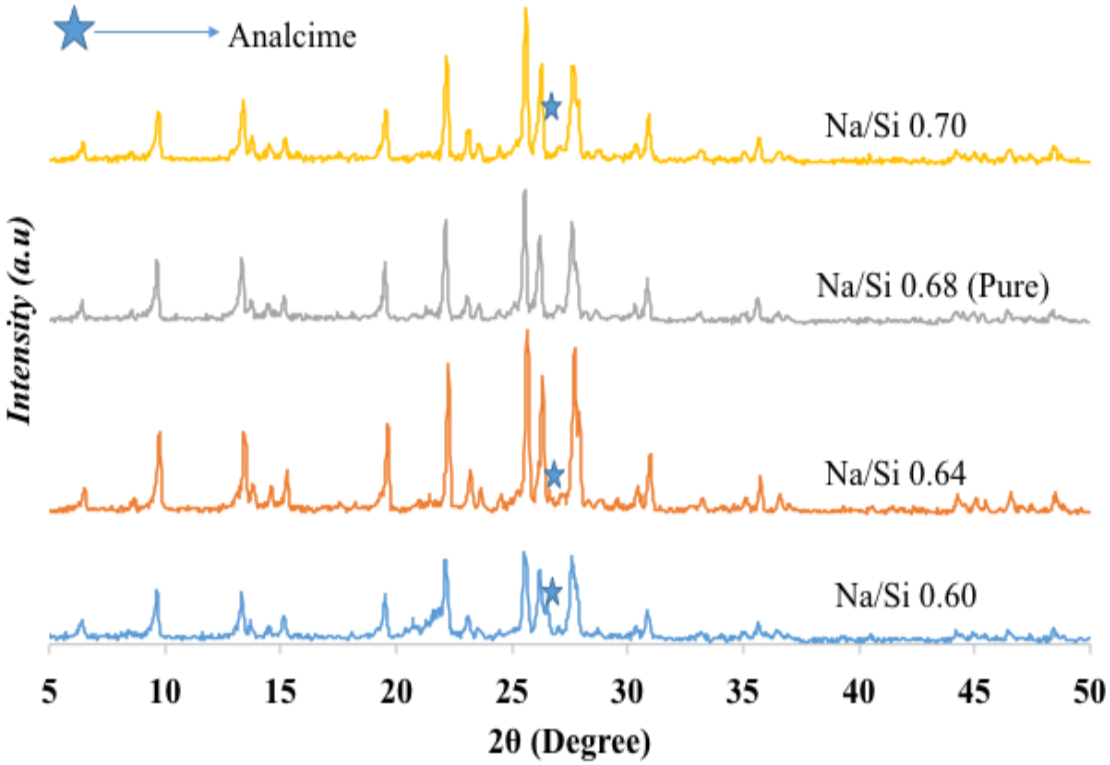

Fig. 2. 4 XRD patterns of mordenite zeolites with different Na/Si ratios at fixed Si/Al of 50 synthesized at 180 ^{o}C for 48 h. using silica gel and sodium aluminate

Fig. 2.5 summarizes the differactograms of pure mordenites obtained at different Si/Al and the corresponding Na/Si ratios at which pure phase of the mordenite were obtained. It was clear that pure products of different gel Si/Al ratios were obtained at different cationic content of the gel. Thus, concentration of the alkali is the driving force to pure crystals. The alkalinity of the gel solution is also a determining factor for mordenite crystallinity, morphology and crystal purity. In the absence of seed and template the alkali acts as the structure-directing agent. Eventual increase in the $^{-}$OH concentration due to increase in the Na/Si ratio allows for the control growth of pure mordenite at higher silica content which controls the transport of the silicates in solutions probably during the ageing time to give the pure products. The $^{-}$OH modifies the

nucleation process [35] by increasing the rate of crystal growth of the mordenite [30]. Hincapie *et al* [26] was the first to obtained small mordenite from low gel Si/Al which he justified using the Lowenstein's rule, which was in accord with effect of the alkali concentration that determine the framework to be obtained [35]. The increase in the crystal size with increase in the $^{-}$OH/Si ratio was due to the increase in the pores and an eventual crystal size growth. It was also reported elsewhere [30] that the increase in crystal size and crystallinity was due to the increasing in the gel Na/Si content as observed in this studies.

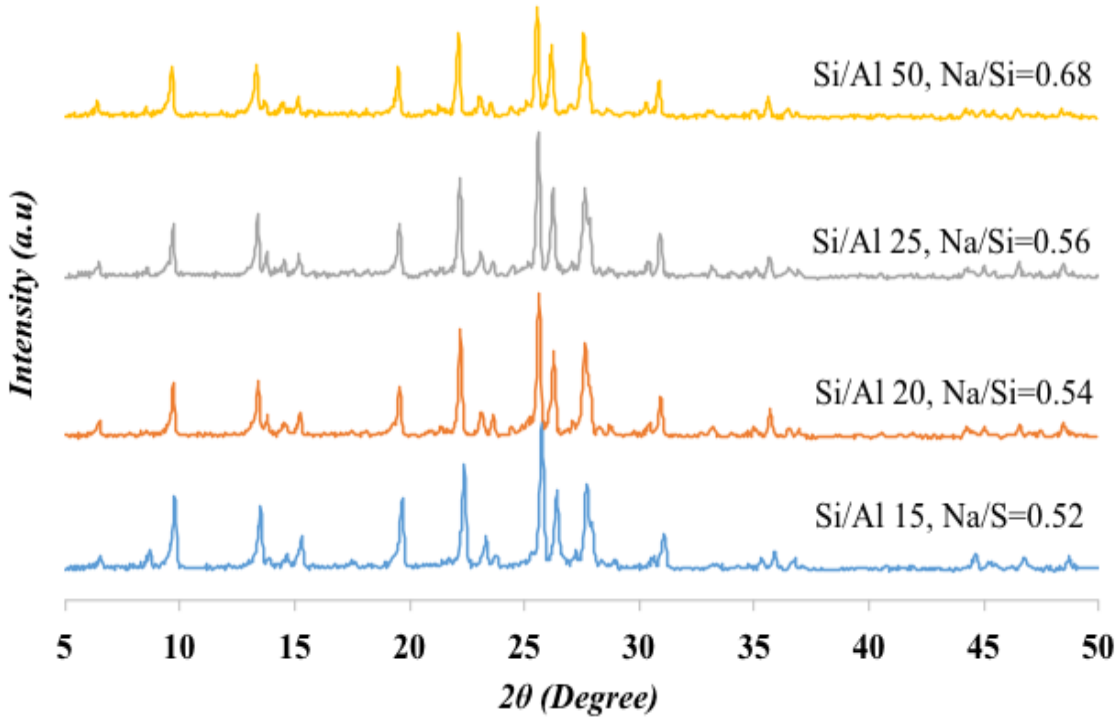

Fig. 2. 5 XRD patterns of pure MOR with different Si/Al obtained at different -OH/Si ratios synthesized at 180 ^{o}C in 48 h using silica gel and sodium aluminate

2.3.2 Effect of Silica source

Fig. 2.6 is a typical differactograms depicting the effect of different silica source on the crystallinity of mordenite synthesized from a gel with 15 Si/Al molar ratio. Mordenite synthesized from water glass and tetra ethyl orthosilicate, displayed a strong sharp peak, which is attributed to silica [105], but no evidence of mordenite peaks is present in the differactograms. In the case of tetra ethyl orthosilicate, this could be due to the effect of ethanol by product formed during the aging, formation of which affect the solvent polarity by reducing the concentration of the alkali OH present. Consequently affecting the dissolution and transport of silicates which cause slower crystal growth, giving mainly the silica as the product [105]. Furthermore, there is evidence of formation of diethyl ether during the aging reactions, which was noticed by formation of organic phase in the main solvent (water) and prevents the silica transport.

The XRD patterns showed pure mordenite was obtained with Colloidal silica, Silica gel and fumed silica. When fumed silica was used the gel composition was modified due to the lower density of fume silica, 100 grams of water was used to obtain a homogeneous mixture. To understand the Morphology of these pure MOR the FE-SEM images were snapped. A prism-like morphology was obtained using colloidal silica which could be attributed to the well dispersed hydrated SiO_2 of the colloidal silica [44]. While a short prism-like crystals were observed when fumed silica was used and longer flat prism when the silica gel was used (Fig. 2.7). Similar morphology was reported elsewhere [45], which was said to be due to the gel dispersion procedure. These prism-like crystals of size range 6-7 μm were also reported elsewhere [43]. The small spherically shaped crystals of size 1 μm observed growing along with prismatic

morphology, were reported by Wang et al when he used TEAOH as an organic template [106].

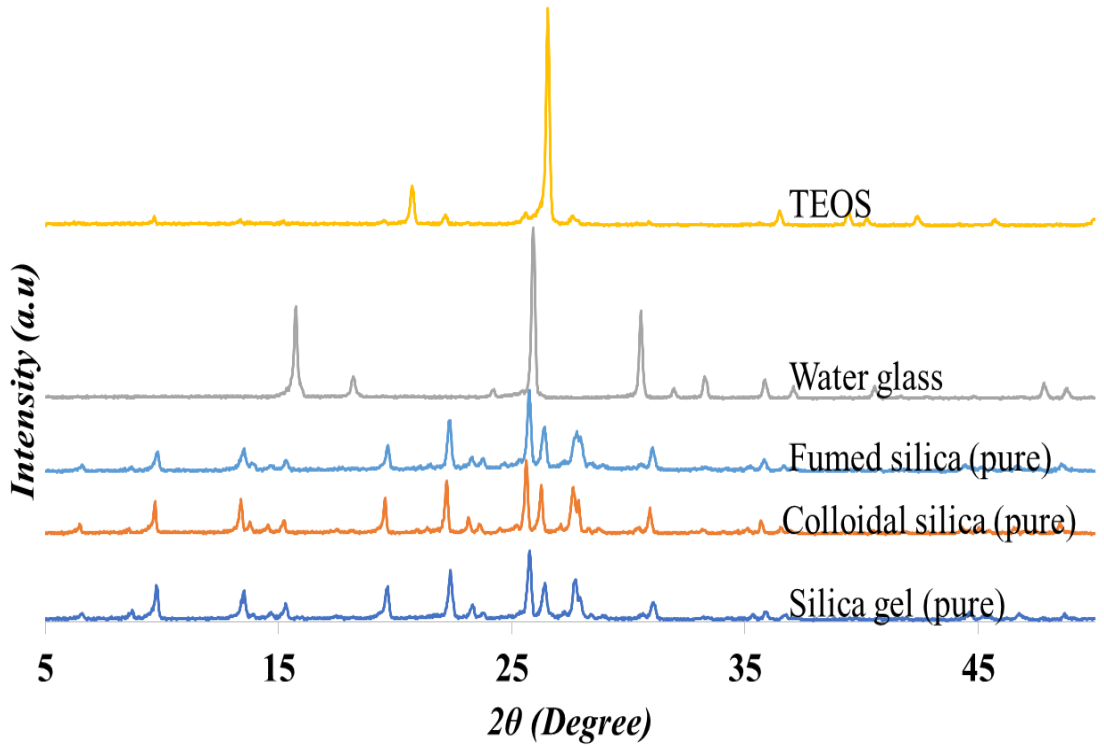

Fig. 2. 6 XRD patterns of MOR samples at Si/Al ratio 15 synthesized at 180 ^{o}C for 48 h using different Silica source

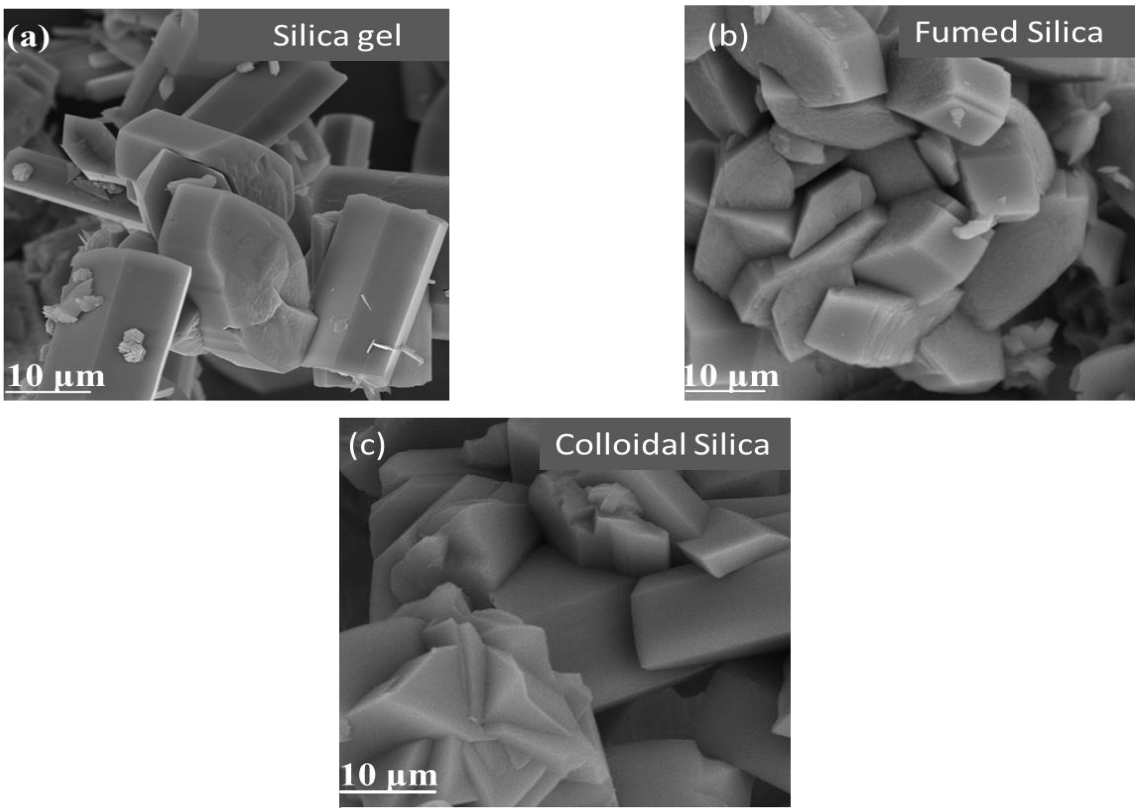

Fig. 2. 7 SEM of MOR samples with 15 Si/Al molar ratio and 0.52 Na/Si molar ratio synthesized at 180 ^{o}C for 48 h using different Silica source (a) Silica gel (b) Fumed silica (c) Colloidal silica

2.3.3 Effect of Si/Al molar ratio

Fig. 2.8 displays the differactograms of mordenite synthesized from gel of different Si/Al ratio in the range of 15-30 at constant Na/Si ratio of 0.52. Pure mordenite at a fixed Na/Si of 0.52 was obtained for only Si/Al ratio of 15 and 20, while experiments with Si/Al ratio of 25 and 50 produce Analcime peaks along with the mordenite phase, which is regarded as impurity. The Analcime is becoming more obvious as the Si/Al is increased at the same Na/Si ratio. Pure mordenite at Si/Al ratio 25 and 50 were obtained by changing Na/Si contents. It was observed that by increasing the Na/Si ratio pure MORs at higher Si/Al ratios were successfully formed as discussed and justified above.

Inorganic cationic species are known to induce crystallization in zeolites and affect crystal purity and morphology as reported in [35].

Fig. 2.9 Display the FE-SEM micrographs of mordenite synthesized from gel of different Si/Al ratios. It was noticed that the crystal size increase with increased Si/Al ratio. The morphologies of the products vary with the Si/Al ratio. At the lowest Si/Al of 15, formation of spherically aggregated crystals in addition to the prisms was observed. The small spheres have been first reported by Mao *et. al.* [107] as assembly of small stripe-like crystals and contributed to the broadening of the peaks in the differactograms. By increasing the gel Si/Al ratio from 25 to 30 the morphology is changing from flat prism to rod-like crystals. At Si/Al molar ratio of 30 a rod-like morphology was 100 %. However, the Analcime peaks were sharp and almost 30 %. In conclusion it can inferred that the crystal size and shape increase as the Si/Al ratio is increased, also the uniformity and morphology of the crystals is improved as the Si/Al is increased

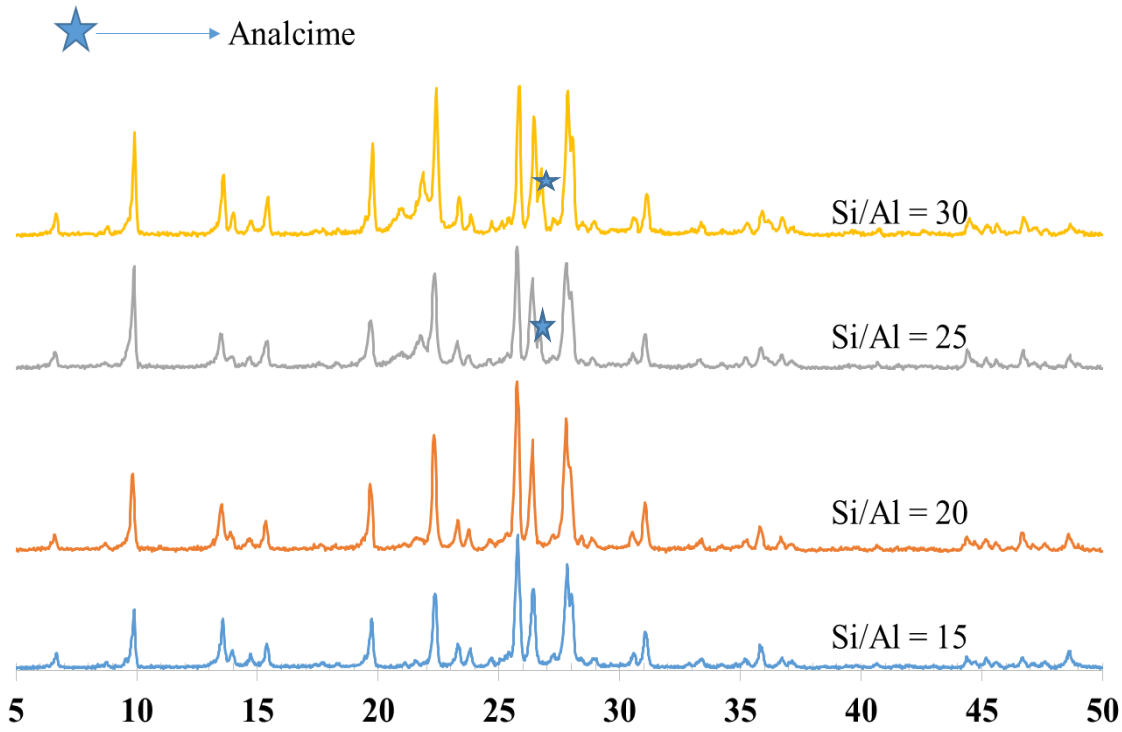

Fig. 2. 8 XRD patterns of mordenite zeolites with different Si/Al ratios at fixed Na/Si of 0.52 synthesized at 180 ^{o}C for 48 h

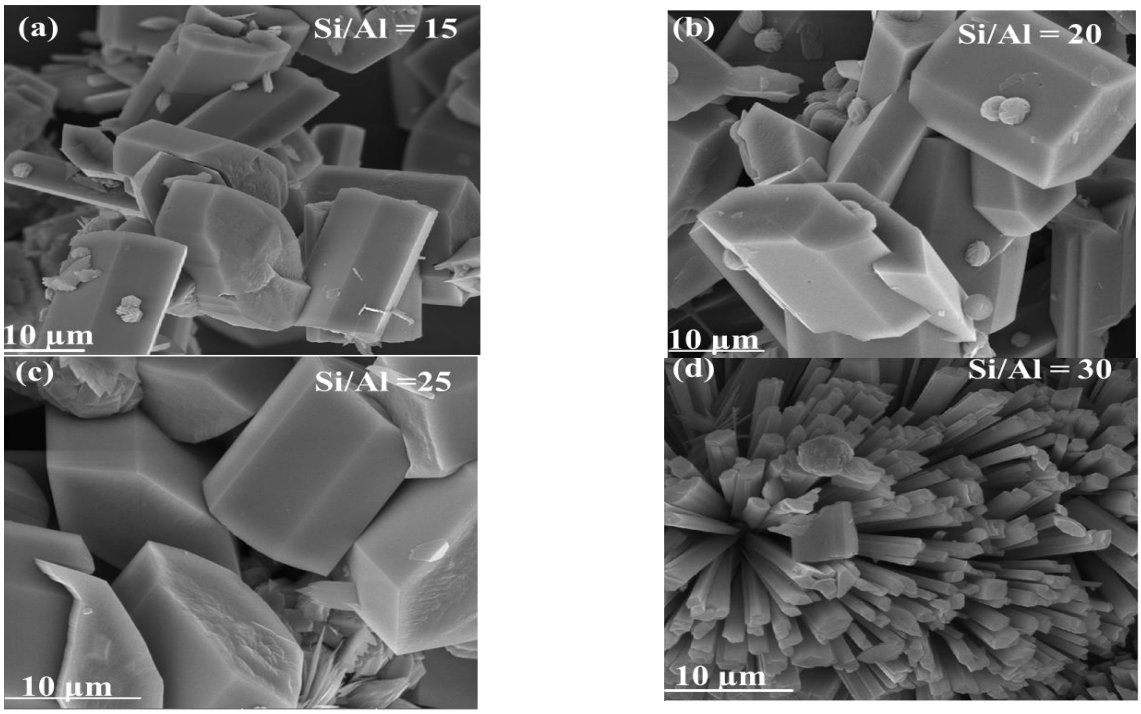

Fig. 2. 9 FE-SEM micrographs of mordenite zeolites with different Si/Al ratios at fixed Na/Si of 0.52 synthesized at 180 ^{o}C for 48 h (a) 15, (b) 20, (c) 25 and (d) 30

2.3.4 Effect of Crystallization temperature

To study the effect of crystallization temperature mordenite synthesized with colloidal silica at Si/Al 15 was hydrothermally treated at 150 ^{o}C, 160 ^{o}C and 170 ^{o}C. Sample synthesized at 150 ^{o}C was amorphous. While sample treated at 160 ^{o}C and 170 ^{o}C displayed a typical mordenite differactograms as shown in Fig. 2.10. The sample heated at 160 ^{o}C exhibit good crystallinity and smaller size as can be justified from the diffraction peaks which were less broadened, less intense and sharped. Increasing the temperature leads to larger crystals and high crystallinity [26, 108]. Although its known that zeolites crystal growth increase with temperature in an active crystallization mode, but an anisotropic effect is observed in most cases [109]. From the SEM images in Fig. 2.11 the sample synthesized at 160 showed a short prism-like structure in contrast to that prepared at 170 ^{o}C that displayed irregular crystals structure and size.

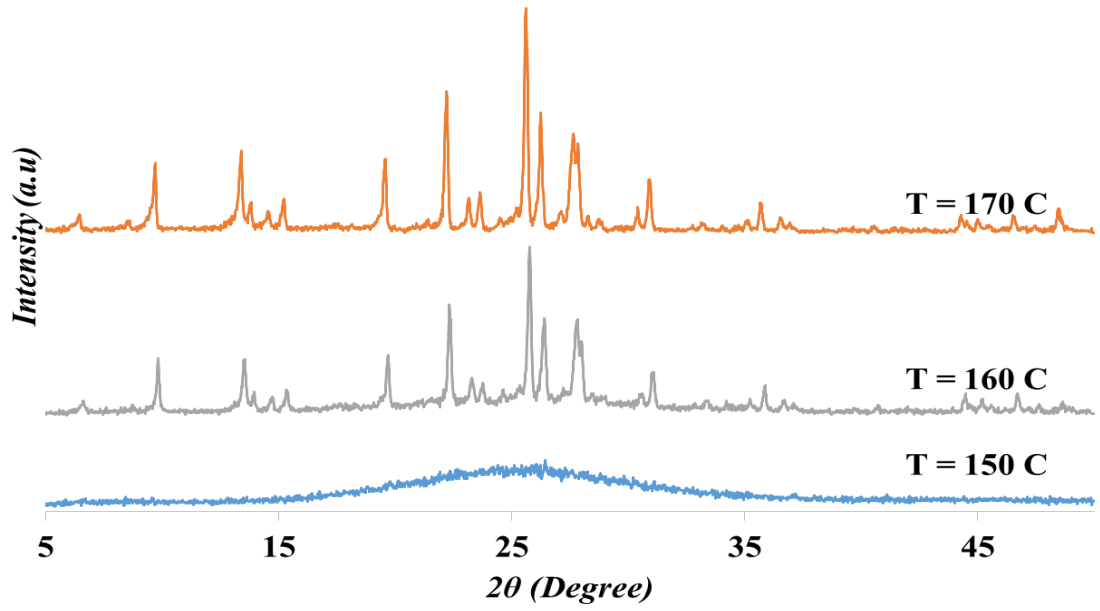

Fig. 2. 10 XRD patterns of mordenite using colloidal silica synthesized at 180 **o**C for 48 h at different temperatures using colloidal silica

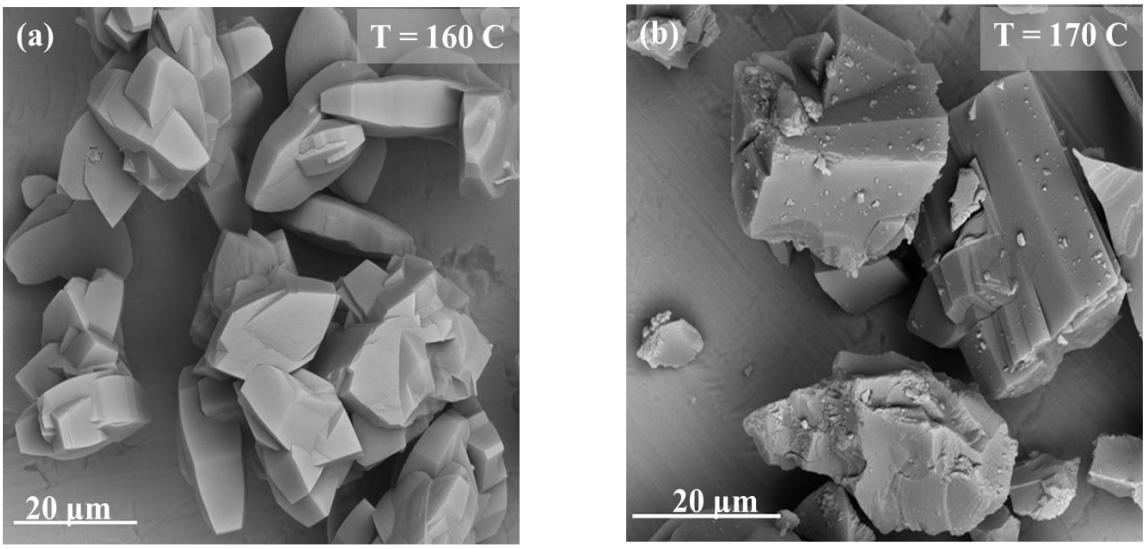

Fig. 2. 11 FE-SEM micrographs of MOR zeolites of 15 Si/Al molar ratio and 0.52Na/Si molar ratio synthesized at different temperatures (a) 160 ^{o}C, (b) 170 ^{o}C

2.3.5 Effect of aging time

To investigate the effect of aging time 1h, 12 h and 24 h ageing was performed using colloidal silica with a gel of 15 Si/Al molar ratios. Fig. 2.12 showed the differactograms, both ageing produce pure mordenite with a typical powdered pattern as obtained by Aly *et. al.* [43] who also used 20 h aging for mordenite synthesis without organic template. The morphology of the products were studied by FE-SEM shown in Fig. 2.13 It was found that mordenite aged at 24 h exhibit a 100% short small platy prism structure. While ageing performed in 12 h produce an unusual white jointed particles crystal that could not be actually distinguished. Comparing sample obtained from 24 h aging with the former experiment conducted with 1 h ageing the morphology was a mixture of sphere like crystals and prism-like crystal. As reported by Simoncic Petra [110] allowing more time lead to complete dissolution of the silica and formation of larger crystals, while giving less time lead incomplete nucleation or crystal growth.

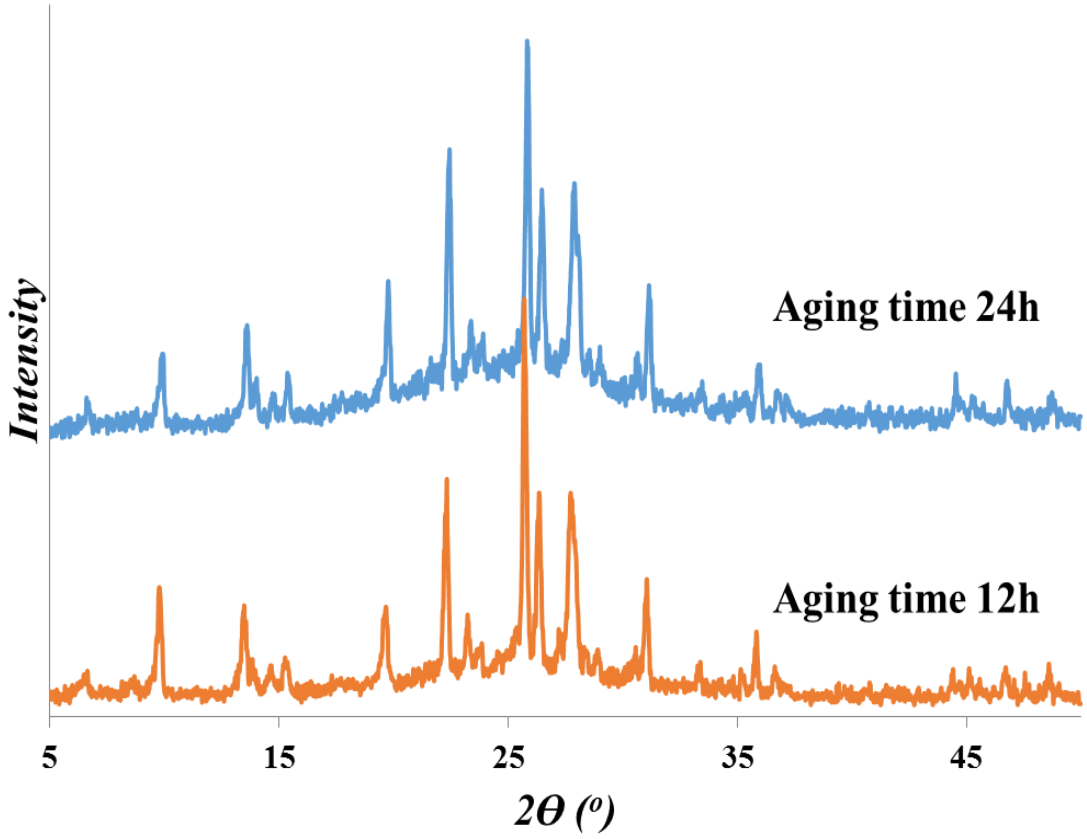

Fig. 2. 12 XRD of MOR synthesized at 180 ^{o}C using colloidal silica at different aging time in 48 h

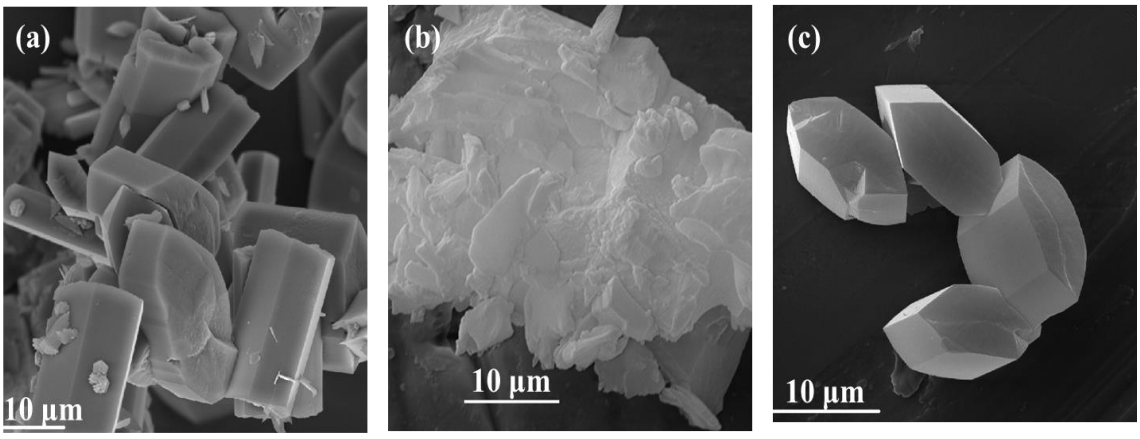

Fig. 2. 13 FE-SEM micrographs of MOR zeolites of 15 Si/Al molar ratio and 0.52Na/Si molar ratio aged at different times (a)1h (b) 12 h and (c) 24 h

2.4 Conclusion

A novel Organic template-free and seeded-free synthesis of mordenite zeolite was successful. The influence or the control effect of the alkalinity ratio was evident in aluminosilicates synthesis. Mordenite zeolite of Si/Al ratio 15, 20, 25 and 50 were successfully obtained by playing with the alkali concentration, which was the major controlling factor in the crystallization of pure mordenite phase. It was observed that higher Si/Al ratio requires higher Na/Si ratio. Crystallization of mordenite with higher Si/Al at the same Na/Si ratio produced Analcime.

Chapter Three

Synthesis, Characterization and Application of Phosphate-Modified Mordenite Zeolite: Enhanced Cyclic Voltammetric Response in Ferro/Ferric Cyanide System and Electrocatalytic Detection of Thiocyanate

Abstract

Mordenite zeolite with average size of 17 μm was synthesized hydrothermally from the gel composition of 9.4 Na_2O: Al_2O_3:40 SiO_2:1040 H_2O in the absence of organic template and without seed addition. XRD, EDS and FE-SEM confirmed the crystallinity, elemental composition and morphology of MOR crystals, respectively. The pure mordenite was modified by impregnation with 5 wt.% H_3PO_4. The effect of the phosphorous impregnation was studied using solid state NMR. The electrochemical behavior of phosphate mordenite was investigated in carbon paste via cyclic voltammetry. The highest current density (5.6 x 10^5 μA/cm^2) was obtained from the composite electrode containing 5% of the phosphate mordenite. The electrode showed a linear response at the scan rate range of 5 to 400 mV s^{-1} towards the ferrocyanide ($K_4Fe(CN)_6$). The electroactive surface area of 22.58 mm^2 and total electrode surface coverage of 2.24 x 10^{-3} mol cm^{-2} were obtained. The effect of the framework silico-aluminophosphate interface on the mordenite surface was confirmed by voltammetric oxidation of thiocyanate. The behavior of the phosphate-mordenite carbon paste electrode (P-MCPE) was greatly affected by pH. Its dependence on the concentration of the thiocyanate showed a linear range with R^2 of 0.9967 using square wave voltammetry.

3.1 Background

Zeolites, particularly aluminosilicates, are well known for their industrial application especially in oil refining, petrochemicals and fine chemicals production owing to their large surface area, pore volume, acidity, uniform microporous channel and excellent hydrothermal and chemical stabilities [19].

Mordenite is a high-silica, hydrophobic and 1-dimensional zeolite with the typical composition $Na_8\ Al_8\ Si_{40}\ O_{96}\ (H_2O)_{24}$ as first discovered and reported by Meier [111]. The siliceous (high silica content) material, is normally an assembly of channels which were enclosed by 8 and 12-membered rings of SiO_4 and AlO_4 with a unit cell parameters a = 18.1 Å, b = 20.5 Å & c = 7.5 Å, while the void volume is 0.14 ccg^{-1}(cubic centimeter per gram) and framework density of 17.2 T atoms / 1000 $Å^3$ (where T is tetrahedral Si or Al) [41, 112]. Mordenite has orthorhombic symmetry, and belongs to the *cmcm* space group. The framework in the (001) direction contains elliptical micropore (6.7 x 7.0 Å) channels parallel to *c-axis* and (2.6 x 5.7 Å) channels parallel to the *b-axis* leading to the uni-dimensional nature as a result of difficulty to sorption of most molecules due to the tightness of the later channels of mordenite [41, 113].

Mordenite has been recently reported to be a suitable substrate for hosting semiconductors, chemical sensors and non-linear optical materials owing to its shape selectivity, acidity and thermal stability [113]. Ion-exchange in the zeolite is accompanied by changes in pore size, ion-conductivity, adsorption, catalytic activity and selectivity [113]. Thus, metal ion incorporation, pore size engineering and partial dealumination are most common chemical modification procedures employed to adjust the characteristics properties of mordenite [113]. Partial and controlled dealumination of

zeolites is mostly achieved by mild acid treatment, which resulted in removing aluminium extra-framework and narrowing the pore diameter [114]. As an innovative modification method, changing zeolites diffusivity with phosphorous has attracted great concern [52]. It was found that even at low phosphorous loading, shape selectivity of zeolites is improved due to contraction of the pore diameter [114]. The introduction of phosphorus into zeolites has been proven to facilitate the adjustment of acid sites and more effective control of hydrogen transfer reaction [83]. Most of the effort invested on phosphorus modification has been invested to increased para-selectivity during the isomerization of xylene or disproportionation of toluene [114]. In recent years, phosphorus modification of zeolites has been used to enhance selectivity to lighter olefins [68, 69, 72, 80, 83, 115-117].

Owing to the negative charge in the zeolites framework, potential selectivity should be observred based on the charge on a molecule. Xu *et al* reported that the absorbed molecules-zeolite interaction, hydrophobicity or hydrophilicity, and ion-exchanged capacity of zeolite can all be altered by changing the framework Si/Al molar ratio [6]. In chemical and gas sensors applications, compound with desirable sensing property is assembled into the zeolite cages or channels to enhance and modify the intrinsic zeolite property [6]. These intrinsic properties may be coupled with an electrochemical reaction of interest to generate a new responsive electrochemical surface that can be categorized in the so-called chemically modified electrodes (zeolites modified electrodes). The composition, response time, ionic strength, thermal stability and usable pH range of the material surface can be electrochemically investigated [85]. The first use of zeolite as a membrane electrode in potentiometric technique led to the eventual

advances in zeolite modified electrodes (ZMEs) [118]. Zeolite modified electrodes received great interest in the late 1980s due to their high stability low cost and potential industrial applications [85].

Manea *et al* successfully established the composition of zeolite doped with silver in composite electrode using cyclic voltammetry (CV). The electrode showed a linear dependence of current against both analytes during simultaneous determination of nitrites and nitrates in aqueous solution using Multiple-pulse Amperometry [95]. It was investigated and reported elsewhere that the peak current depends on electroactive surface area from cyclic voltammetry data [119]. The electrochemical mechanism in mordenite zeolite catalytic process in mordenite-poly (ethylene oxide) oligomer electrode was investigated using cyclic voltammetry, the mordenite framework Al-O bond was found to be prone to destruction at high positive potential, owing to the negative charge of the framework aluminium [120]. Table 3.1 summarizes some ZMEs and the techniques used in their characterization and application.

Table 3. 1 Review of some zeolite modified electrodes

SN	Zeolite Modified Electrodes (ZMEs)	Characterization technique	Application	Comments	Ref.
1	**Surfactant modified zeolite**	FT-IR, Potentiometry	Potentiometric determination of nitrates in water	Linear response to 1 x 10^{-6} to 1 x 10^{-3} M nitrates species with a detection limit of 1 x 10^{-6} M and slope of 59.4±0.7mV per decade	[121]
2	**SiO_2-Al_2O_3 mixed oxide carbon paste**	Cyclic voltammetry	Anodic stripping voltammetric determination of Lead (II)	Three times Decreased detection limit 1.07 x 10^{-9} mol L^{-1}. Selectivity linear increase in peak current	[122]
3	**Mordenite MOR-CPE**	Cyclic Voltammetry	Determination of Atenolol	Enhanced sensitivity with low cost of preparation	[123]
4	**Mordenite in poly (ethylene oxide oligomer)**	Cyclic Voltammetry	Probing electrochemical mechanism in catalytic process	Resistance to high potential and the risk of losing Al-O bond in the tetrahedral Al framework	[120]
5	**Nickel dispersed on natural phosphate fixed on copper.**	Cyclic voltammetry	Electrocatalytic oxidation of methanol	Better electrocatalytic activity than Ni. Linear increase with concentration	[124]

Thiocyanate commonly exists as potassium thiocyanate or sodium thiocyanate. It is a conjugate base to thiocyanic acid. The anion is oxidized to sulfate and cyanide during metabolism in acidic medium by peroxidase [125]. As a result, discrimination of smokers can be made by thiocyanate measurement for its high production due to tobacco smoke degradation [126]. Higher concentration of thiocyanate might leads to coma condition as it affect the process of dialysis of protein [127]. Moreover, thiocyanate as part of industrial effluents might present significant toxicity to aquatic lives and hence its detection is a highly important research pursuit. Although spectroscopic and chromatographic approaches have been employed in this experimentation, the ease of preparation, stability, selectivity and sensitivity of the so-called chemically modified electrode might be advantageous. The electrochemical technique employed for thiocyanate detection depends mainly on the construction of potentiometric sensors. The used of superconducting material based on copper oxide for the oxidation of thiocyanate was reported by Badri *et al* [127]. However, cyclic voltammetry was used which less sensitive technique compared to the square wave voltammetry.

The aim of this work was to investigate the behavior of a novel phosphate mordenite carbon paste electrode (P-MCPE). The synthesized mordenite was converted into the proton form by ion-exchange using ammonium nitrate solution, afterward post synthesis phosphorous impregnation was carried out. A novel phosphate mordenite carbon paste electrode (P-MCPE) was constructed from the phosphate mordenite. Cyclic voltammetry was used to further investigate the electrode properties. The best new composite electrode was employed in the electrochemical detection of potassium thiocyanate via square wave voltammetry.

3.2 Experimental

3.2.1 Materials

PTFE-line autoclave was used in the zeolite synthesis. Silica gel (Sigma-Aldrich grade 7734 pore size 60Å, 70-230 mesh) was used as silica source, Sodium aluminate 13404 Sigma- Aldrich was used as aluminium source. Sodium hydroxide pellets PRS-CODEX 98% was used to control pH of the gel. Orthophosphoric acid (85% Sigma-Aldrich) was used for the post synthesis impregnation. For the electrochemical characterization, Potassium ferrocyanide $K_4Fe(CN)_6$ was as the analyte in characterizing the electrode and KCl was used as supporting electrolyte, anhydrous sodium phosphate monobasic (Sigma-Aldrich), anhydrous sodium phosphate dibasic (Sigma-Aldrich) and phosphoric acid were used to make buffer of different pH (3 to 9) which were used to study the effect of pH. Potassium thiocyanate was used to study the efficacy of the electrode in the electrocatalytic oxidation of thiocyanate. Low viscosity paraffin oil was used as a binder in the preparation of the carbon paste electrode. Parent proton mordenite H-MOR and phosphate mordenite zeolite 5P-MOR were synthesized. Mortar and pestle was used for mixing carbon graphite and phosphate zeolite. Ag/AgCl electrode was used as the reference electrode and platinum as the counter electrode in the electrochemical measurements. All experiments were conducted at room temperature.

3.2.2 Synthesis and phosphorus modification of mordenite zeolite

Mordenite synthesis was started according to the gel dispersion procedure reported by Hincapie *et al.* [26]. A gel with composition 9.4 Na_2O: Al_2O_3:40 SiO_2:1040 H_2O was treated hydrothermally in a PTFE-lined autoclaves at 180 ^oC for 48 h in the absence of both seed and organic template. The Product was washed several times until

the pH became less than or equal to 7. The product was then calcined in air circulating oven at 550 ^{o}C. The proton form (acidic mordenite) was obtained by converting it to ammonium form by ion-exchanged using ammonium nitrate, which was calcined to get the pure proton form.

Phosphorus modification was done based on the post synthesis impregnation procedure reported by Dyballa *et al* [66]. A predetermined amount of mordenite zeolites was suspended in 1.5 ml of 5wt. % H_3PO_4 and the slurry was allowed to evaporate by heating at 40 ^{o}C after which the product was calcined.

3.2.3 Characterization of the phosphate mordenite

The morphology of the mordenite and phosphates mordenite zeolite was investigated by field-emission scanning electron microscopy (FE-SEM) using LYRA 3 Dual Beam (Tescan). The crystallinity was confirmed by using a diffractometer (Miniflex, Rigaku) equipped with Cu Kα radiation (1.5405 Å) at 2θ 5° to 50° using a scan rate of 0.03° per step and a counting time of 3 s for each step. ^{27}Al NMR of both parent and modified samples and ^{31}P NMR of the phosphorus mordenite were conducted to investigate the effect of phosphorus impregnation using Bruker Lamda-200 Multi Nuclear Magnetic Resonance (NMR) Spectrometer with Solid-state facility.

3.3 Electrochemical characterization

3.3.1 Preparation of zeolite modified electrode

Phosphate mordenite carbon paste electrode was prepared as guided by the work of Ardakani *et al* [89]. A mixture of 100 mg containing constant amount of 30% low viscosity paraffin oil as binder and different ratios of the graphite to phosphate mordenite

zeolite was mixed manually in a mortar. The Paraffin oil was added by means of a dropper and mixed for 20 min until a uniformly wetted paste was obtained. The paste was then packed into the end of 40 mm Teflon tube at the end of which a 0.1 mm hole electrode contact surface was made. Pushing an excess of the paste out of the tube and polishing it on a weighing paper obtained a new surface. Carbon paste electrode was prepared in the same way without adding zeolites to the mixture. The amount of the 5P-MOR was varied from 5% to 20% with a constant amount of paraffin oil at 30% while graphite was varied with the zeolite amount. The electrodes were named 0-5P-MCPE, 5-5P-MCPE, 10-5P-MCPE, 15-5P-MCPE and 20-5P-MCPE according to whether the carbon paste electrode contain 5%, 10%, 15% and 20% of the 5P-MOR, respectively.

3.3.2 Voltammetric measurement using cyclic voltammetry

The electroactive surface area, the current dependence in ferrocyanide and working potential of the phosphate-mordenite carbon paste electrode were obtained by cyclic voltammetry using a CHI 760E Potentiostat equipped with a three-electrode cell. The phosphate mordenite carbon paste electrode (PMCPE), a platinum wire as auxiliary electrode, and a KCl saturated Ag/AgCl reference electrode. The Ag/AgCl reference is kept in 1 M KCl solution when not in use. The electrochemical behavior of 5P-MCPE was examined in potassium ferrocyanide $K_4Fe(CN)_6$. The electrode was then used for the electrocatalytic oxidation of thiocyanate ion in phosphate buffer, the effect of different pH of the phosphate buffer of 0.1 M concentrations was studied and a calibration curve was established.

3.4. Results and Discussion

3.4.1 Characterization of mordenite zeolite and phosphate mordenite zeolite

The XRD powder pattern of the synthesized mordenite (H-MOR) and phosphorous modified mordenite (P-MOR) zeolites is shown in the Fig. 3.1 The sample peaks where typical of a mordenite phase and the morphology was compared to that published elsewhere [107] and confirmed that a pure mordenite phase was obtained. It is also noted that the crystallinity of the mordenite was highly retained after phosphorus modification. Flat prism-like crystals were the dominant phase of the morphology as shown in Fig. 3.2. The phosphorus modification was confirmed by energy dispersion X-ray spectroscopy (EDS) that gave an average phosphorus surface amount of 2.20 wt.% of total zeolite amount of 1.0 g.

The effect of phosphoric acid treatment was further investigated by solid state ^{27}Al NMR and ^{31}P NMR. Fig. 3.3 shows the ^{27} Al NMR of the parent mordenite and the phosphorus modified mordenite zeolite. The signal at around 55 ppm is attributed to the tetrahedral Al-framework while the small and broader signal occurring around 0 ppm is attributed to the octahedral framework aluminium (OFAl) as reported in the literature elsewhere [128]. From the two spectra, it is observed that the gross amount of Al has decreased after phosphorus modification, with a sharp decrease of octahedral Al signal. This indicates the formation of new local silico-aluminophosphate (SAPO) surface as reported in [57, 65]. To confirm the addition of phosphorus ^{31}P NMR was conducted on the modified mordenite sample and the spectrum is shown in Fig. 3.4 A clear sharp peak at around -30 ppm evolved, confirming strong chemical interaction between the phosphate from the phosphoric acid and the zeolite bronsted acidity which is in

accordance with the hydrogen bonding formation as proposed by Kaeding in his model [54]

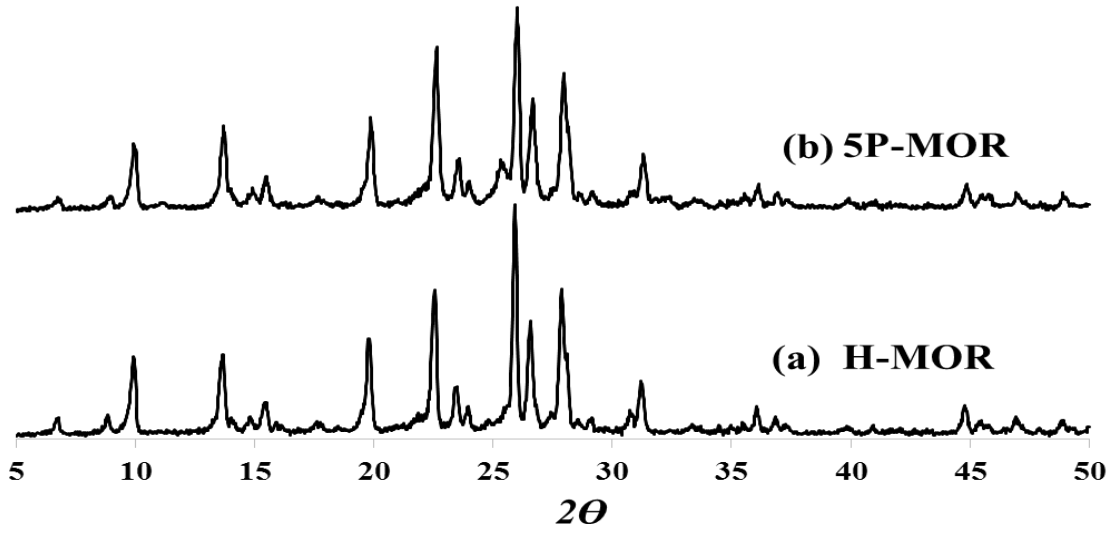

Fig. 3. 1 XRD patterns of mordenite zeolites (a) Parent HMOR and (b) 5P-MOR with 0.52 Na/Si molar ratio and 20 Si/Al molar ratio synthesized at 180 ^{o}C for 48 h using silica gel

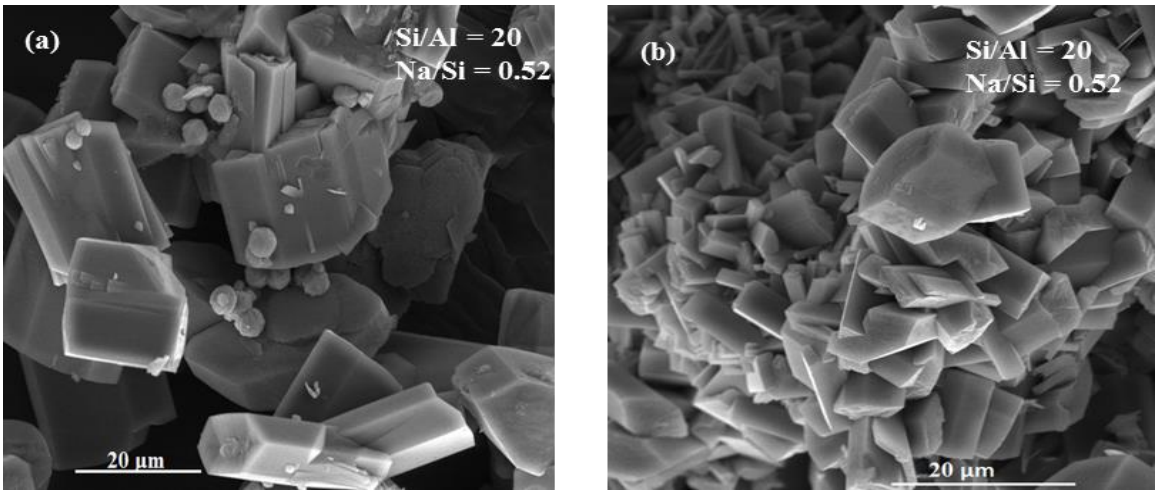

Fig. 3. 2 FE-SEM micrographs of mordenite zeolites of 20 Si/Al molar ratio and 0.52 Na/Si molar ratio crystallize at 180 ^{o}C (a) H-MOR, (b) 5P-MOR

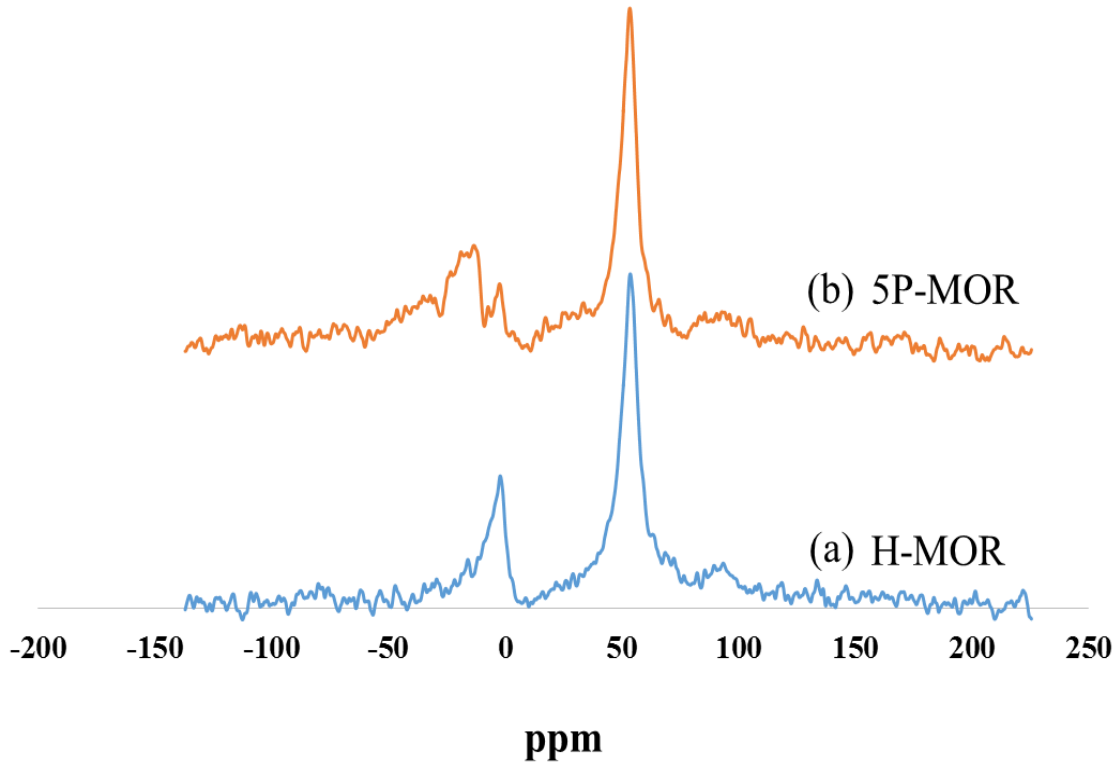

Fig. 3. 3 Aluminium ^{27}Al NMR of (a) H-MOR, (b) 27Al NMR of 5P-MOR

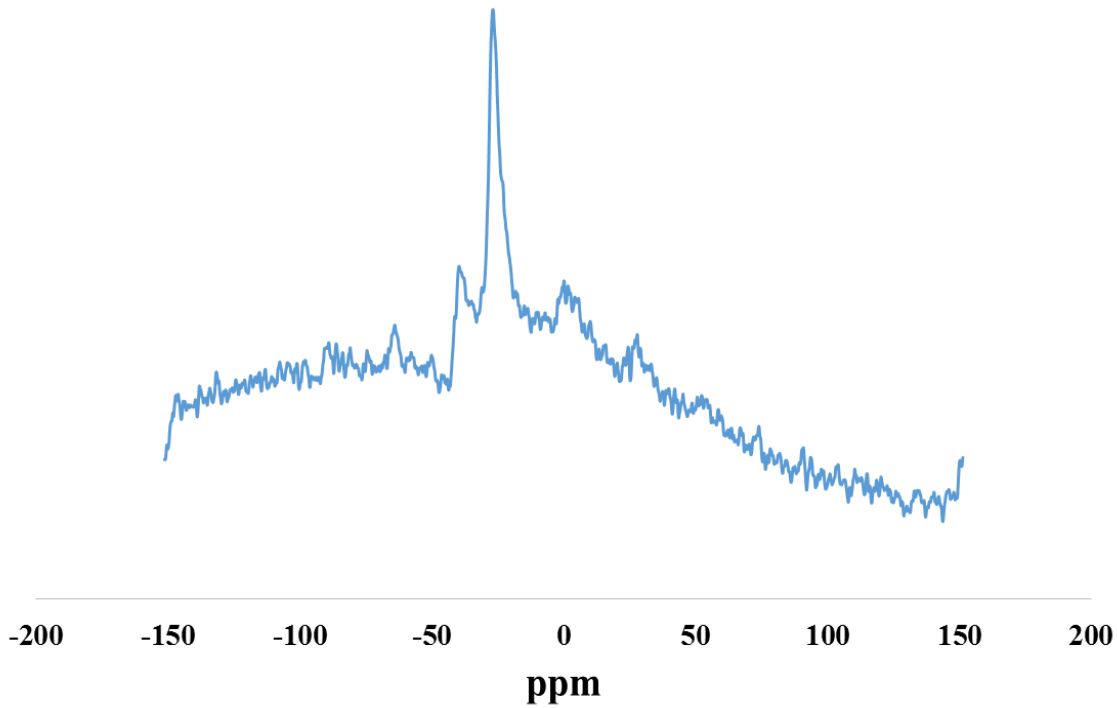

Fig. 3. 4 Phosphorus ^{31}P NMR of 5P-MOR with 0.52 Na/Si molar ratio and 20 Si/Al molar ratio

3.5 Electrochemical Evaluation

3.5.1 Effect of percentage of mordenite in carbon paste electrode

The cyclic voltammograms of the 5P-MCPEs were shown in Fig. 3.5A. The percentage of the 5P-MOR was varied from 0% to 20% 5P-MCPE composite at constant paraffin oil content of 30% to give five different carbon paste electrodes designated as 0-5P-MCPE, 5-5P-MCPE, 10-5P-MCPE, 15-5P-MCPE and 20-5P-MCPE, in all cases the initial number indicates the percent of the 5P-MOR. The CV of the 5% 5P-MCPE was recorded between -0.4 V to 0.8 V at 100 mV s^{-1}, a current approximately 5.6 x 10^5 μA/cm^2 was obtained. The bare carbon paste (containing 0% of 5P-MOR) gave 4.8 x 10^5 μA/cm^2, following the 5-5P-MCPE. Thus, as reported the zeolite in the composite

electrodes enhance ion accessibility of the ferrocyanide species to its pores and channels which at lowest concentration, increased the accumulation of the analyte at electrode surface [87]. It can be seen that, the highest (threshold) electrode surface coverage was attained which is proportional to the peak current. In the higher concentrations, this threshold electrode surface coverage was exceeded. It was also reported elsewhere [23] that the surface saturation occur when the population of redox species at the electrode surface surpass the total area of the electrode and hence an overlapping and steric effect result in lower ion accessibility. This effect leads to a decreased electroactive area and peak current at high coverage owing to higher amount of the phosphate mordenite. We, therefore, propose that the current limitation due to the aluminophosphate surface of the mordenite is obeying diffusional model.

Fig. 3.5B shows the peak current trend in graphical manner. The plot of the peak current versus the percentage modifier showed a non-linear increase of the peak current with maxima at 5% 5P-M0R.

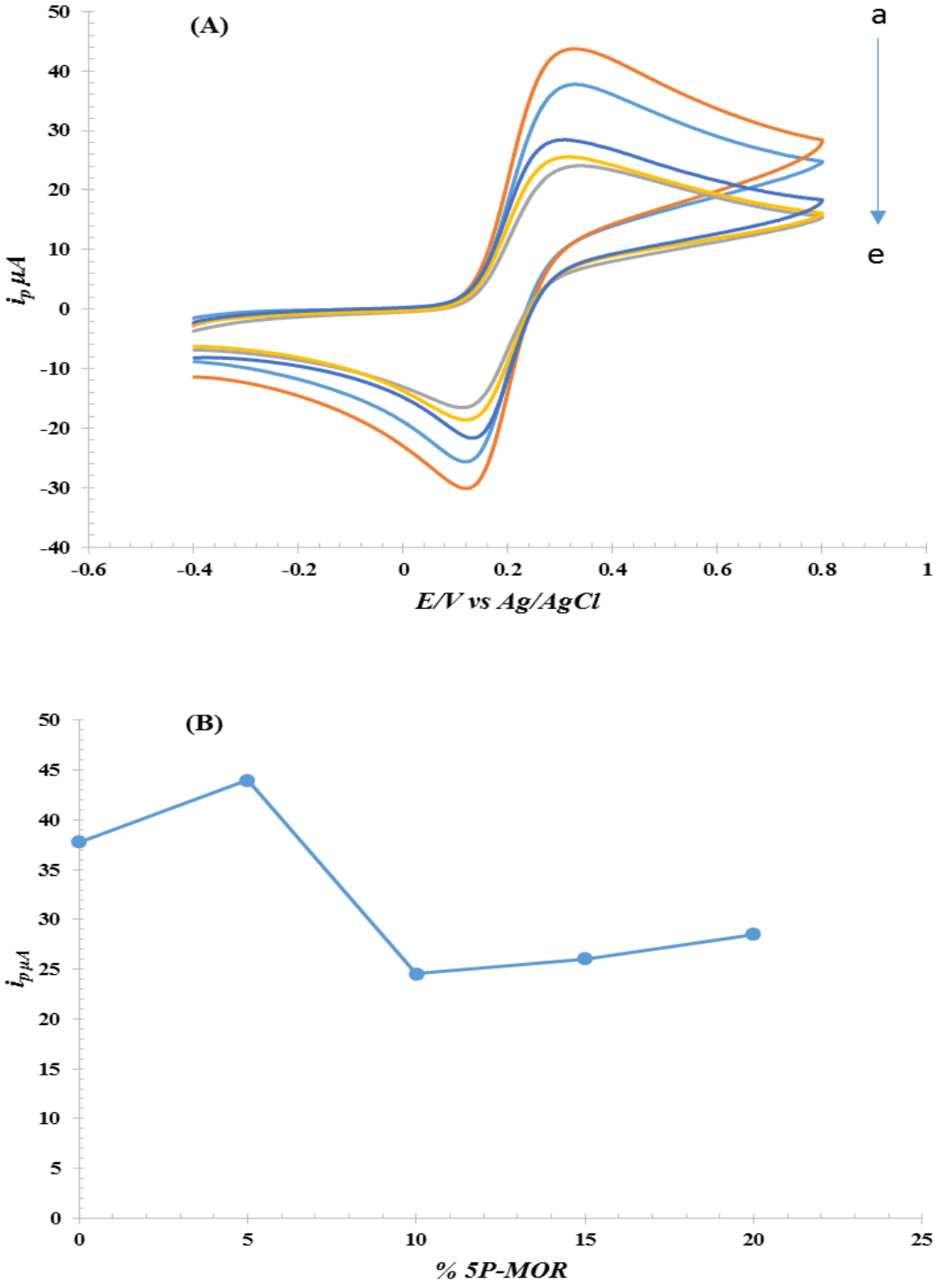

Fig. 3. 5 (A) Comparison of CVs (B) Plot of peak current vs % modifier of carbon paste electrode containing (a) 5%5P-MOR (5-5P-MCPE), (b) 0% 5P-MOR (0-5P-MCPE) (c) 20% 5P-MOR (20-5P-MCPE), (d) 15% 5P-MOR (15-5P-MCPE) (e) 10% 5P-MOR (10-5P-MCPE) in 10 mM $K_4Fe(CN)_6$

3.5.2 Effect of scan rate

The 5% 5P-MCPE **(**5-5P-MCPE**)** behaves linearly with respect to the ferro/ferric cyanide system from 5 mV s^{-1} to 400 mV s^{-1} with R^2 of 0.9921, suggesting a pure diffusion behavior as reported elsewhere [129]. Fig. 3.6 shows the voltammograms at various scan rates. The relationship between peak current and square root of the scan rate obtained from the *Randles-Sevcik* Equation (Equation ***3.1***) is shown in Fig. 3.6. The electroactive surface area (A) of the electrode was estimated.

$$i_p = 2.69 \times 10^5 n^{3/2} v^{1/2} D^{1/2} AC \qquad \textit{Eqn. 3. 1}$$

Where i_p is the anodic peak current, *n* the number electron transfer, *A* the electrode surface area, *D* the diffusion coefficient, ***v*** the scan rate and *C* the concentration of the $K_4Fe(CN)_6$. The electroactive surface area was found to be $A=22.58\ mm^2$. Compared with the bare carbon paste electrode, the estimated electroactive surface area was *12.71* mm^2. This clearly justified the extended surface area of the 5P-MCPE over the bare carbon paste electrode.

Assuming that the surface of the electrode is homogeneous and molecules of the analyte are spherical, then the theoretical number of redox species can be calculated by dividing the total electrode area by the diameter of the molecules [23]. Thus, the concentration of the redox species are then directly proportional to the surface area, hence based on Equation 3.2 below, the immobilized redox species at the surface of the modified electrode were considered to control the oxidation-reduction current as they are responsible for the formation of monolayer Langmuir isotherm [23, 94]. It has been shown that the analyte concentration at the electrode is not the same as in the bulk solution. The relationship between peak current of the ferrocyanide and scan rate is

shown in Fig. 3.7 From these plots the surface coverage of the redox species on the electrode (Γ^*) can be calculated by employing the Equation 3.2, also the charge transfer corresponding to the surface coverage can be obtained from Equation 3.3

$$I_p = \frac{n^2 F^2 A\Gamma^* v}{4RT} \qquad \textit{Eqn. 3. 2}$$

$$\Gamma = \frac{Q}{nFA} \qquad \textit{Eqn. 3. 3}$$

Where *A* is the electrode surface area ($7.85 \times 10^{-5}\ cm^2$) calculated from $A = \pi R^2$, *n* is the number of electrons involved in the reaction (1 electron in this case), I_p is the peak current. The total surface coverage (Γ^*) is then calculated as $2.24 \times 10^{-3}\ mol\ cm^{-2}$. According Equation 3, this corresponded to charge transfer of 1.70×10^{-2} C compared to $1.28 \times 10^{-3}\ mol\ cm^{-2}$ leading charge transfer of 9.7×10^{-2} C for the bare carbon paste electrode. Hence, this justifies further the enhancement achieved with the phosphate mordenite with less charging current.

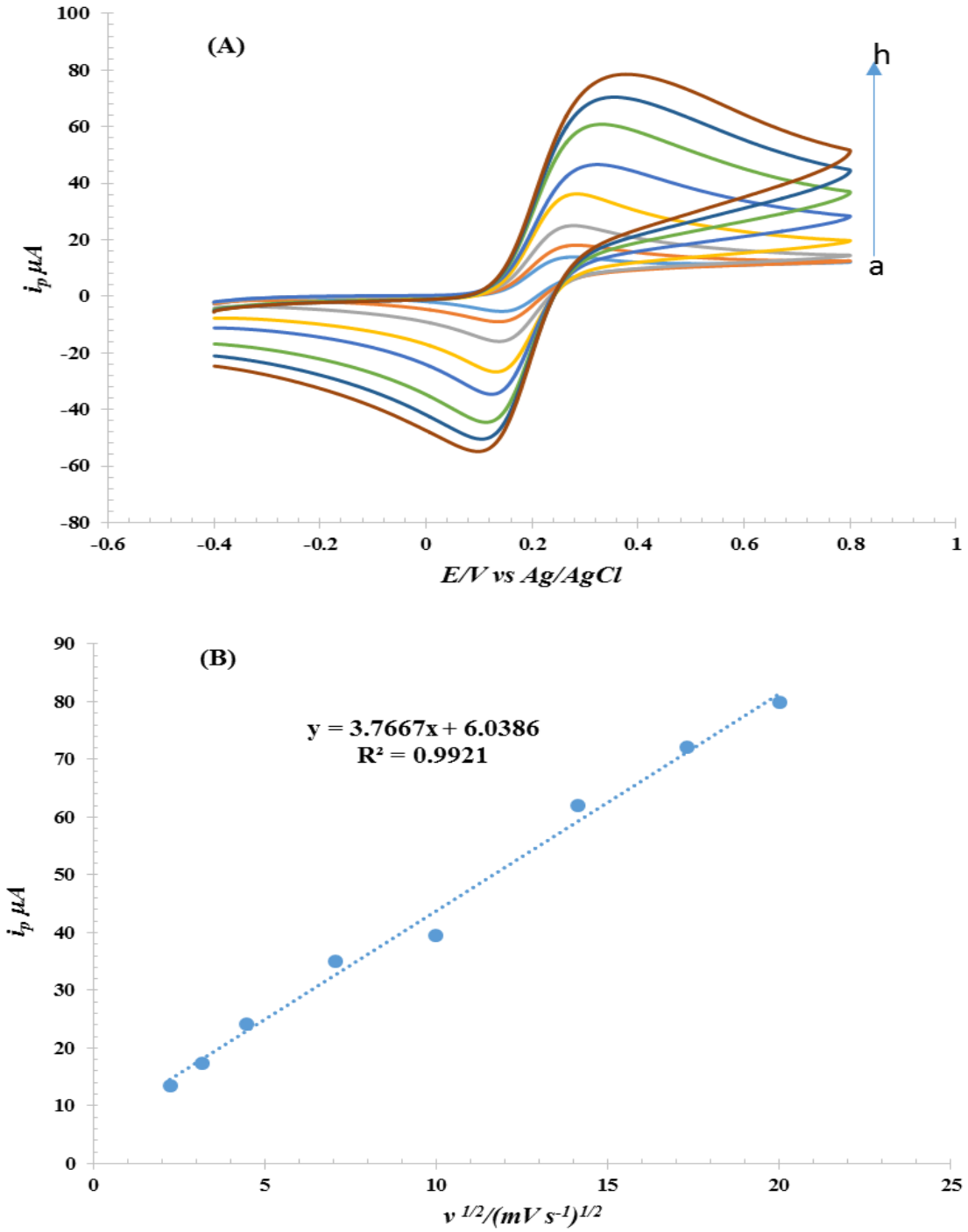

Fig. 3. 6 (A) CV of 5-5P-MCPE at different scan rates a. 5 mV b. 10 mV c. 20 mV d. 50 mV e. 100mV f. 200mV g. 300 mV and h. 400 mVs-1 in 10 mM $K_4Fe(CN)_6$ and 0.1 M KCl (B) Plot of peak current vs scan rate

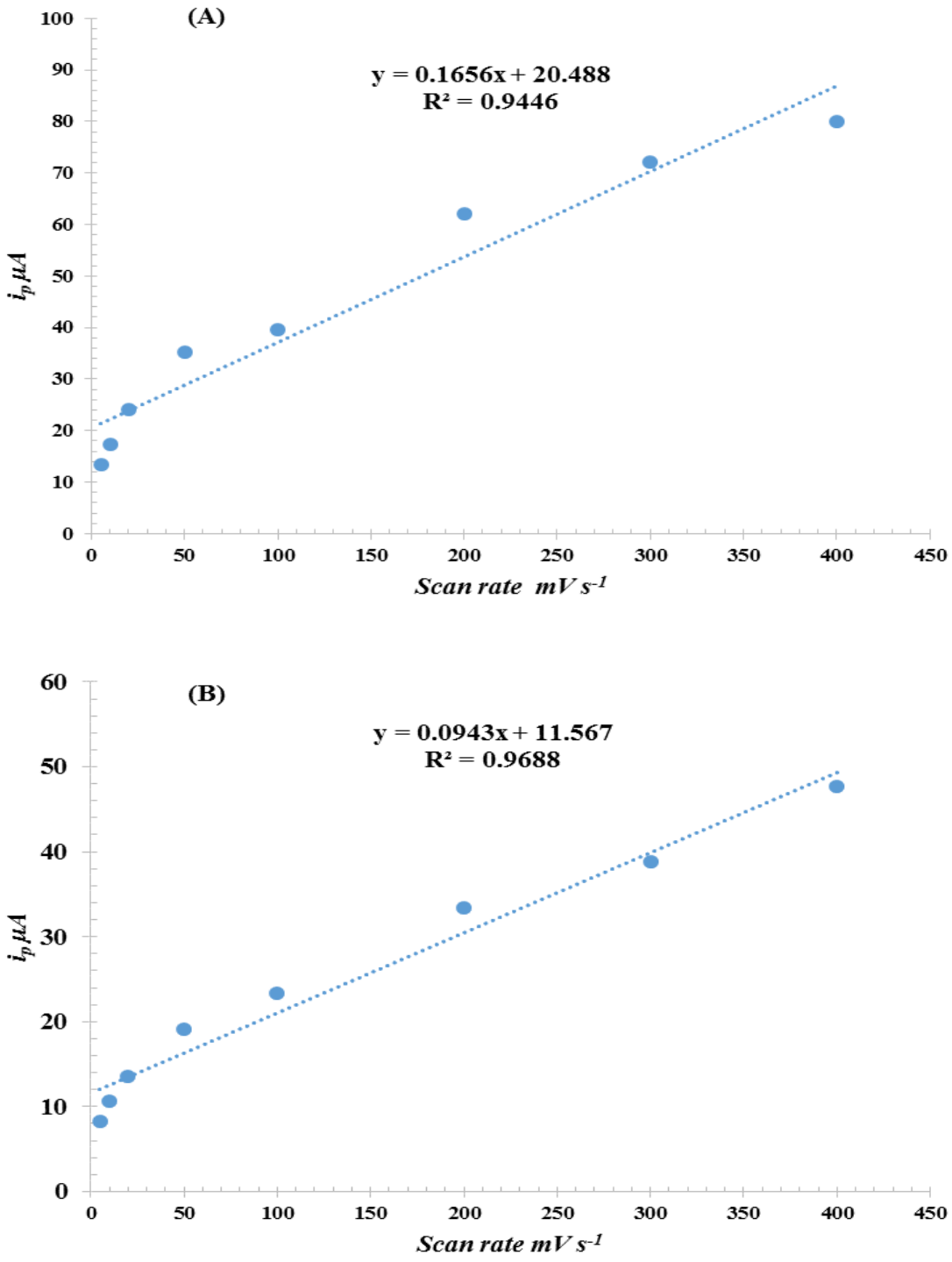

Fig. 3. 7 Plot of Peak current vs scan rate in the presence of 10 mM $K_4Fe(CN)_6$ in 0.1 M KCl on (A) 5-5P-MCPE and (B) bare carbon paste electrode

3.5.3 Oxidation of thiocyanate

Having established that the phosphate in the P-MOR has impact on the activity of the carbon graphite electrode composition, we thought it was crucial to investigate how the P-MOR could impact the electrocatalytic behavior of composite electrode as phosphate zeolites are known for their stability and selectivity in catalytic reactions [65, 130]. For this study, we select thiocyanate SCN^-, as a model analyte. Fig. 3.8A shows the relative square wave voltammograms obtained in 50 μM SCN^- solution at 5-5P-MOR and bare carbon paste electrodes in phosphate buffer saline PSB (pH 7). The buffer was chosen because of its good record in electrochemical applications and the neutral pH was used so that the catalytic effect of the P-MOR will be purely understood. An enhanced current density (5.73×10^4 μA/cm^2 compared to 3.8×10^4 μA/cm^2) of the 5-5P-MCPE was observed. As discussed earlier this resulted from the higher surface coverage provided by the phosphate mordenite [87]. Figure 3.8 B displays square wave voltammograms for the electrocatalytic oxidation of 50 μM thiocyanate.

Based on the above observation we proposed a mechanism in which the SCN^- forms hydrogen bonding with the hydrogen of the phosphate group there by fastening the accumulation and increasing concentration of the SCN^- at the electrode surface. Moreover, electrostatic attraction between the tetrahydroxyphosphonium ion positive charges also brings the thiocyanate to the graphite surface [40].

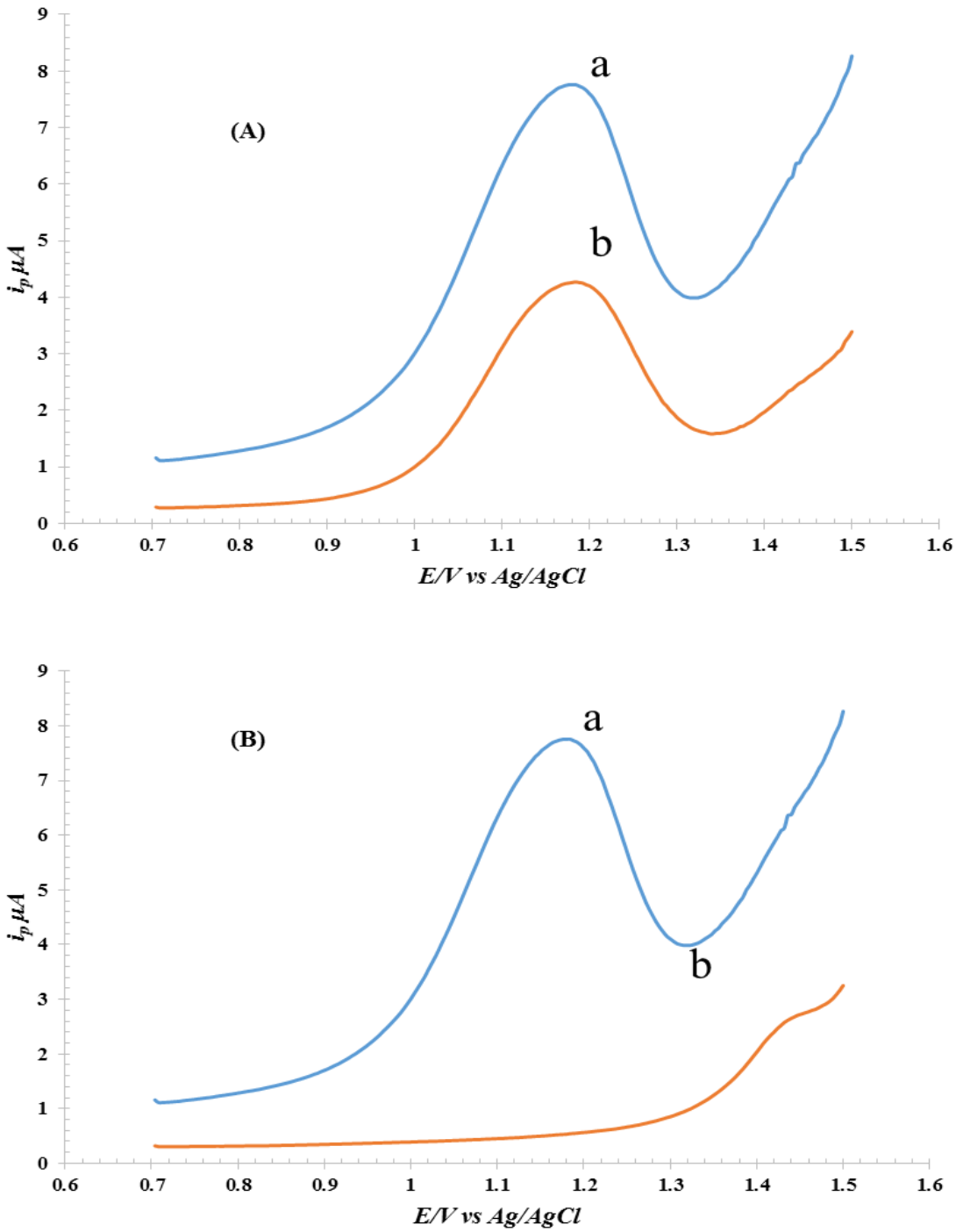

Fig. 3. 8 (A) Comparison of SWV of (a) 5-5P-MCPE and (b) Bare CPE. (B) SWV of 5-5P-MCPE in pH 7 buffer (a) in the presence of 50 µM SCN^- (b) in the absence of SCN^-

3.5.4 Effect of pH

Fig. 3.9 shows the effect of pH, which was studied on 50 μM, SCN^- in 0.1 M phosphate buffer (pH range 3 to 9) prepared from sodium dihydrogen phosphate, disodium hydrogen orthophosphate and phosphoric acid. An irregular increase in the peak current with pH was observed. The highest current was achieved at pH 8 which confirms the catalytic detection of the SCN^- as the pH ensure the reservation of the hydrogen atoms of the phosphate mordenite and this agrees with our proposed mechanism. This behavior could be attributed to the phosphorus content of the modifier, which was reported in [58] to modify the diffusivity of the zeolite material and hence govern the dynamic process at the electrode surface making it purely diffusion control and allowing more molecules to converge at the electrode surface.

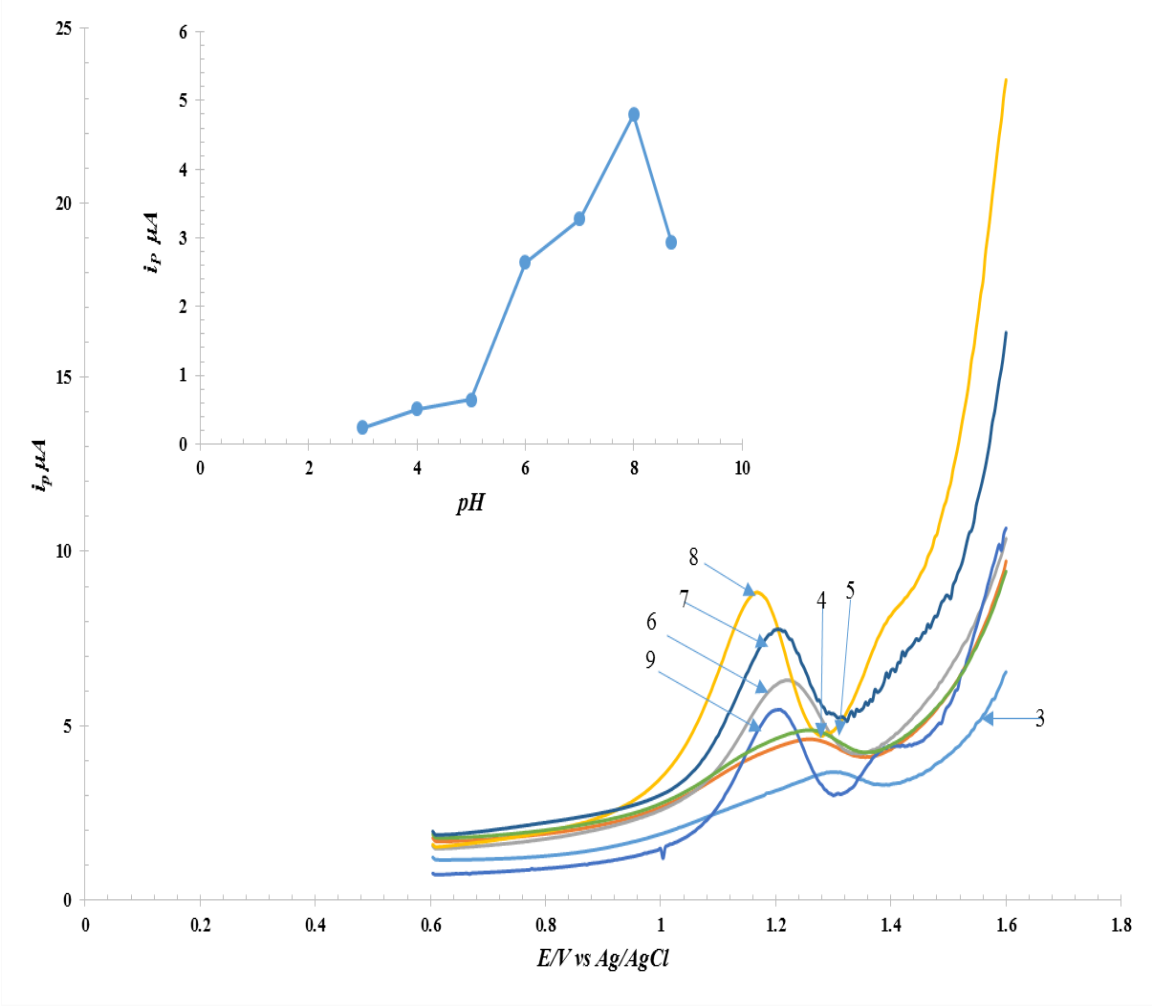

Fig. 3. 9 SWV of 5-5P-MCPE in 50 µM SCN^- in phosphate buffer of different pH. Inset is the relationship of peak current ad pH.

3.5.5 Calibration plots

Fig. 3.10 shows the square wave voltammograms of SCN^- and the calibration plot showing the relationship of peak current with concentration of SCN^- (10 to 150 µM). The peak current showed a linear increase within the concentration range of 1.0 x 10^{-7} mol L^{-1} to 1.50 x 10^{-4} mol L^{-1} of SCN^- (i_p = 0.0773[SCN^-] + 0.1699) R^2 = *0.997*). The reproducibility and stability of the electrode was determined by registering 7 consecutive cyclic voltammograms, a relative standard deviation of 2.3 % was observed which demonstrated excellent precision of the electrode.

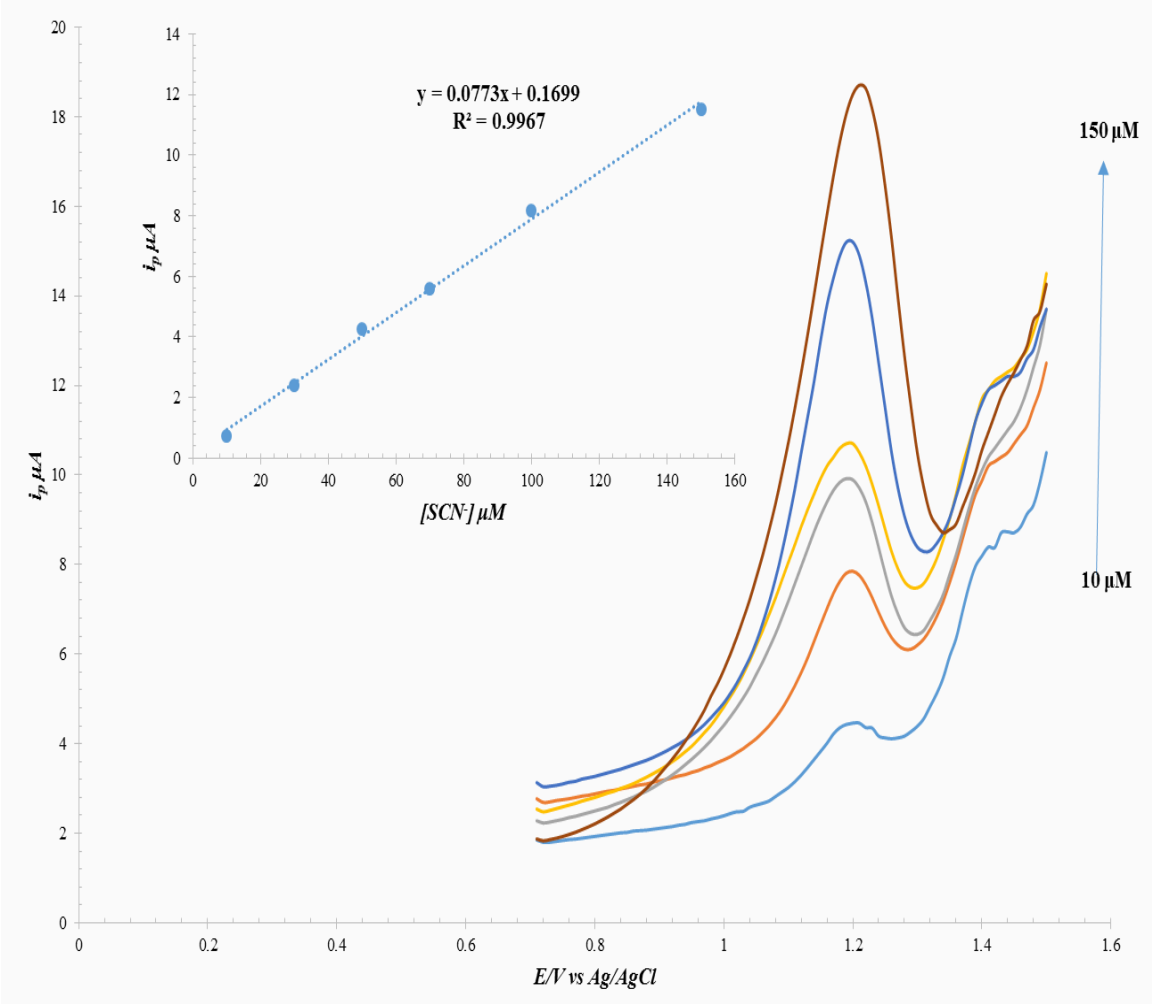

Fig. 3. 10 Calibration, dependence of the peak current on concentration of SCN^- (10 µM to 150 µM) Graph. Inset is the relationship of peak current with concentration.

3.6 Conclusions

Hydrothermal alkaline-control, template-free and seed-free synthesis of mordenite was successful achieved. The addition of phosphorus led to the control diffusivity of the phosphate mordenite. ^{27}Al NMR and ^{31}P NMR confirmed that fundamental chemical changes occurred due to the phosphate zeolite-interaction. ^{27}Al NMR studies had revealed that dealumination of the mordenite aluminium framework occurred due to the phosphoric acid treatment. The newly generated silico-aluminophosphate surface also showed an increase in catalytic activity. Cyclic voltammetric technique was utilized for the characterization of the phosphate zeolite carbon paste electrode in ferro/ferric cyanide system. The electroactive surface area was determined using the *Randles-Sevcik* equation as $22.58\ mm^{2}$ and total electrode surface coverage of $2.24 \times 10^{-3}\ mol\ cm^{-2}$ compared respectively to $12.71\ mm^{2}$ and $1.28 \times 10^{-3}\ mol\ cm^{-2}$ of the bare. The electrode 5-5P-MCPE containing 5% of 5P-MOR showed a maximum current density of 5.6×10^{5} $\mu A/cm^{2}$ in 10 mM ferrocyanide. The electrocatalytic detection of thiocyanate on 5-5P-MCPE was enhanced and a dynamic range of 10 to 150 μM was obtained. The electrode demonstrated strong precision (RSD 2.3%). Thus the construction and electrocatalytic application of phosphate mordenite for the first time was successfully studied and has shown promising application as electrochemical sensor for industrial applications.

Chapter Four

Synthesis, Characterization and Electrocatalytic Activity of Phosphate Mordenite Towards Nitrite Oxidation in Aqueous Solution

Abstract

In this work template-free synthesis of mordenite was carried out. Post synthesis impregnation using phosphoric acid was applied to add phosphate group. The Phosphate modification leads to disruption of bridging hydroxyl and silanol groups as confirmed by FT-IR result. The EDX showed that the framework Si/Al ratio decrease with p-loading and the ^{27}Al NMR revealed the formation of aluminophosphate at the surface of mordenite. Using CV and SWV the phosphate mordenite was investigated for the electrocatalytic oxidation of nitrite. The effect of different electrolyte and pH were studied and the calibration curve of nitrite at phosphate mordenite carbon paste electrode showed a linear dependence within nitrite concentration range of 10 μM to 250 μM with correlation coefficient of $R^2 = 0.9999$. Standard deviation of 3.3 % was observed after registering 5 consecutive cyclic voltammograms of 5 mM NO_2^-, each time at newly reproduced surface.

4.1 Background

Due to its excessive use as preservatives and additive in consumer products, nitrite became present in our food and water bodies. Nitrite was used as reactive anode for corrosion inhibition [131]. Thus, the existence of nitrite in water is indisputable. The damaging effect of nitrite to human system became obvious from its ability to oxidize Fe^{+2} to Fe^{+3} in the hemoglobin thereby making it unable to bind oxygen [132]. Nitrite has been also reported as the reactive reagent for the formation of nitrosamines which are carcinogens [133]. Consequently, investigation and construction of analytical tools to detect nitrite would ensure environmental safety and promote public safety.

Scientists have taken the challenge by the introduction of various analytical techniques involving spectroscopic [134], chromatographic [135], electrophoresis [136], chemiluminescence [137] for nitrite determination. However, the cost associated with these techniques and the time required for detection encouraged the invention of new techniques with better feasibility, reproducibility and less time consuming.

Electrochemical techniques have been often utilized in this pursuits due to their simple setup, fast response, excellent sensitivity above all their availability on small scale [138]. Carbon paste electrodes have shown great advantages above solid ones owing to their chemical inertness, appreciable potential range, insignificant capacitive current, ease of preparation and compatibility with various analysis in different media.

Inclusion of inert material such as zeolites and layered double hydroxides in composite electrodes has shown intensive interest in electrochemical analysis [139, 140]. Non-conductive materials such as zeolites, layered double hydroxides and clays possess surfaces that affect the mobility of electron [87]. They offer the following advantages;

increasing stability and reproducibility of surfaces, reduced over potential in diffusion control processes, and limited oxygen interferences. On account of their ion exchange ability, zeolites allow electron transfer at the surface of their framework when charge specie is move in or out of the zeolite. The pores of zeolites allowed for ion accessibility which can facilitate the deposition and adsorption of detectable ions [141].

The aspiration of electrode modification with zeolites, arouse from their potentials as electrocatalyst and chemical sensors in a size and shape selective analytical investigation [142]. Mordenite type zeolite, due to its resistance to thermal decomposition, stability to acidic medium and its ability to being selective, has been used as substrate in the construction of such devices as chemical sensors. Semiconductors and optical fibers [143]. The selectivity of mordenite is attributed to its high Si/Al molar ratio and two channels sizes with one being large 12-membered ring (7.0 x 6.7 Å) and a small channel of 8-membered ring (5.7 x 2.6 Å) [5]. The later channel is too tight and accessible only by smaller molecules. Thus, mordenite is considered as 1-D zeolite.

Phosphate zeolites have been extensively developed due to the thermal stability towards dealumination and propylene selectivity of phosphorous zeolites during catalytic cracking reactions [63, 64, 66, 83]. When phosphorous is added to zeolite in the form of phosphoric acid, phosphate group attached itself to the zeolite framework through the oxygen (O-atom) in the framework. Thereby, constraining the sizes of the channels windows and pore openings [48]. Mordenite distinctive features can be good requirement for phosphatation which will lead to highly selective, thermal and acid resistance aluminophosphate surface in which the reacting Al-framework is protected [61]. Such

surfaces, due to the formation of positively charged phosphate group can be selective to anionic species especially nitrite in electrochemical studies.

This work explores the fundamental chemical and physical changes that followed phosphorous addition to mordenite type zeolite by some spectroscopic techniques. We also investigate the electrocatalytic behavior of the modified mordenite in nitrite electrochemical oxidation in various electrolytic solutions and at different pH.

4.2 Experimental

4.2.1 Materials

Prepared gels were treated in 100 ml PTFE-lined stainless steel autoclaves with a volume. All samples were synthesized using Silica gel (Sigma Aldrich grade 7734 pore size 60Å, 70-230 mesh), Sodium Aluminate 13404 Sigma Aldrich was used as Aluminium sources. The alkalinity of the gel 98% was control Sodium hydroxide (NaOH) pellets PRS-CODEX alkalinity. Orthophosphoric acid (85% Sigma-Aldrich) was used in the phosphate modification. Phosphate mordenite zeolite (P-MOR) was synthesized in our laboratory. Carbon graphite powder was used in the construction of the carbon paste electrode. The phosphate mordenite and the carbon graphite were bound using a low viscosity paraffin oil. Mortar and pestle was used for mixing carbon graphite and phosphate zeolite. The fabricated electrodes were characterized in the analyte solution KNO_2 and KCl (Fluka chemika) was used as supporting electrolyte. The effect of different electrolytes was investigated in 0.1 M solution of, acetate buffer prepared from sodium acetate (Fluka chemika) and Acetic acid (Fischer scientific) and phosphate buffer prepared from phosphoric acid (85% Sigma-Aldrich), anhydrous sodium dihydrogen

phosphate (Fischer Scientific), anhydrous disodium hydrogen phosphate (Fischer Scientific) and sulphate buffer prepared from ammonium sulphate and sulfuric acid. Ag/AgCl electrode was used as the reference electrode and platinum as the counter electrode in the electrochemical measurements. All experiments were conducted at room temperature.

4.2.2 Synthesis of mordenite zeolite

The Gel dispersion method reported by Hincapie *et al.* [26] was used in the zeolites synthesis. Gel of different Si/Al at different Na/Si ratios was prepared in the equal amount of water. Stipulated amount of sodium hydroxide pellets were dissolved in water followed by the addition of sodium aluminate under stirring condition at room temperature. After a clear solution was obtained the silica gel was then introduced. All gels were aged for 1 h before transferring them into a PTFE-lined stainless steel autoclaves. Hydrothermal treatment was carried out at 180 ^{o}C for 48 h without the addition of both seed and template. After 48 h the product were removed from the oven, quenched and washed several times with DI water using centrifuged until the pH became less than 7. The washed products were dried in an air circulating fume hood.

To obtain the proton form of the Mordenite zeolite (H-MOR), Ion exchange was performed by microwave irradiation. Two sequential ion exchanges were carried out by adding 20 g of 2 M Ammonium nitrate (NH_4NO_3), which was prepared, by adding 16 g of ammonium nitrate in 100 ml of DI water. Then 20 g of this solution was used against each 1 g of the zeolite. The temperature of the microwave was ramped to 85 ^{o}C in 5 min and later dwelled at 85 ^{o}C for 10 min. the products were washed once by DI after each ion exchanged and finally, the products were washed three times using DI water in a

centrifuge and dried. The dried products were calcined in oven under airflow for 15 h with ramping rate of 2.9 ^{o} min^{-1} for 3 hrs. The temperature was then dwelled at 550 ^{o}C for 12 h. Products were finally obtained in the H-MOR formed.

4.2.3 Phosphate modification

Phosphorus modification was conducted based on post synthesis impregnation according to the procedure reported by Corma *et al* [63]. 1 g mordenite zeolite (H-MOR) was suspended in aqueous solution of phosphoric acid containing the desired phosphorous amount. Three different phosphorous loading (0.5 wt.%, 0.75 wt.% and 1.0 wt.%) were prepared. In each case a liquid to solid ratio 10 (wt/wt) was established. The slurry was evaporated at 60 ^{o}C to obtain the solid product. The modified mordenite samples were described as xP-MOR-n, where x indicates the phosphorous loading and n indicates the Si/Al ratio of the mordenite zeolite.

4.2.4 Characterization

The crystallinity of the mordenite was checked using a diffractometer (Miniflex, Rigaku) equipped with Cu Kα radiation (1.5405 Å). Peak patterns were recorded at 2θ from *5* ° to *50* ° using a scan rate of 0.03 ° per step and a counting time of 3 s for each step. Field-emission scanning electron microscopy (FE-SEM) LYRA 3 Dual Beam (Tescan) equipped with energy dispersive X-ray spectrometry (EDX, Oxford Instruments) operated at an acceleration voltage of 30 kV was used to check the morphology of the purified products. Bruker Lamda-500 Multi Nuclear Magnetic Resonance (NMR) Spectrometer with solid-state facility (Proton and multinuclear FT spectra are accessible) was used to investigate the effect of phosphorus impregnation by

conducting ^{27}Al NMR and ^{31}P NMR on both parent and modified samples. FT-iR was also used to further characterize the samples after phosphorus addition.

Table. 4. 1 Synthesis plan for different phosphorous-modified mordenite

Si/Al	**15**	**20**	**25**
Al_2O_3 Source	$NaAlO_2$	$NaAlO_2$	$NaAlO_2$
Na_2O/SiO_2	0.52	0.54	0.56
Silica source	Silica gel	Silica gel	Silica gel
Temperature (^oC)	180	180	180
Time (h)	48	48	48
P-Loading	0.5 wt. %	0.5 wt. %	0.5 wt. %
	0.75 wt. %	0.75 wt. %	0.75 wt. %
	1.0 wt. %	1.0 wt. %	1.0 wt. %

4.3 Electrochemical characterization

4.3.1 Preparation of phosphate mordenite carbon paste electrode

The preparation method of the carbon paste electrode described by Ardakani *et al* [89] was adopted in this work. Desired amount of the P-MOR was mixed with graphite powder while the paraffin oil binder was kept constant at 30 %. A total of 100 mg mixture was formed in each case. The carbon graphite and P-MOR was first mixed using mortar and pestle before adding the oil binder. After the paraffin oil was added, it was mixed again until a homogenously wetted paste is obtained. The pasted was carefully packed into a 40 mm Teflon tube and a 0.1 mm electrode contact hole was made at one

end of the tube. Pushing excess paste out and polishing on a weighing paper created new surface. The electrodes where named based of the P-loading on mordenite and based on the percentage of P-MOR in the mixture. Thus, 0-5P-MCPE, 5-5P-MCPE, 10-5P-MCPE, 15-5P-MCPE and 20-5P-MCPE were obtained corresponding respectively to bare, 5%, 10%, 15% and 20% percentages of the P-MOR.

4.3.2 Voltammetric measurement

The characteristic oxidation peak current of nitrite ion on the surface different phosphate mordenite carbon paste electrodes (P-MCPEs) were recorded via cyclic voltammetry using CHI 760E Potentiostat equipped with a three electrode cell. The P-MCPEs were used as the working electrode, platinum wire as auxiliary electrode, and a KCl saturated Ag/AgCl reference electrode was used. The optimum p-loading, Si/Al ration and percentage P-MOR were established by recording cyclic voltammograms of 10 mM NO_2^- ion at the different P-MCPEs. The total surface coverage of the electrode was determined by varying the potential scan rate. The optimum electrolyte/buffer solution and working pH were determined. Finally a calibration curve was established and the stability of the electrode was investigated. The different composite electrodes can be identified by the letters in the following description, y-xP-MCPE-n in this case y is added to show the percentage of the phosphate mordenite in the carbon paste electrode, x and n have been described above.

4.4 Results and discussion

4.4.1 Crystallinity mordenite zeolite and phosphate mordenite zeolite

The crystallinity of parent MOR and P-MOR with different Si/Al ratios 15, 20 and 25 and those loaded with varying phosphorous concentration were investigated at 2Θ from 5 ^{o}C to 50 ^{o}C with a rate of 3 ^{o}/min. MOR samples with Si/Al ratios of 15, 20 and 25 showed the pure mordenite phase with excellent crystallinity at corresponding Na/Si of 0.52, 0.54 and 0.56 (Fig 4.1). Compared to the work of Hincapie *et al* [26] mordenite with Si/Al ratio 20 synthesized for 48 h showed almost 110% crystallinity in a seed assisted gel dissolution method. Also, compared with the standard mordenite powdered pattern from *IZA* (International Zeolite Association), the synthesized mordenites exhibit excellent crystallinity. Gel Si/Al ratio has shown no observable impact on the crystallinity of synthesized MOR, as the number and intensity of major peaks were relatively equal. The XRD peaks showed some broadening at base of the peaks, that is more obvious in MOR-15 (Si/Al = 15). This is attributed to the uncommon aggregates of small-sized strip-like crystal that formed spheres as reported elsewhere [107]. Fig. 4.2 to 4.4 show the X-ray powdered pattern of MOR prepared from gel of different Si/Al ratios.

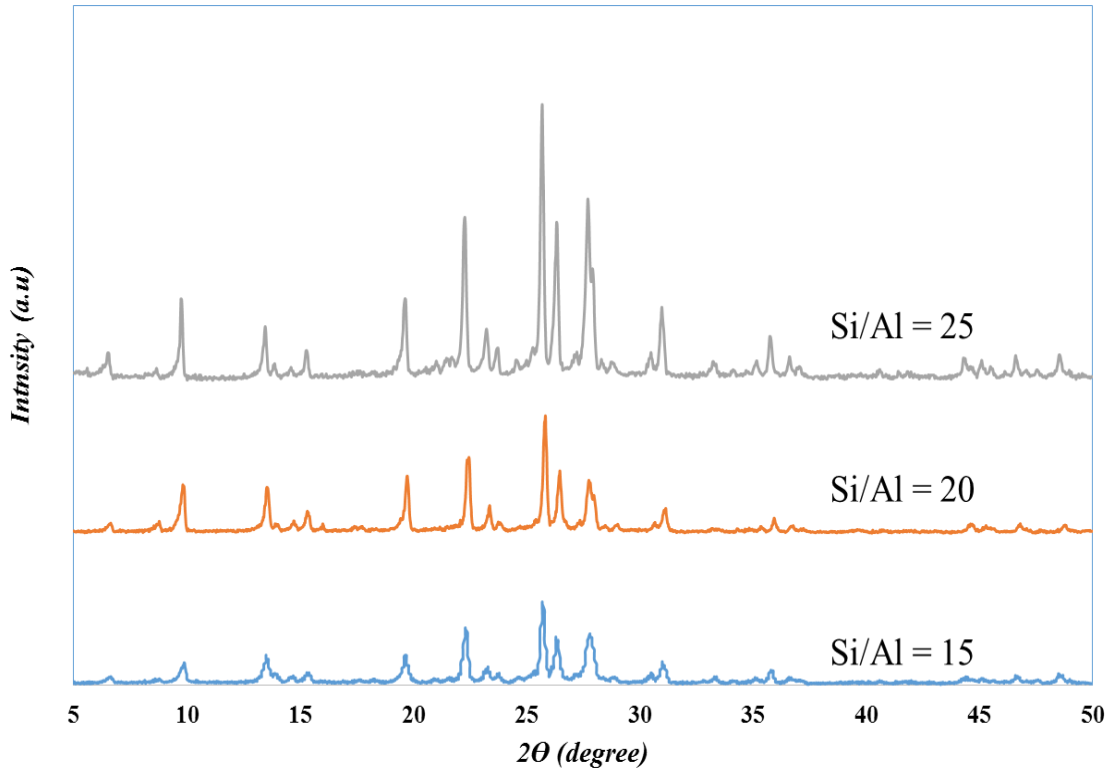

Fig. 4. 1 XRD powdered pattern of mordenite prepared from gel of different Si/Al ratios synthesized at 180 ^{o}C for 48 h using silica gel

The crystallinity of the P-MOR samples containing different P-loadings was also checked between 5 ^{o}C to 50 ^{o}C of 2θ. It was observed from the slight diminished peak intensity that crystal size and particle size were reduced after phosphoric acid treatment. The broadening effect was marginal due to acid treatment. These could be a consequence of dealumination [66]. Fig. 4.2 to Fig. 4.4 show the XRD of the P-MOR Si/Al of 15, 20 and 25 respectively, compared to their parents H-MOR.

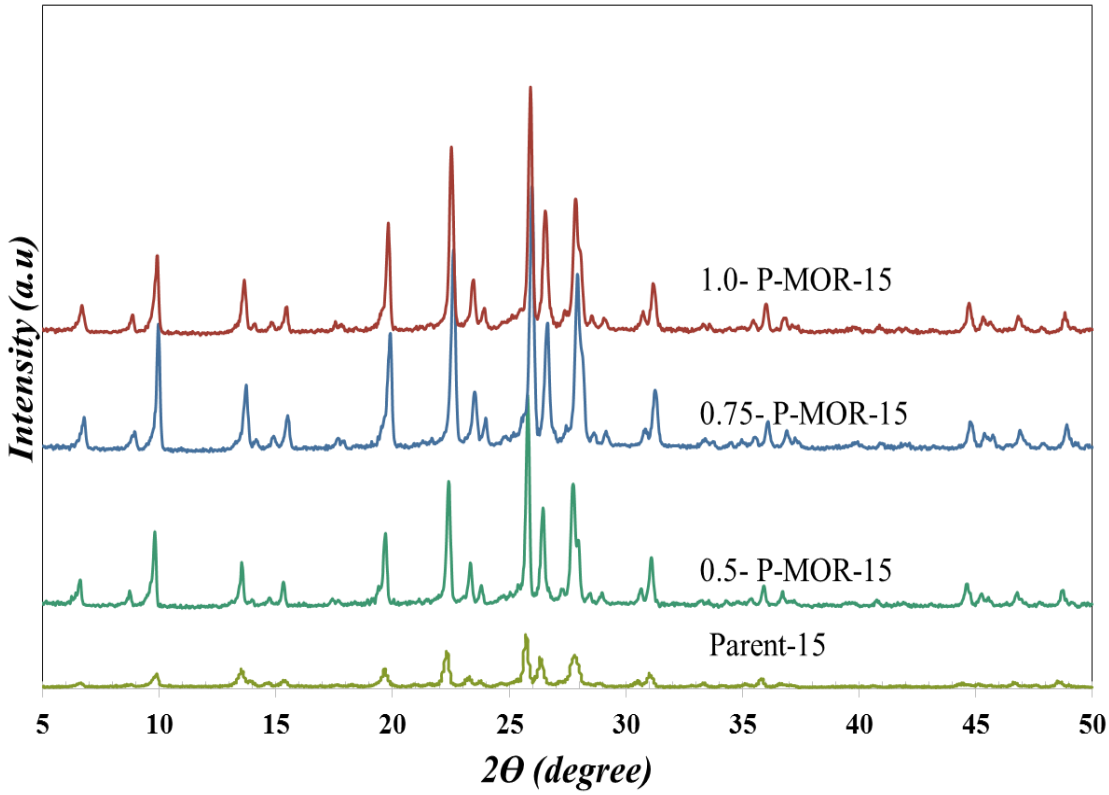

Fig. 4. 2 XRD powdered pattern of mordenite sample Si/Al 15 synthesized at 180 ^{o}C for 48 h using silica gel impregnated with 0.5 wt.%, 0.75 wt.% and 1.0 wt.% Phosphorous.

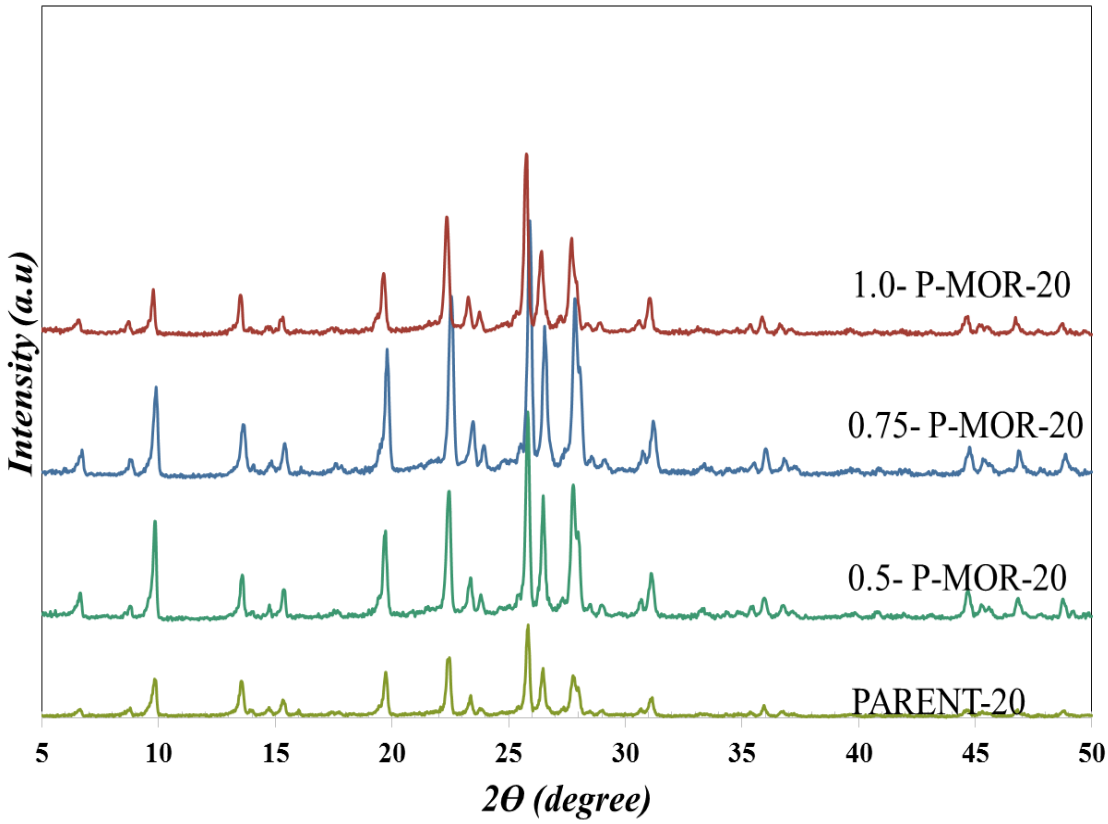

Fig. 4. 3 XRD powdered pattern of mordenite sample Si/Al 20 synthesized at 180 ^{o}C for 48 h using silica gel impregnated with 0.5 wt.%, 0.75 wt.% and 1.0 wt.% Phosphorous.

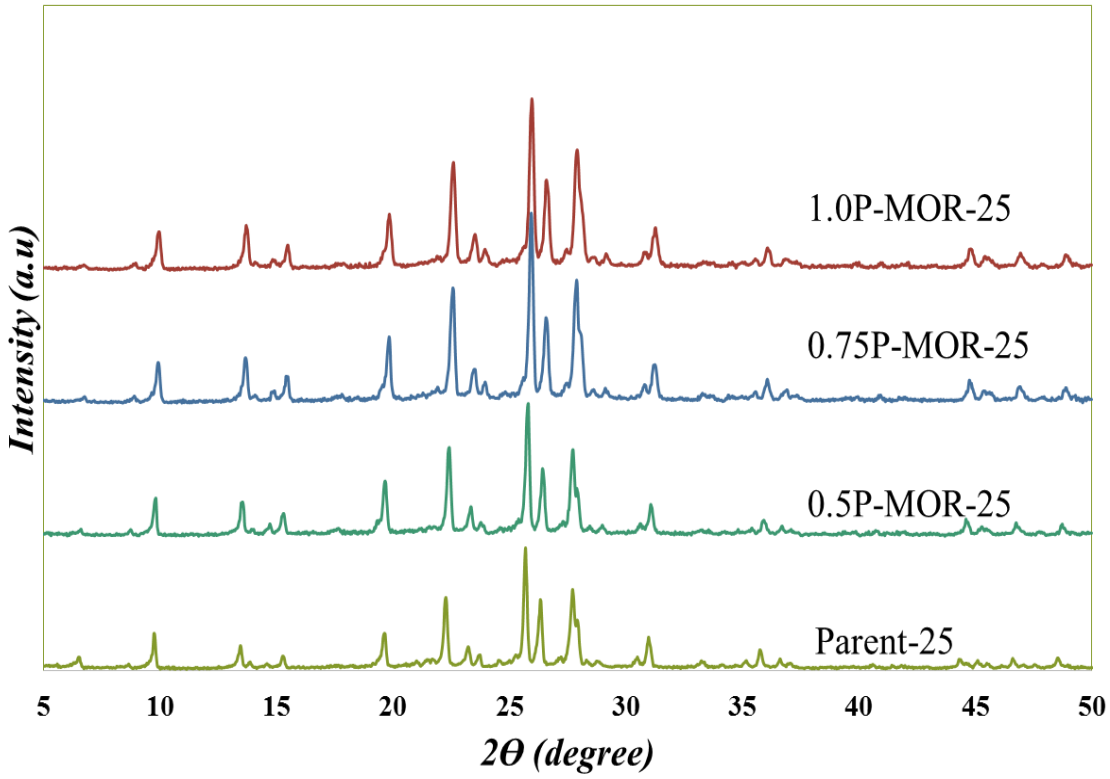

Fig. 4. 4 XRD powdered pattern of mordenite sample Si/Al 25 synthesized at 180 ^{o}C for 48 h using silica gel impregnated with 0.5 wt.%, 0.75 wt.% and 1.0 wt. % Phosphorous.

4.4.2 Morphology

Fig. 4.5 to Fig. 4.7 display the FE-SEM micrographs of P-MOR of different Si/Al ratios each loaded with 3 different P amount. In the case MOR-15 crystal, short prism morphology was obtained. Moreover, some strength sphere were observed with high magnification which were all reported elsewhere [107]. The broadening of the base of XRD peaks was evident to the presence of the spheres. It was confirmed from the FE-SEM images that the crystal sizes increase as the Si/Al ratio increase. This was actually due to higher alkali in the case of the MOR-25 leading to higher rate of silica transport during the crystal growth phase. It could also be due to the decrease in the competition between Al-framework and Si-framework. As reported elsewhere [144, 145] cations induce crystal formation and led to large crystal.

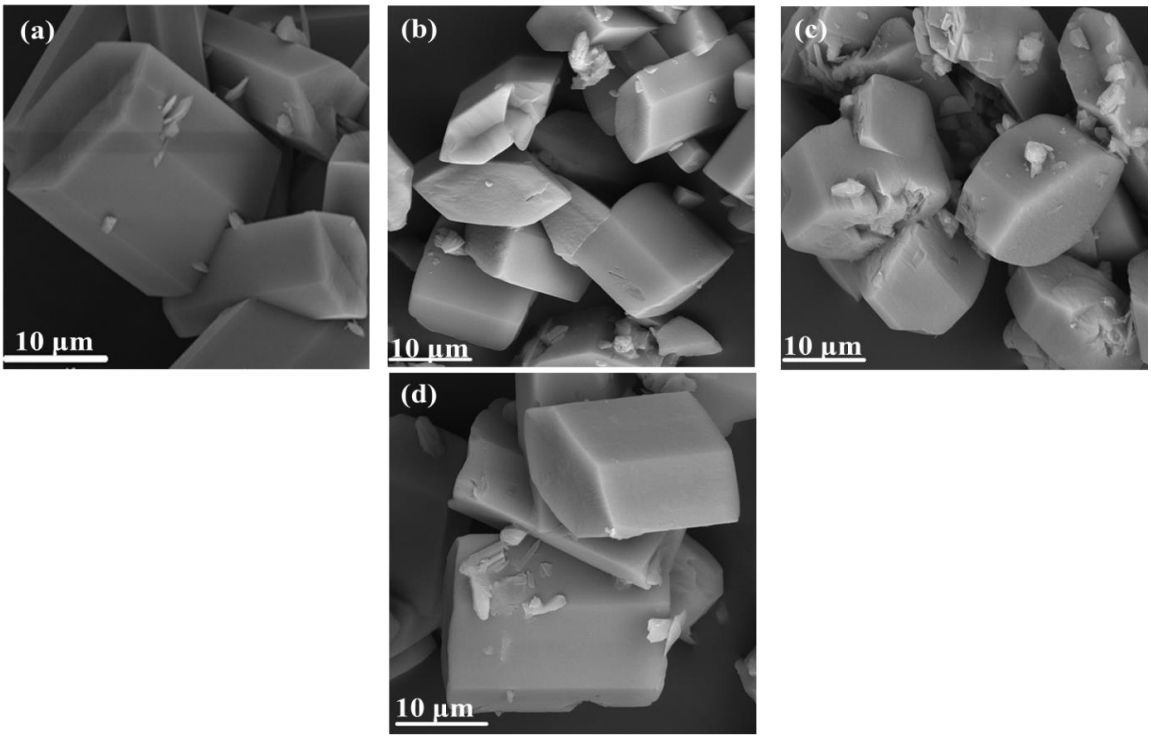

Fig. 4. 5 FE-SEM of MOR samples 15 Si/Al molar ratio and 0.52 Na/Si molar ratio crystallized at 180 ^{o}C in 48 h impregnated with different P-loading on 0.5g MOR (a) H-MOR (b) 0.5P-MOR (c) 0.75P-MOR (d) 1.0P-MOR

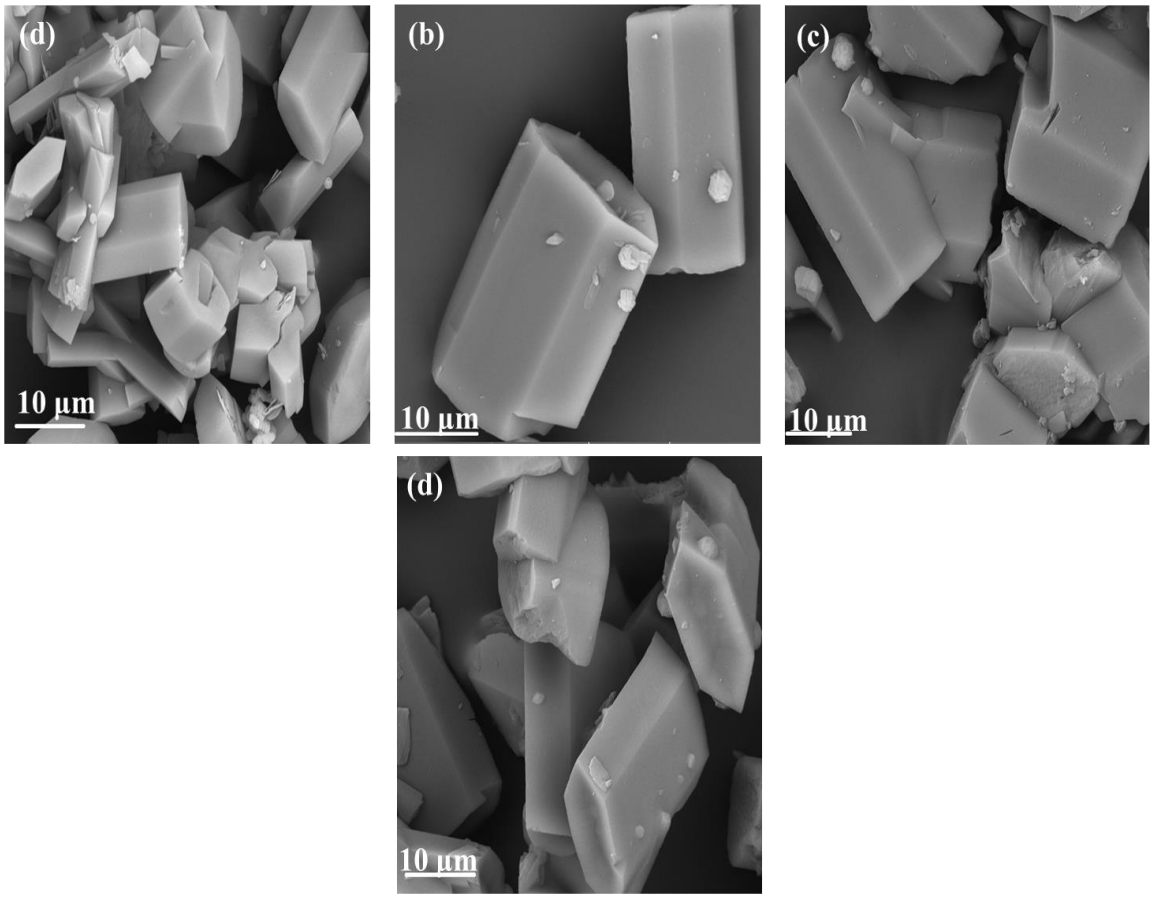

Fig. 4. 6 FE-SEM of MOR 20 Si/Al molar ratio and 0.52 Na/Si molar ratio crystallized at 180 ^{o}C in 4 h impregnated with different P-loading (a) H-MOR (b) 0.5P-MOR (c) 0.75P-MOR and (d) 1.0P-MOR

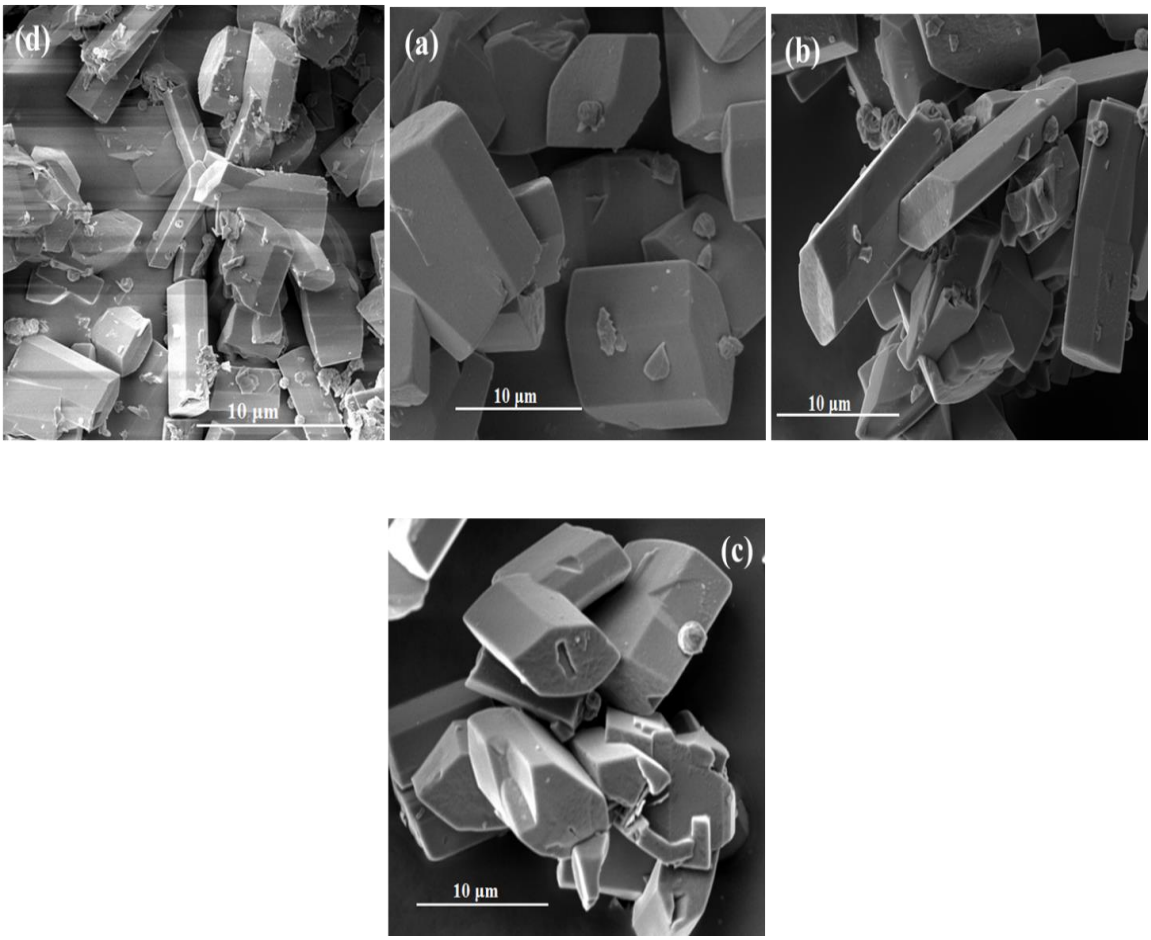

Fig. 4. 7 FE-SEM of MOR samples 20 Si/Al molar ratio and 0.52 Na/Si molar ratio crystallized at 180 ^{o}C in 4 h impregnated with different P-loading (a) H-MOR (b) 0.5P-MOR (c) 0.75P-MOR (d) 1.0P-MOR

4.4.3 Effect of phosphorus impregnation

To confirm the attachment of phosphorus to the mordenite framework, energy dispersion X-ray spectroscopy (EDX) was employed on the P-MOR(s). Qualitatively it shows some peaks of phosphorous in the spectrum. It was a less powerful technique to quantitatively account for the exact amount of phosphorus loaded on the zeolite mordenite. However, the elemental composition from the EDX summarized in Table 4.1 shows a systematic drop in the framework Si/Al ratio, which was due to the leach out of the framework aluminium caused by the direct phosphatation [66]. The actual amount of phosphorous incorporated at each loading on the different mordenite zeolites was summarized in Table 4.2. The EDX spectra of the P-MOR samples with Si/Al molar ratios of 15, 20 and 25 loaded with 3 different amount of phosphate group were shown in Fig. 4.8 to Fig. 4.10

Table. 4. 2 EDX results on the effect of P-loading on the framework Si/Al of MOR

P-MOR	P-loading (wt.%)	Framework Si/Al (wt. /wt.)
P-MOR-15	0.5 wt. % of P	7.135
	0.75 wt. % of P	7.502
	1.0 wt. % of P	7.714
P-MOR-20	0.5 wt. % of P	6.686
	0.75 wt. % of P	8.424
	1.0 wt. % of P	9.611
P-MOR-25	0.5 wt. % of P	7.538
	0.75 wt. % of P	7.897
	1.0 wt. % of P	9.080

Table. 4. 3 Amount of phosphorous incorporated results obtained from XRF

P-MOR	P-Loading (wt.%)	P-incorporated (wt.%)
P-MOR-15	0.5 wt.%	0.57
	0.75 wt.%	0.70
	1.0 wt.%	0.87
P-MOR-20	0.5 wt.%	0.59
	0.75 wt.%	0.64
	1.0 wt.%	0.83
P-MOR-25	0.5 wt.%	0.64
	0.75 wt.%	0.77
	1.0 wt.%	0.89

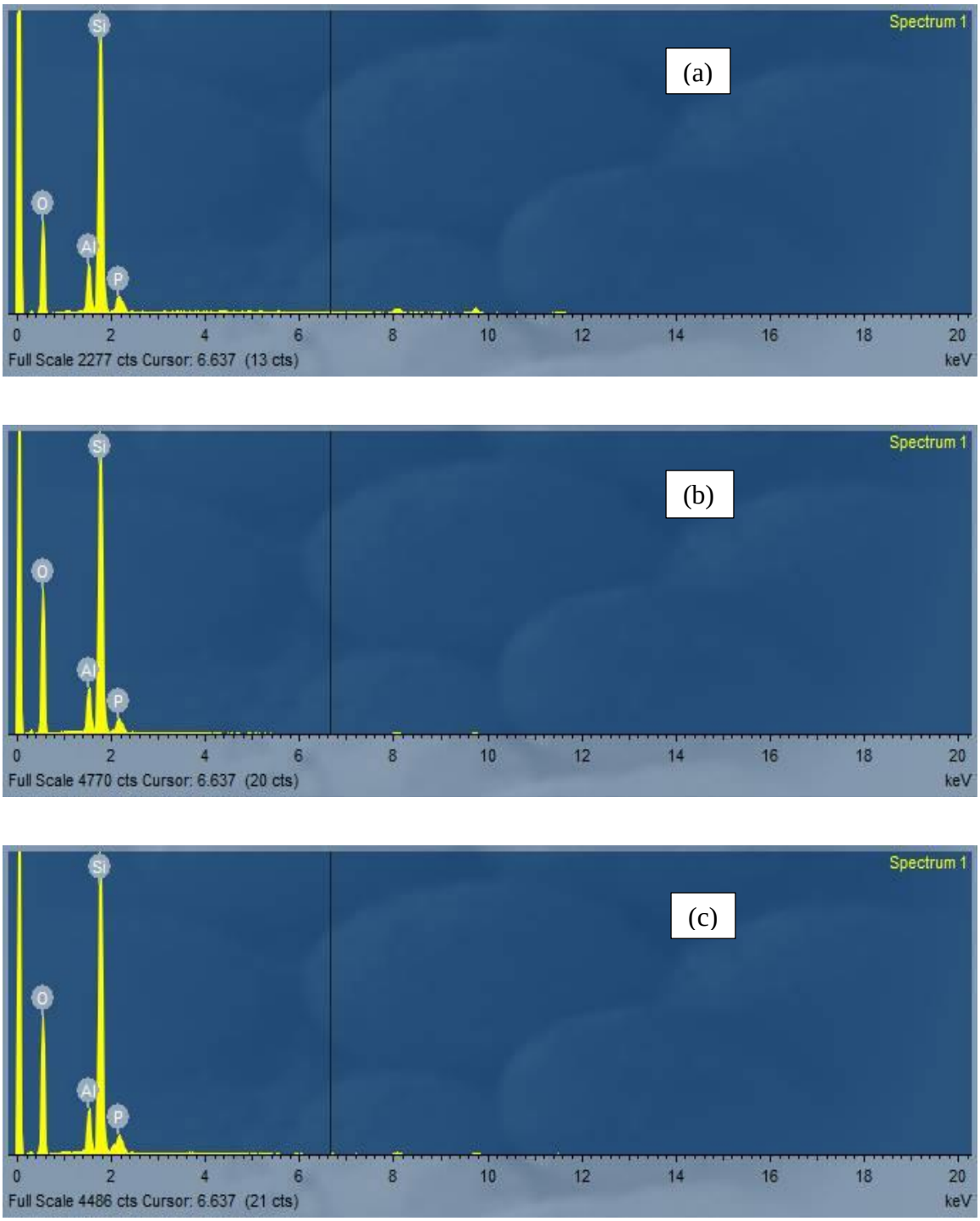

Fig. 4. 8 EDX spectrum of MOR of 15 Si/Al molar ratio impregnated with different p-loading (a) 0.5P-MOR-15, (b) 0.75P-MOR-15 and (c) 1.0P-MOR-15

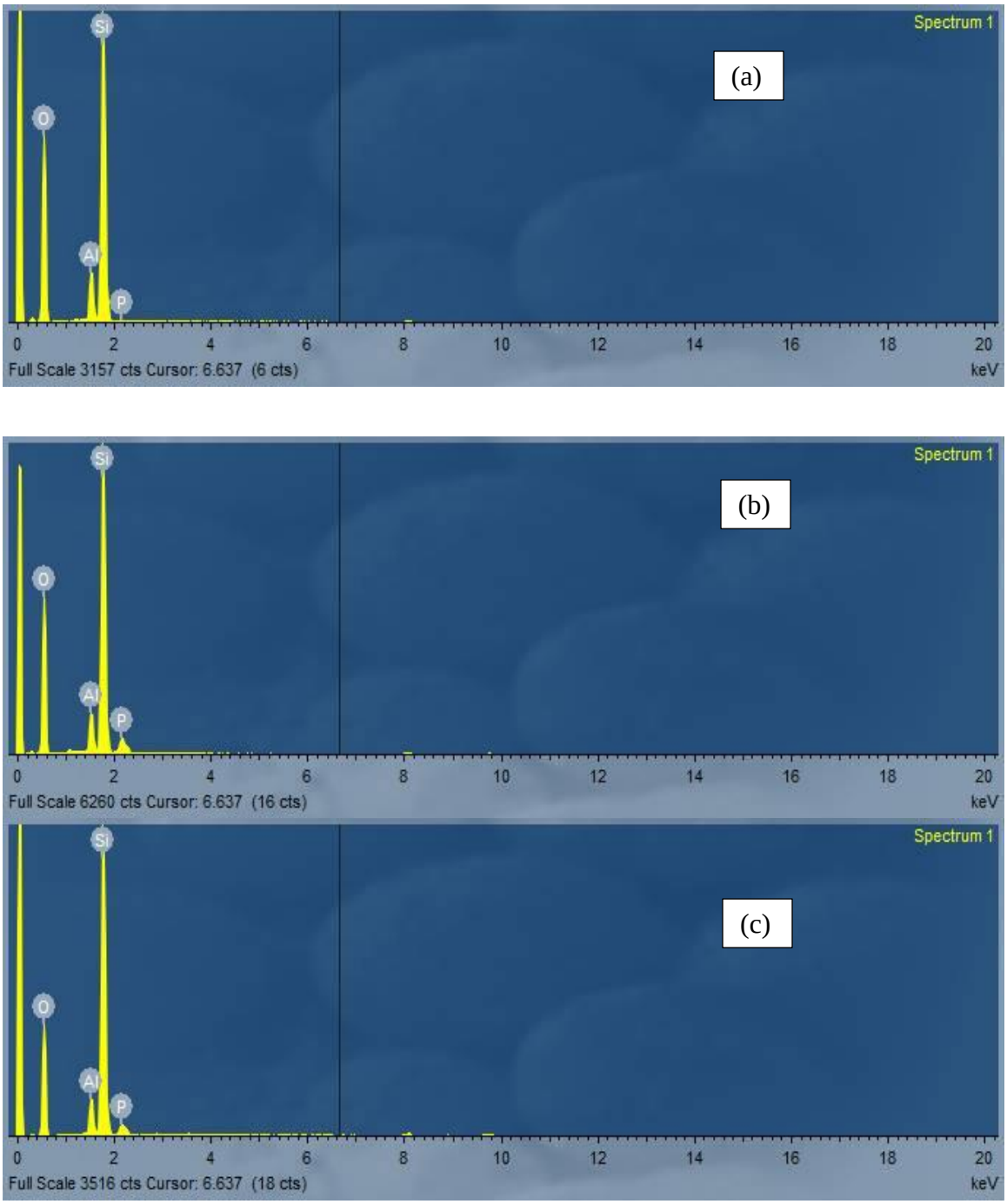

Fig. 4. 9 EDX spectrum of MOR of 15 Si/Al molar ratio impregnated with different p-loading (a) 0.5P-MOR-20, (b) 0.75P-MOR-20 and (c) 1.0P-MOR-20

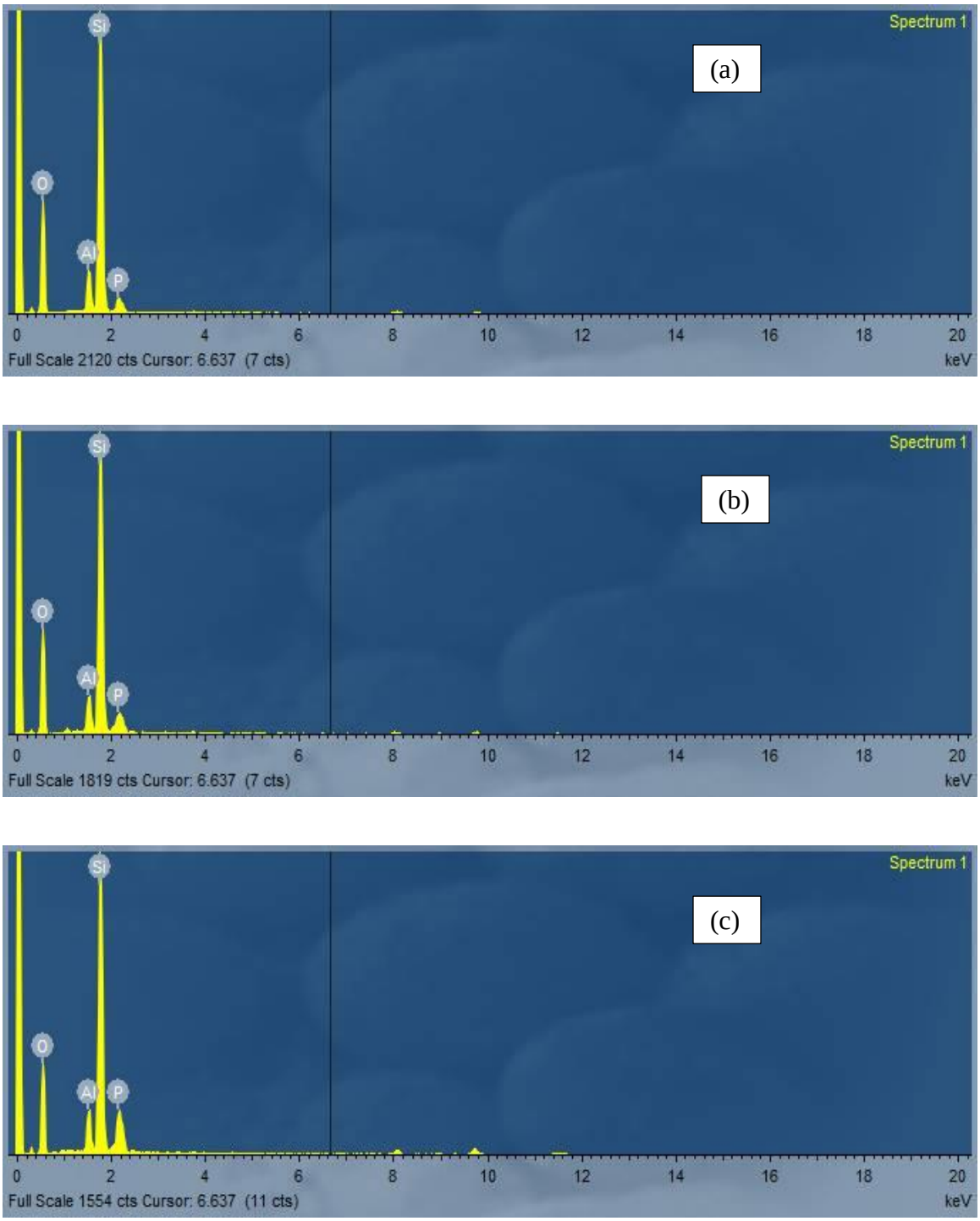

Fig. 4. 10 EDX spectrum of MOR of 15 Si/Al molar ratio impregnated with different p-loading (a) 0.5P-MOR-25, (b) 0.75P-MOR-25 and (c) 1.0P-MOR-25

Caro et al [58] reported from ^{1}H NMR investigation carried out on ZSM-5, the phosphoric acid pass through channels. Van Donk [62] reported the existence of extra-octahedral coordinated Al-framework that increase diffusion limitation in mordenite which was greatly reduced by mild acid treatment. Guided by the fact that both coordinated framework can be revealed in ^{27}Al NMR spectrum, we recorded both ^{27}Al NMR and ^{31}P NMR spectra on MOR and P-MOR samples. Comparing ^{27}Al of the phosphate mordenite and that of the parent H-MOR mordenite there is decrease in intensity of the peaks which is more obvious to the peak corresponding to the octahedral Al, due to the removal of aluminium from framework.

This direct framework dealumination was a consequence of the orthophosphoric acid impregnation and post thermal-treatment by calcination and it's the reason for the eventual decreased in concentration of Brønsted acid sites as inferred from the work of Caro *et al* [146]. The dealumination observation was also confirmed by the wok of Jianwen Li *et al* in [80] on phosphorus-Nickel co-modification of ZSM-5. The ^{27}Al NMR of the phosphoric acid treated mordenite and the parent mordenite zeolite are presented. Fig. 4.11 to Fig. 4.13 display the ^{27}Al NMR of the P-MOR.

The ^{31}P NMR spectra of the P-MOR-15 samples were recorded to complement the discussion made on the results of ^{27}Al NMR. The peak around -30 ppm in Fig. 4.14 corresponding to phosphorous was increasing with increasing P-loading, which is expected on P-MOR-20 and P-MOR-25. This clearly confirms strong chemical interaction between the phosphate group and the mordenite framework aluminium through oxygen, forming aluminophosphate surface reported elsewhere [61, 147]. This is

also reaffirmation to the increase in the framework Si/Al ratio due to dealumination observed by the EDX and the ^{27} Al NMR.

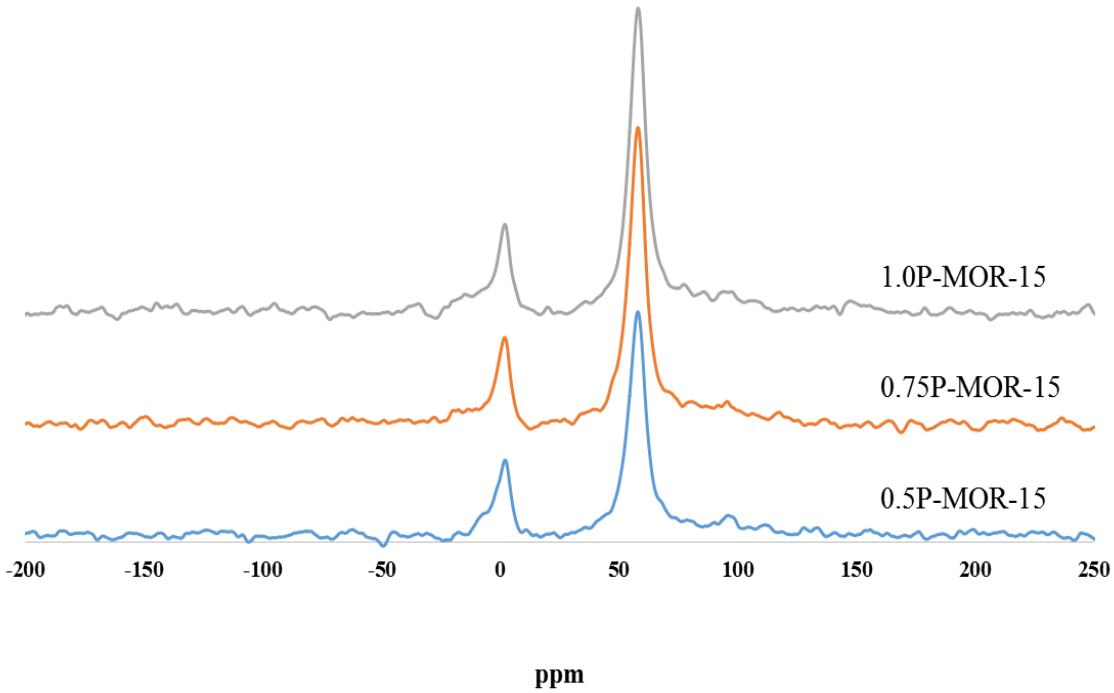

Fig. 4. 11 ^{27}Al NMR P-MOR-15 of 15 Si/Al molar ratio impregnated with different P-loadings

.

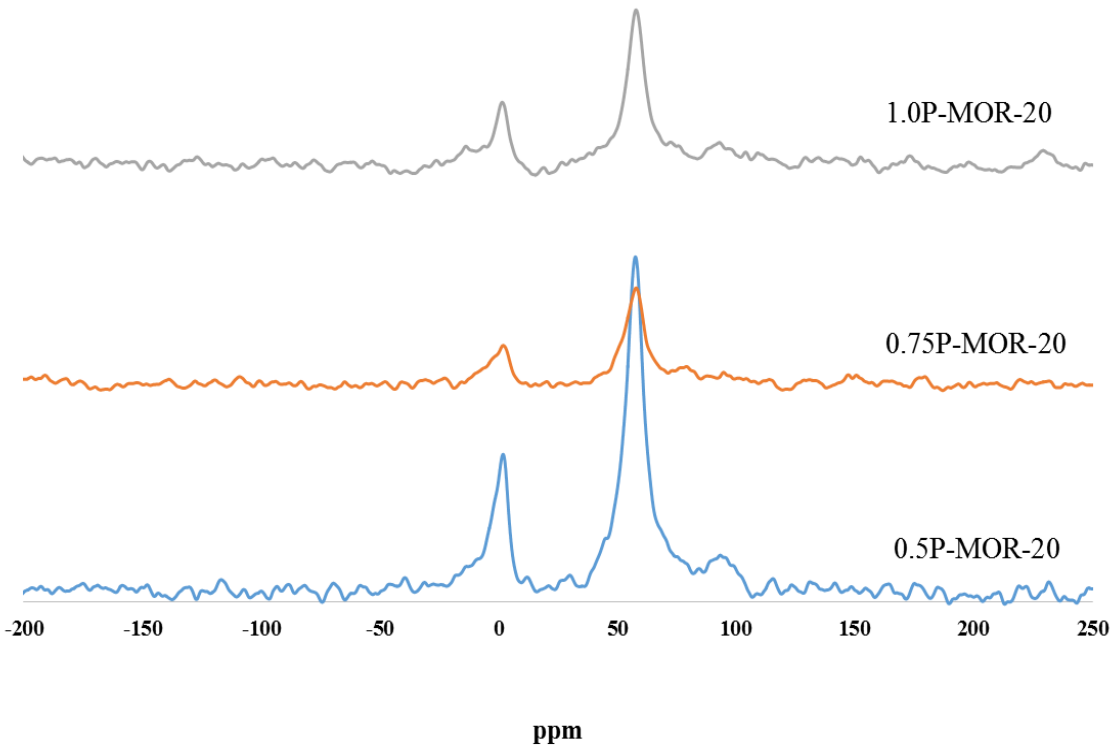

Fig. 4. 12 ^{27}Al NMR P-MOR-15 of 15 Si/Al molar ratio impregnated with different P-loadings

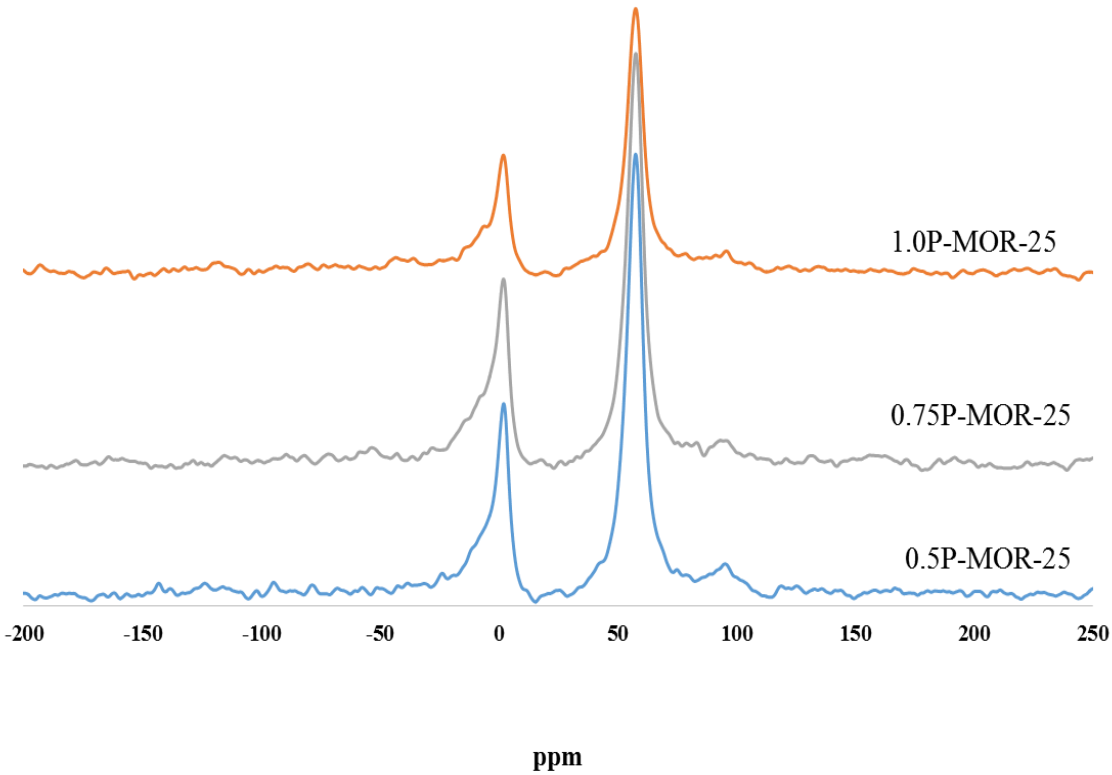

Fig. 4. 13 ^{27}Al NMR P-MOR-15 of 15 Si/Al molar ratio impregnated with different P-loadings

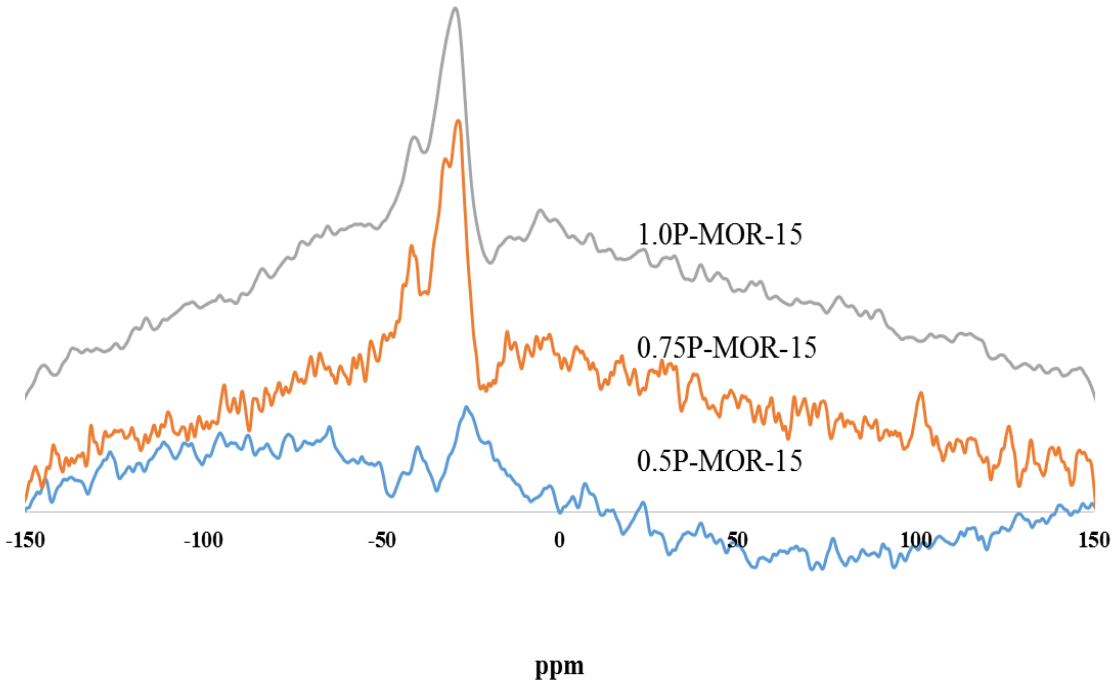

Fig. 4. 14 ^{31}P NMR P-MOR-15 of 15 Si/Al molar ratios impregnated with different P-loadings

4.4.4 FT-iR studies

Fourier transform infrared spectroscopy (FT-iR) has been used to obtain structural information from the bronsted acidity of zeolites. Peculiarly, the stretching region of the –OH can supply rich information on the type of hydroxyl group bound to the zeolite which are vital to its chemistry [148]. The acidic hydroxyl group constitutes the so-called bronsted acidity. Recently, mordenite has been reported to comprise six different –OH groups at different locations (showing stretches between 3581 to 3625 cm^{-1}) which are responsible for the bronsted acidity in the zeolites [5]. Thus, we conducted the FT-iR on all samples and compared them with the parent material so that important chemical changes following of phosphoric acid treatment can be understood.

Fig. 4.15 to 4.17 shows the FT-iR spectra of the phosphate mordenites of different Si/Al ratios (P-MOR-15, P-MOR-20 and P-MOR-25). It was noticed as can be seen in Figures the sharpness of the strong stretching around 3450-3650 cm^{-1} corresponding to the silanol and external bridging groups at the surface [5, 50], were diminishing with increasing P-loading. While the appearance of a weak band at around 3680 cm^{-1} was obvious which is due to –OH group in the amorphously formed aluminium phosphate [50]. The direct consequence of this, is the generation of a more active hydrophobic surface with possible mesopores [149], the formation of a protonated amorphous aluminium phosphate layer [150] and the formation of positively charged phosphate group [50]. The effect is becoming stiffer as the framework Si/Al is increased, which is obvious due to the hydrophobic nature of silica and decreased in the bronsted acidity in the phosphate mordenite.

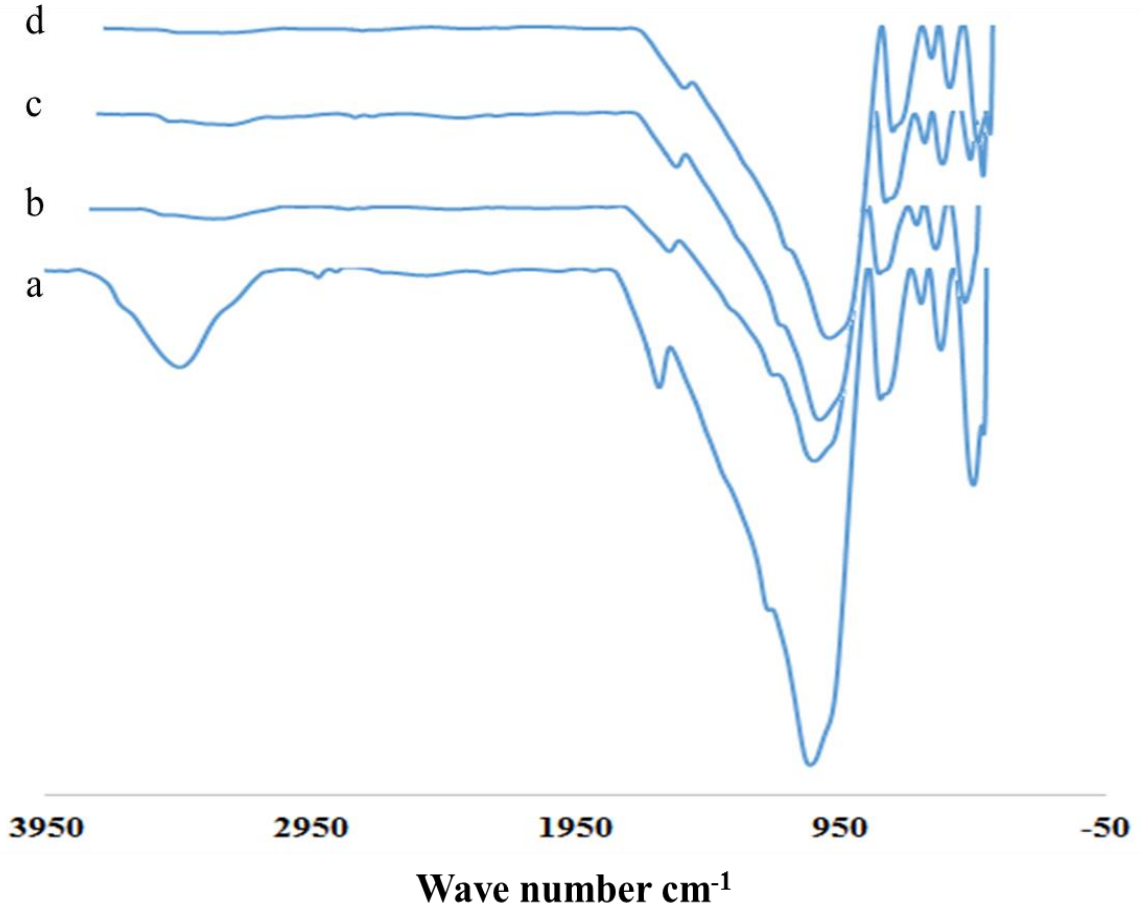

Fig. 4. 15 FT-iR Spectra of P-MOR Si/Al = 15, Na/Si = 0.52 synthesized at 180 ^{o}C for 48 h (a) parent (b) 0.5P-MOR (c) 0.75P-MOR and (d) 1.0P-MOR

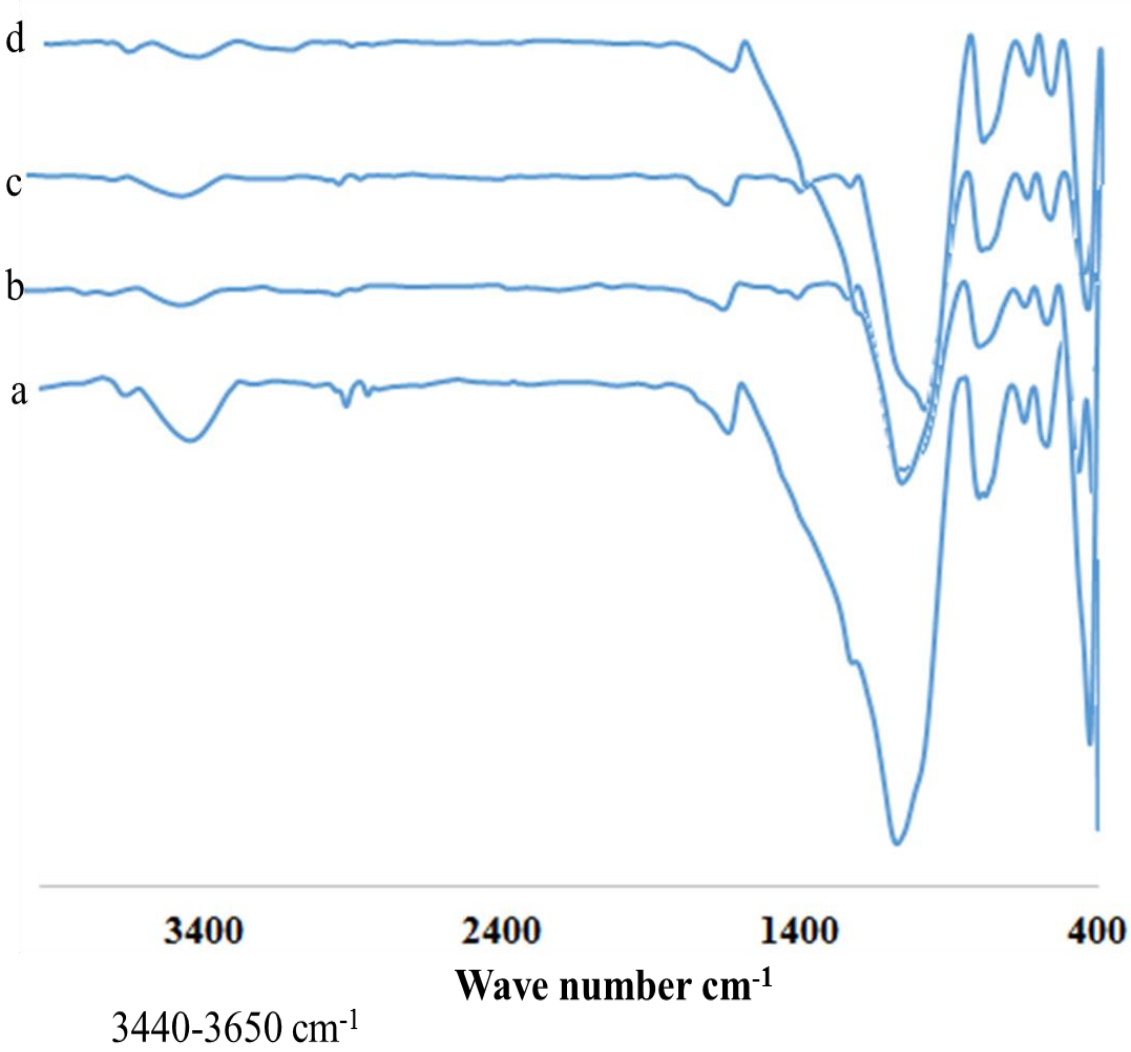

Fig. 4. 16 FT-iR Spectra of P-MOR Si/Al = 20, Na/Si = 0.52 synthesized at 180 ^{o}C for 48 h (a) parent (b) 0.5P-MOR (c) 0.75P-MOR and (d) 1.0P-MOR

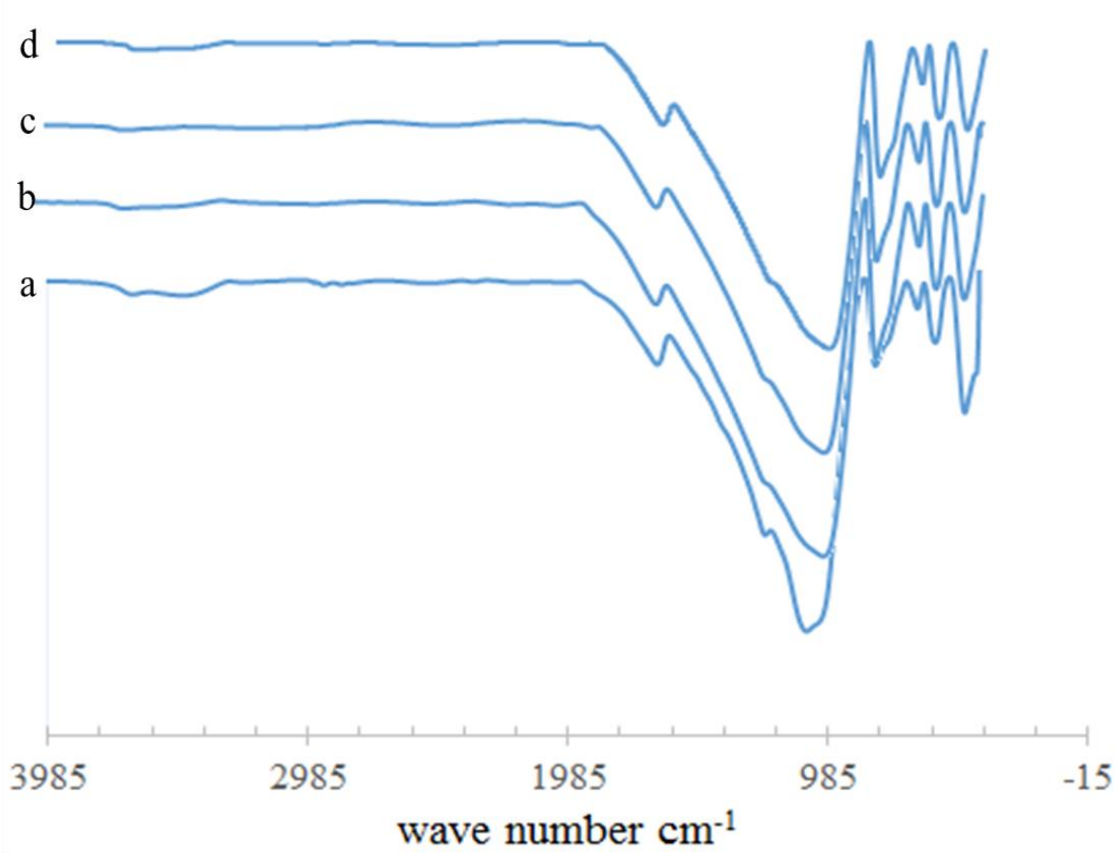

3440-3650 cm^{-1}

Fig. 4. 17 FT-iR Spectra of P-MOR Si/Al = 25, Na/Si = 0.56 synthesized at 180 ^{o}C for 48 h (a) parent (b) 0.5P-MOR (c) 0.75PMOR and (d) 1.0P-MOR

4.5 Electrochemical evaluation

4.5.1 Optimization of P-loading and the bulk Si/Al ratio for NO_2^- detection

Considering the fact that getting maximum current is important, we begin the electrochemical assessment by screening the different phosphate mordenite possessing different Si/Al ratios and P/Al ratios. The cyclic voltammograms of 10 mM NO_2^- in 0.1 M KCl pH 7 at different carbon paste electrodes comprising 5 % each of the phosphate mordenites, 30 % paraffin oil and 65 % carbon graphite were recorded. Also the CV for the unmodified mordenite carbon paste electrode was recorded. For instance, in the case of mordenite with Si/Al ratios of 15 three different phosphate mordenite were produced three different carbon paste electrodes, and another carbon paste electrode were made from the H-MOR-15.

Fig. 4.18 to 4.20 show charts of peak current against the phosphorous loading plotted from the data obtained by CV of 10 mM NO_2^- in 0.1 M KCl at carbon paste electrodes prepared from each of the H-MOR having 15, 20 and 25 Si/Al molar ratio and their respective phosphate mordenite P-MOR. The electrodes are named as follows: MCPE-15, 0.5P-MCPE-15, 0.75P-MCPE-15 and 1.0P-MCPE-15. It can be clearly seen the promotional effect on peak current was obvious by the systematic increase in peak current with p-loading from 0 wt. % to 0.75 wt.%. Thus, the influence of positively charged aluminophosphate surface formed has significant influence towards the mass transport of the nitride ion.

Interestingly, the highest peak current in all cases was observed at 0.75 wt.% phosphorous loading. However, the peak current show some degree on dependence on the MOR Si/Al molar ratios as the highest peak current was obtained with the MOR-25

loaded with 0.75 wt.% phosphorous. Not only the peak current is increased but also a dramatic decrease in the background current was obvious at P-loading of 0.75 on P-MOR-25(0.75P-MCPE-25).

To verify further, the square voltammograms (see Fig. 4.21) of the electrodes prepared from the P-MOR-25 containing varying p-loading were recorded. The same pattern of current increase was observed which shows the reliability of the electrode on the phosphate composition.

As discussed earlier, the hydrophobicity of the mordenite increase with increased Si/Al ratio and phosphoric acid impregnation. However, the structural feature supporting the nitrite oxidation is the formation of the positively charged phosphate groups at the surface of the mordenite [50, 151]. This electrocatalytic character, which is supplemented by the pore-system of the structured catalyst, had in a synergistic manner supported the mechanism proposed by Corma et al.

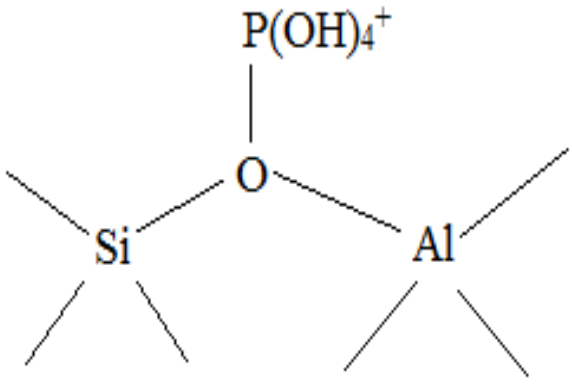

Scheme 4. 1 Adopted mechanism for phosphate zeolite interaction [50]

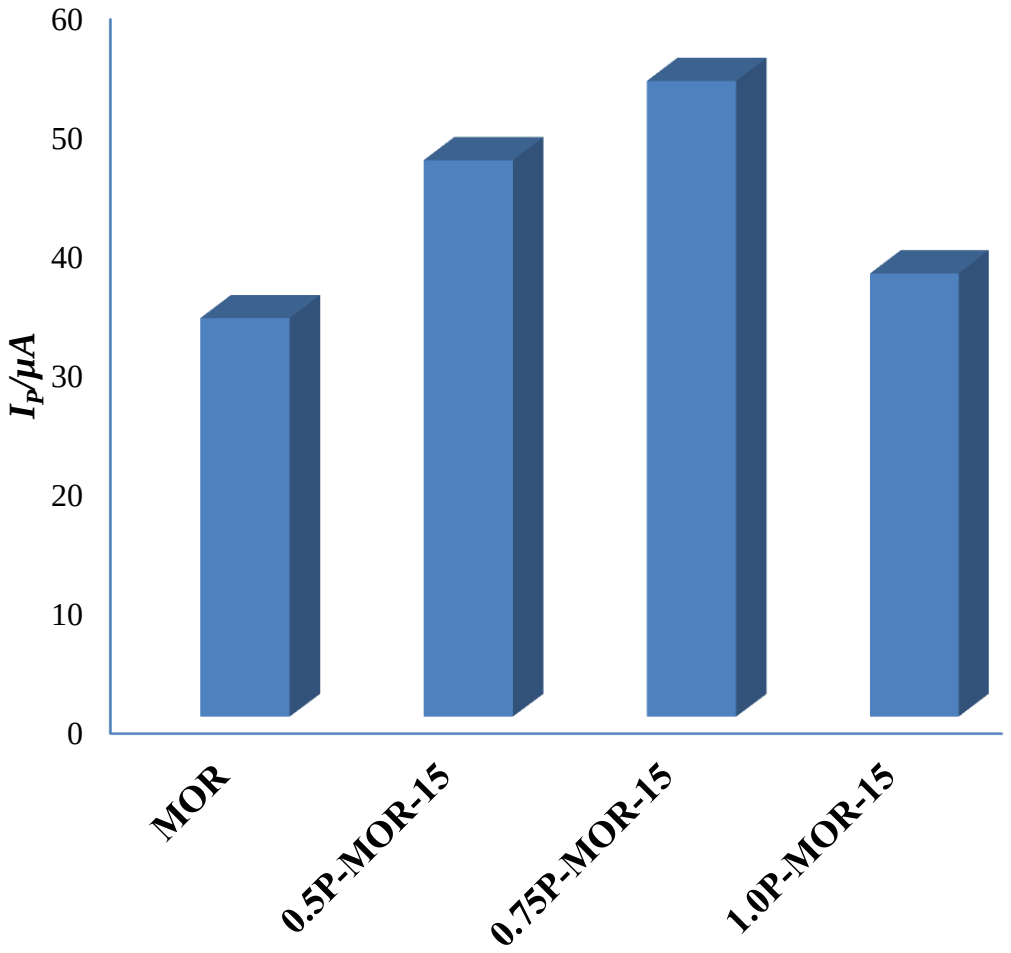

Fig. 4. 18 Chart showing the relation between peak current and phosphorous loading data obtained from CVs of carbon paste electrodes prepared from P-MOR-15 containing different P-loading, at a potential window of 0 mV to 1.8 mV and scan rate of 100 mV s^{-1}

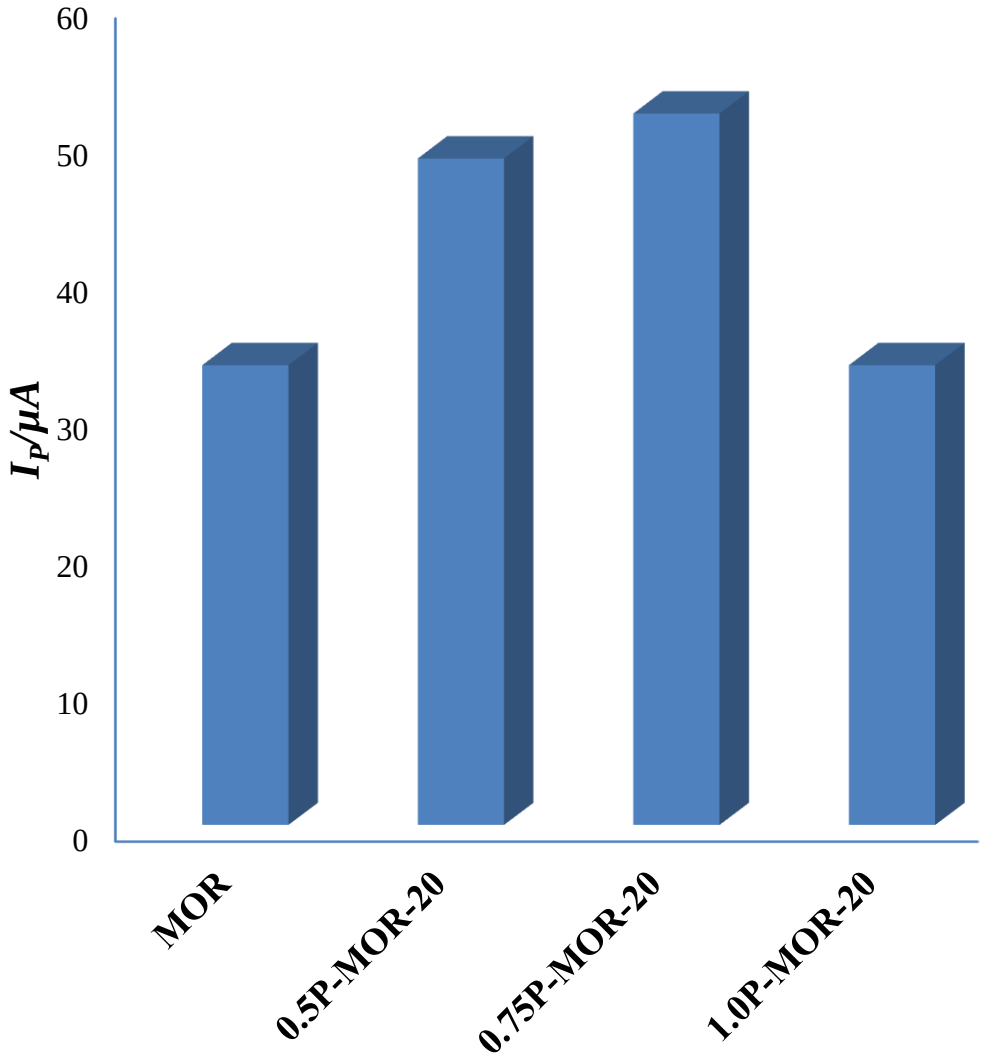

Fig. 4. 19 Chart showing the relation between peak current and phosphorous loading, data obtained from CVs of carbon paste electrodes prepared from P-MOR-20 containing different P-loading, at a potential window of 0 mV to 1.8 mV and scan rate of 100 mV s^{-1}

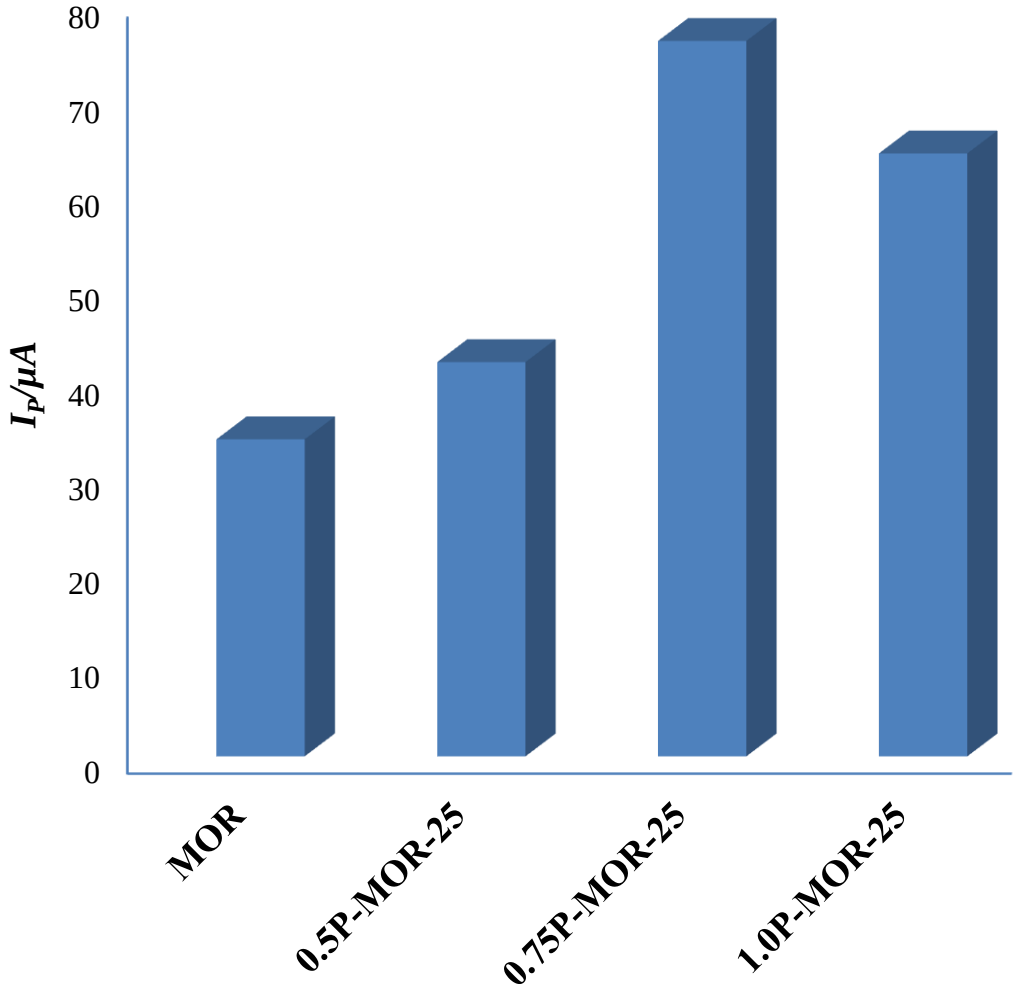

Fig. 4. 20 Chart showing the relation between peak current and phosphorous loading data obtained from CVs of carbon paste electrodes prepared from P-MOR-25 containing different P-loading, at a potential window of 0 mV to 1.8 mV and scan rate of 100 mV s^{-1}

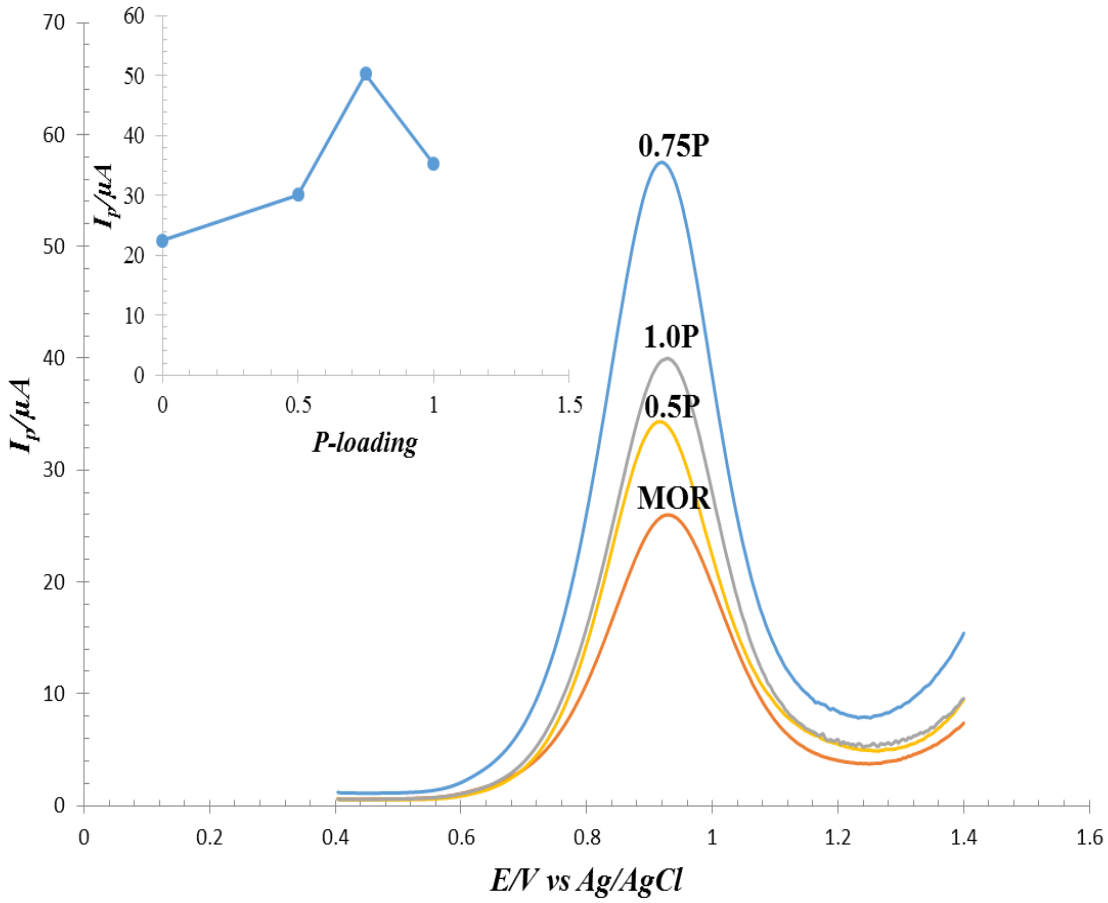

Fig. 4. 21 Comparison of SWVs of carbon paste electrodes prepared from P-MOR-25 containing different P-loading, in the presence of 10 mM NO_2^- in 0.1 M KCl

4.5.2 Influence of the proportion of phosphate mordenite in the carbon paste

Having established that 0.75-MCPE-25 was the best composite containing 0.75 wt.% phosphorous loading on mordenite with 25 Si/Al molar ratio. We then investigated the percentage composition of the 0.75-P-MOR-25 in the carbon paste. By varying the phosphate mordenite percentage from 0 to 20 % five different composite electrodes were produced which are summarized in the Table 4. 4

Table. 4. 4 Electrodes composition

Paraffin oil	Graphite	0.75-P-MOR-25	Composition	Name
30	70	0	Bare CPE	P
30	65	5	5-0.75-P-MOR-25-CPE	Q
30	60	10	10-0.75-P-MOR-25-CPE	R
30	55	15	15-0.75-P-MOR-25-CPE	S
30	50	20	20-0.75-P-MOR-25-CPE	T

Fig. 4.22 and Fig. 23 show square wave voltammograms and the blanks of the **P, Q, R, S and T** carbon paste electrodes. The characteristic oxidation peak current of 10 mM NO_2^- in phosphate buffer pH 7, increase steadily with 0.75P-MOR-15 until it reached 15 % (i.e. composite electrode **S)** and then sharply drop at 20 % (i.e. composite electrode **T**). The current density obtained from square wave voltammograms for the bare carbon paste (i.e. **P**) and the Composite electrode **S** are 51.7×10^5 $\mu A/cm^2$ and 9.5×10^5 $\mu A/cm^2$, respectively. Even **R** showed higher current than **P** (which is the bare carbon paste). The superiority can also be attributed to the adsorption of the nitrite ions to its micropores and the newly generated mesopores leading to an optimum electrode surface coverage. However, at the highest proportion of 20 % the surface coverage exceeded it optimum and electron transfer reaction are retarded due to surface saturation [23].

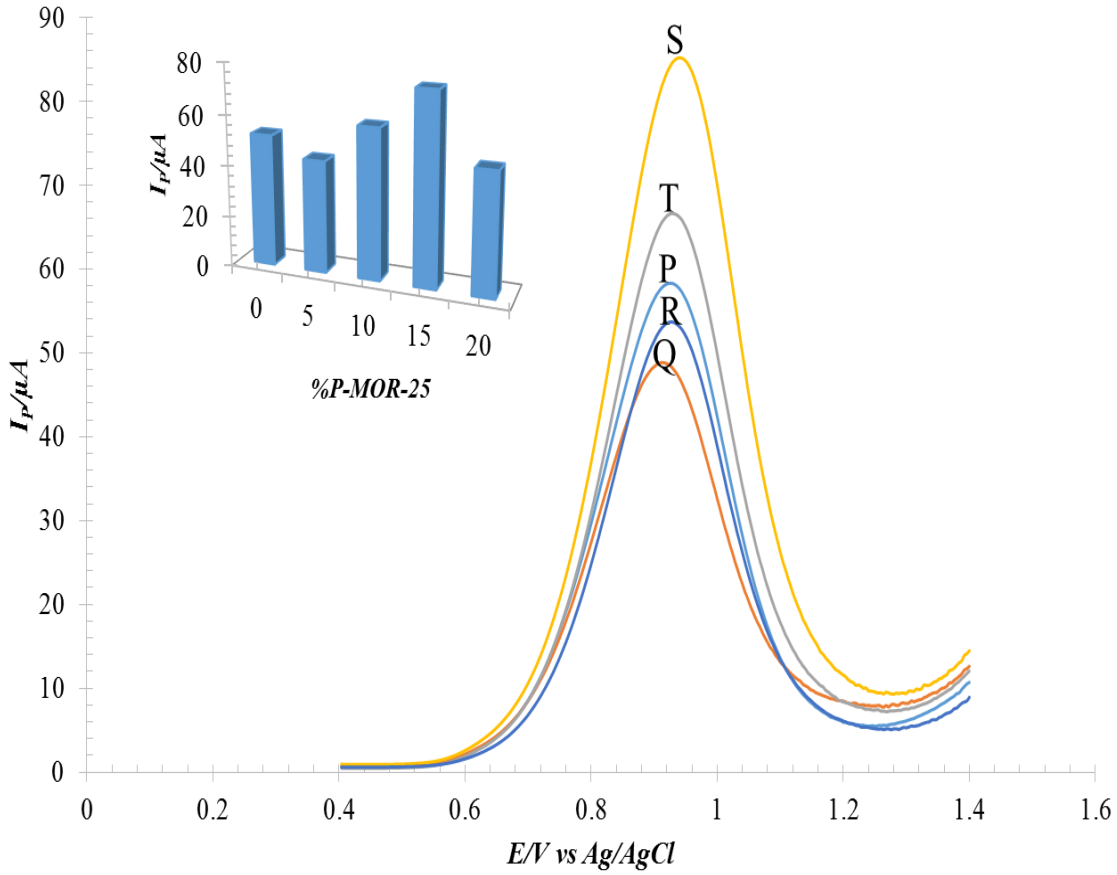

Fig. 4. 22 Comparison of SWVs of different carbon paste electrodes, in presence of 5 mM NO_2^- in phosphate buffer at pH 7. Inset is the relationship of peak current vs % 0.75-P-MOR

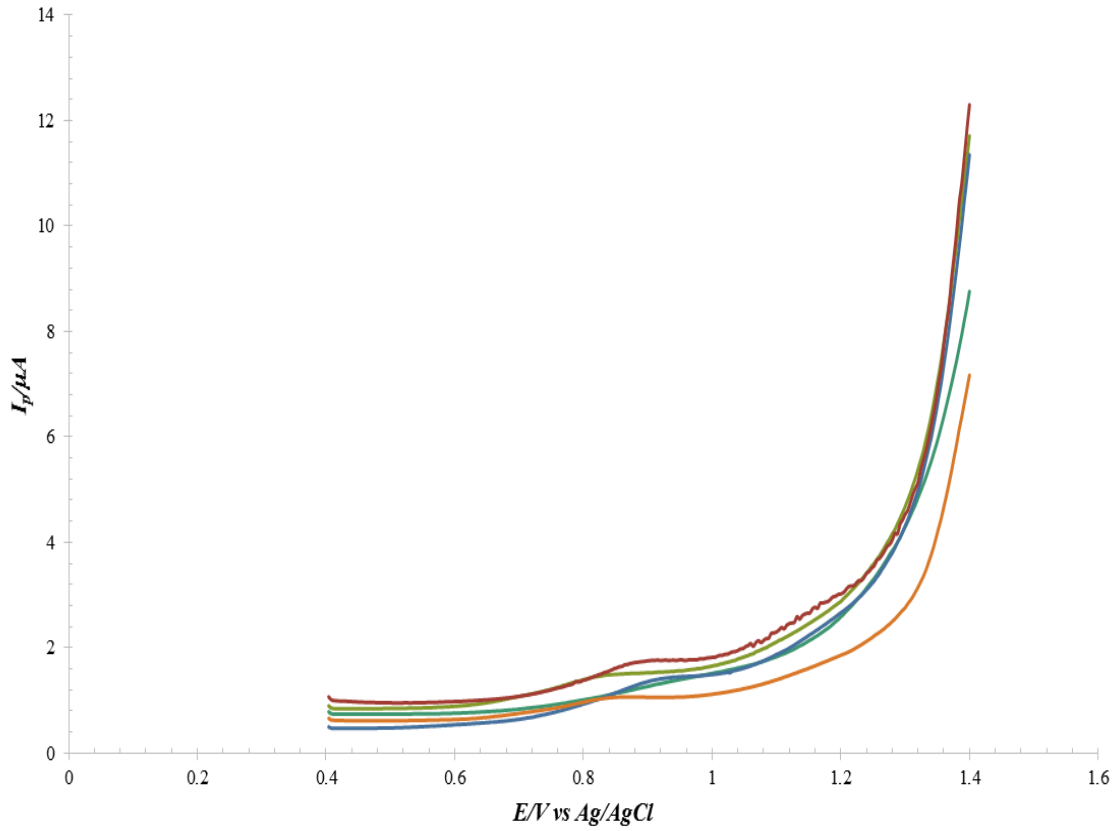

Fig. 4. 23 Comparison of blanks SWVs of different carbon paste electrodes (P, Q, R, S and T)

4.5.3 Comparison with bare carbon paste using CV

Fig. 4.24 shows the compared CVs of the bare carbon paste and the phosphate mordenite carbon paste composite. The electrocatalytic behavior of the best composite **S** was compared to that of the bare in 5 mM NO_2^- in phosphate buffer pH 7 using cyclic voltammetry. The composite electrode **S** depicted a clear irreversible oxidation waveform much higher than that for the bare carbon paste at exactly $E_{1/2}$ = 1000 mV. At this potential oxidation of nitrite was known to occur as demonstrated elsewhere [129, 152, 153]. The irreversibility of the process is obvious by the absence of any reverse peak. Broder *et al* [153] reported that oxidation of nitrite in all media proceeds based on equation 4.1

$$NO_2^- \rightarrow NO_2 + e^- \qquad \textit{Eqn. 4. 1}$$

Presence of water traces favors the nitrite oxidation irreversibly. The nitrite oxidation is a two-electron process. Owing to the fact that water is present in the electrolytic solution used for nitrite detection, in this case, direct oxidation nitrite to nitrate was irreversibly accomplished in one step process. Thus, the following mechanism holds, based on the phosphate interaction with the mordenite framework see scheme 4.2

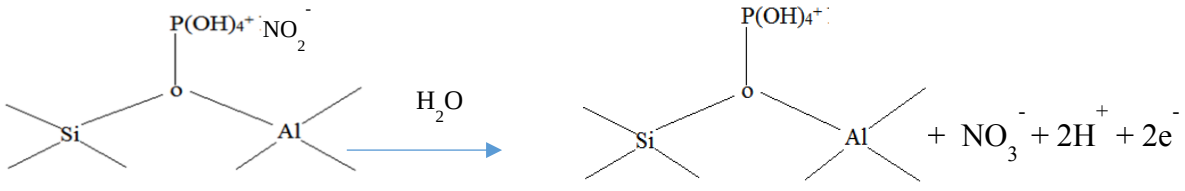

Scheme 4. 2 Mechanism of Nitrite Oxidation

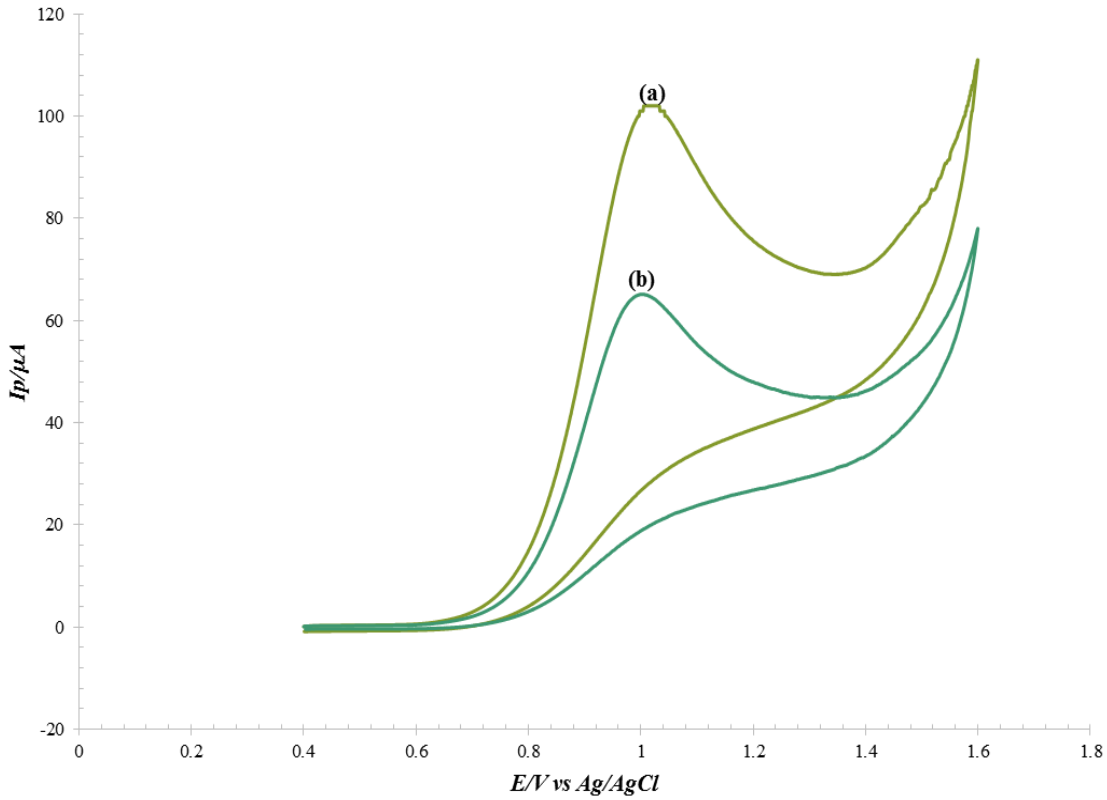

Fig. 4. 24 CV of 15-0.75P-MCPE in the presence of 5 mM NO_2^- in 0.1 M phosphate buffer pH 7 at 100 mV s^{-1} scan rate

4.5.4 Effect of scan rate

Fig. 4.25 depicts the CVs of the variation of peak current with scan rate potential at the **S** electrode in 5 mM NO_2^- solution in 0.1 M phosphate buffer pH 7. The inset plot of the peak current versus square root of scan rate showed a linearity with regression coefficient of R^2 *0.9696* demonstrating that the oxidation of nitrate on the phosphate mordenite carbon paste composite electrode is under diffusion limitation within scan rate range of 10-500 mV s^{-1}. Thus, NO_2^- ions are brought to the surface of the electrode by mass transport.

It was reported elsewhere that in process govern by mass transport, the total electrode surface coverage affects the limitation of the current [23] and that current increase with increased surface coverage. Thus the oxidative peak current I_p, for the nitrite ions adsorbed is express as.

$$I_p = \frac{n^2F^2A\,\Gamma^* v}{4RT} \qquad \textit{Eqn. 4. 2}$$

Where *A* is the electrode surface area (*7.85 x* 10^{-5} cm^2) calculated from A = πr^2, *n* is the number of electrons involved in the reaction (2 electron in this case), I_p is the peak current, F is the faraday constant 96500 C, R is the molar gas constant, *v* is the scan rate and total surface coverage (Γ^*) is then calculated to be 8.96 × 10^{-4} mol/cm^2. Taking the nitrite ions to be spherical and electrode surface to be smoothly homogeneous we can obtain the total electrode surface coverage by plotting the peak current I_p against the scan rate *v*. Fig. 4.26 show the variation of peak current with the scan rate. A strong linear dependence of the scan rate with current is observed with R^2 value of 0998

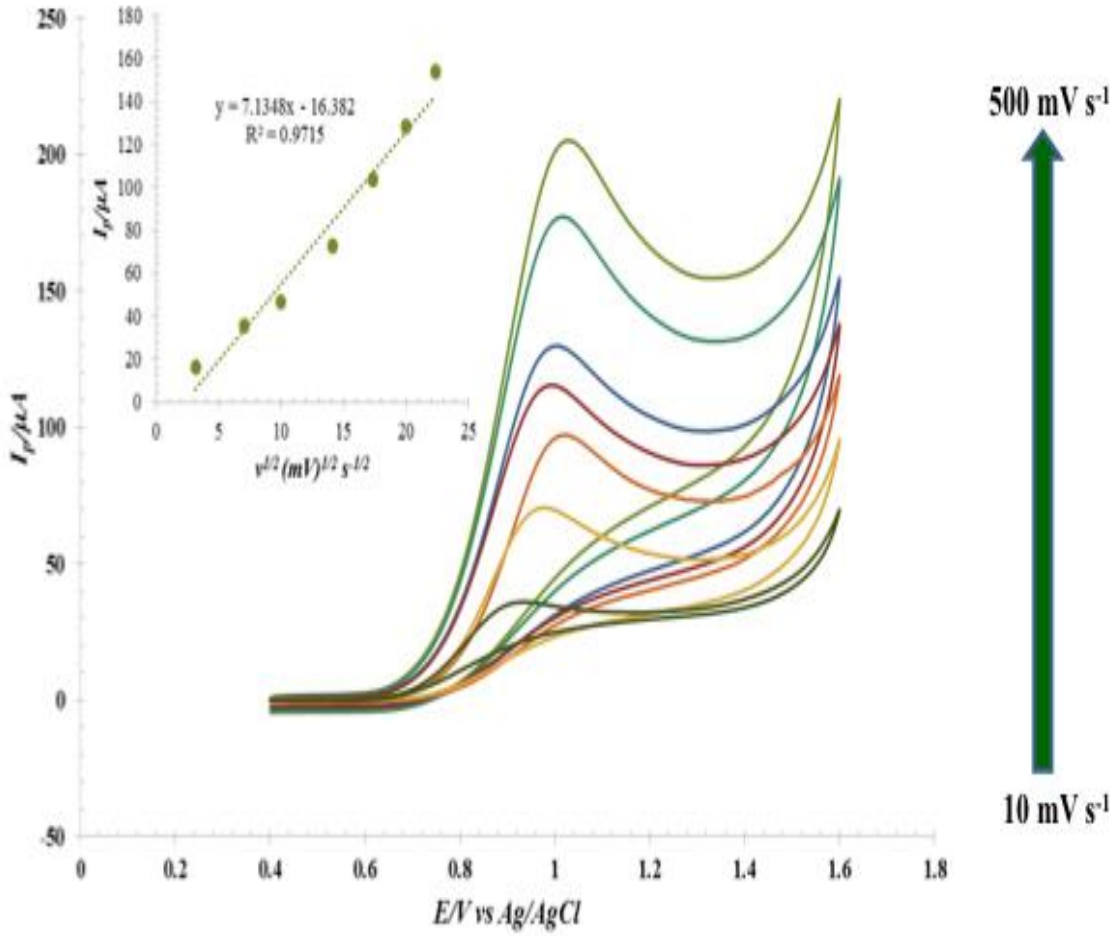

Fig. 4. 25 CVs of the variation of peak current with scan rate potential at the electrode **S** in 5 mM NO_2^- solution in 0.1 M phosphate buffer pH 7. Inset is the plot of peak current vs square root of scan rate

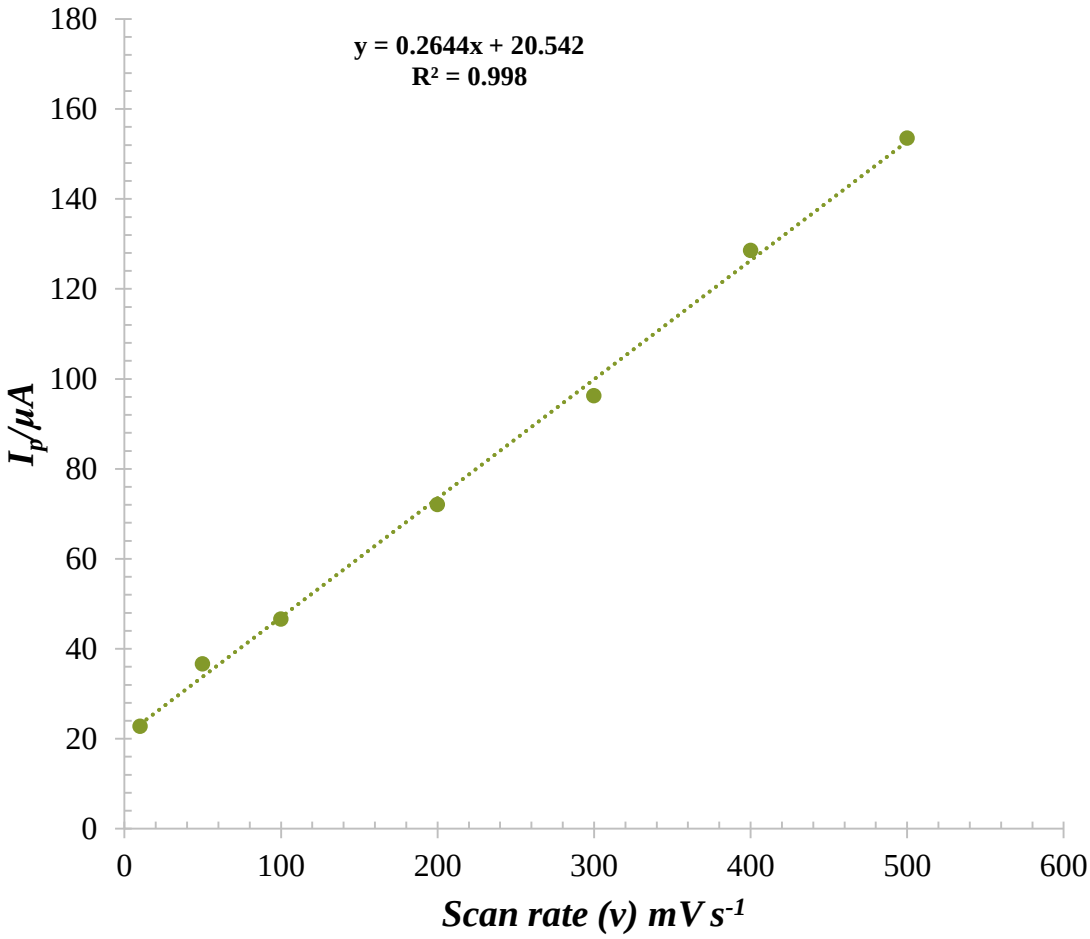

Fig. 4. 26 Plot of peak current vs scan rate

4.5.5 Effect of buffer as electrolyte solution

Having known that the composition and pH of the electrolytic medium affects the performance of electrode surfaces in electrochemical studies [154]. We investigated the effect of different buffer solutions by recording the square wave voltammograms of 5 mM NO_2^- in 0.1 M solutions at pH 7 each of Acetate buffer, phosphate buffer and sulphate buffer shown in Figure 4.27. However, the phosphate buffer favored the oxidation of nitrite as the highest response was produced in the phosphate buffer. Not only is the current enhanced but also the best shape of the peak is obtained in the phosphate buffer. Phosphate buffer had a good record in oxidation of nitrite [129, 152, 155]. The superiority of phosphate buffer is clearly depicted in a chart in figure 4.28

Moreover, in phosphate buffer the size of the phosphate ion is sterically hindered from the positive ion of the protonated phosphate surface of the zeolite, and the cationic sodium ions are selectively repelled. While in the other electrolytic solution especially in the sulphate buffer the anionic sulphate ion is a strong base that can easily block the mechanistic pathway towards nitrite oxidation. The acetate ion is though bulky but a strong nucleophile and can also competes with nitrite, leading to the broadness and shorter oxidation peak.

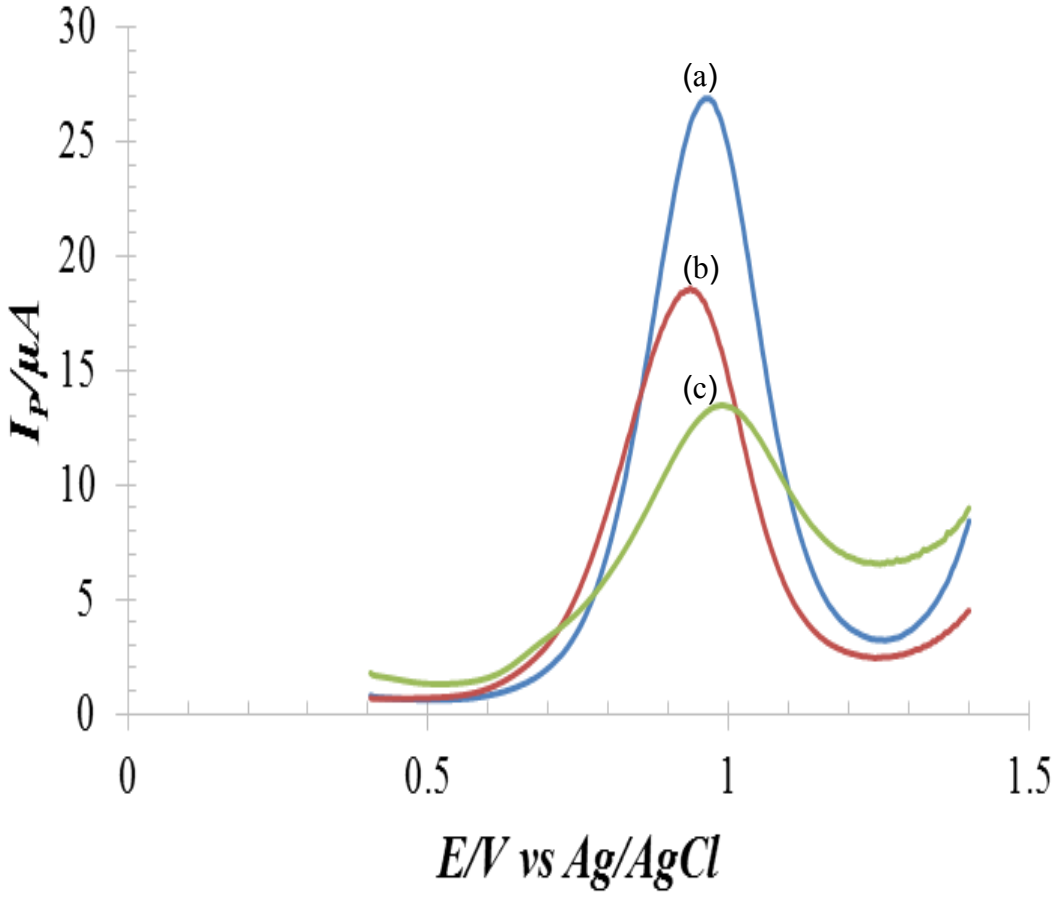

Fig. 4. 27 SWV of electrode **S** in the presence of 5 mM NO_2^- in different buffer solutions (a) 0.1 M Phosphate buffer pH7 (b) 0.1 M Acetate buffer (e) 0.1 M sulphate buffer pH 7

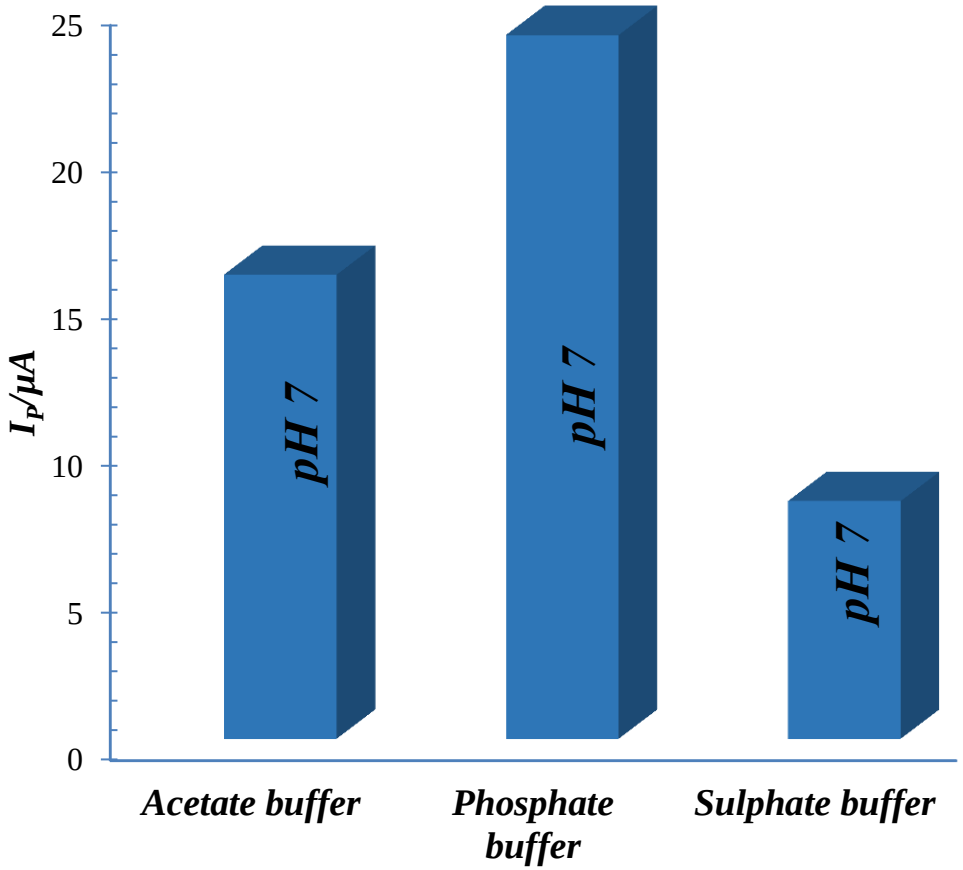

Fig. 4. 28 Dependence of peak current on buffer solution for nitrite detection (data collected from SWV of 5 Mm NO_2^- in 0.1 M solution of each of the buffers at pH 7)

4.5.6 pH dependence of the electrocatalytic oxidation of nitrite

The electrochemical behavior of nitrite ion has been reported to be pH sensitive [155]. The effect of pH was studied by recording the cyclic voltammograms of 5 mM NO_2^- ion in phosphate buffer at different pH. As it can be seen in Fig. 4.29 the oxidation of nitrate is pH sensitive. The oxidation peak current increase progressively with the pH until it reaches a maxima at pH 7, the current suddenly drop at pH 8. The weaker oxidation current of nitrite at lower pH was due to nitrite ion protonation to nitrous acid or subsequent formation of nitric oxide free radical [155]. At higher pH (>3) the current enhancement was attributed to the basicity of the sodium ions that on repulsion from the positive phosphate charge on the mordenite direct the nitrite ion to the electrode surface thereby facilitating the mas transport.

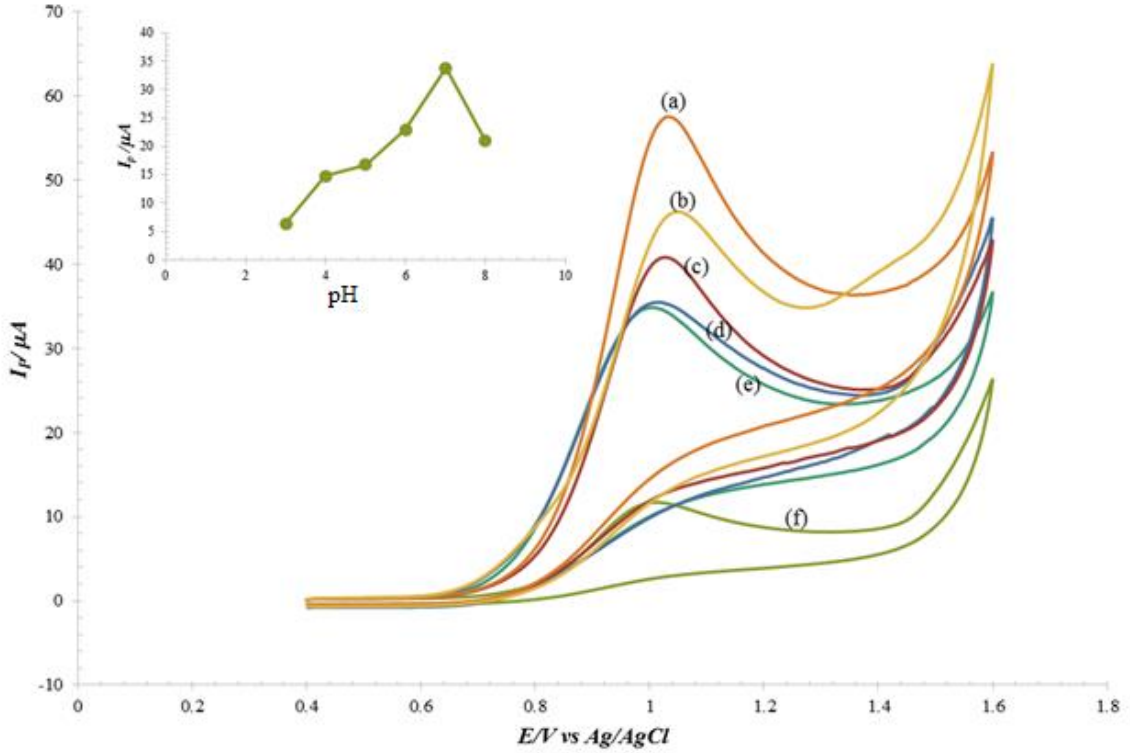

Fig. 4. 29 CV of electrode S in the presence of 5 mM NO_2^- in phosphate buffer at different pH (a) 7, (b) 8, (c) 6, (d) 5, (e) 4 and (f) 3.

4.5.7 Calibration for nitrite oxidation

Having most parameters for nitrite oxidation optimized, it is valuable to test the analytical applicability of the phosphate mordenite carbon paste electrode (electrode **S**). To achieve this, square wave voltammograms of the electrode in different concentrations of nitrite were recorded in 0.1 M phosphate buffer pH 7 were registered. The nitrite oxidation current exhibits excellent linear dependence on nitrite concentration in the range of 1×10^{-5} M to 2.5×10^{-4} M with correlation coefficient of $R^2 \approx 1$. Such a linear relationship in wider dynamic range has never been reported using SWV or CV. It is higher that filed previously using platinum micro rotating electrode [152] with much higher current and that documented in [138] using CV. Equation 4 gives the equation of the regression. The voltammograms and the calibration curve are depicted in Fig.4.30

$$\mathbf{I_p\,(\mu A) = 0.0142[NO_2^-] + 0.0313} \qquad \textit{Eqn. 4. 3}$$

The stability of the electrode was studied by recording 5 different cycles using cyclic voltammograms in 5 Mm NO_2^-. It was found the current is dropping slightly with number of cycles given a relative standard deviation of 3.3%.

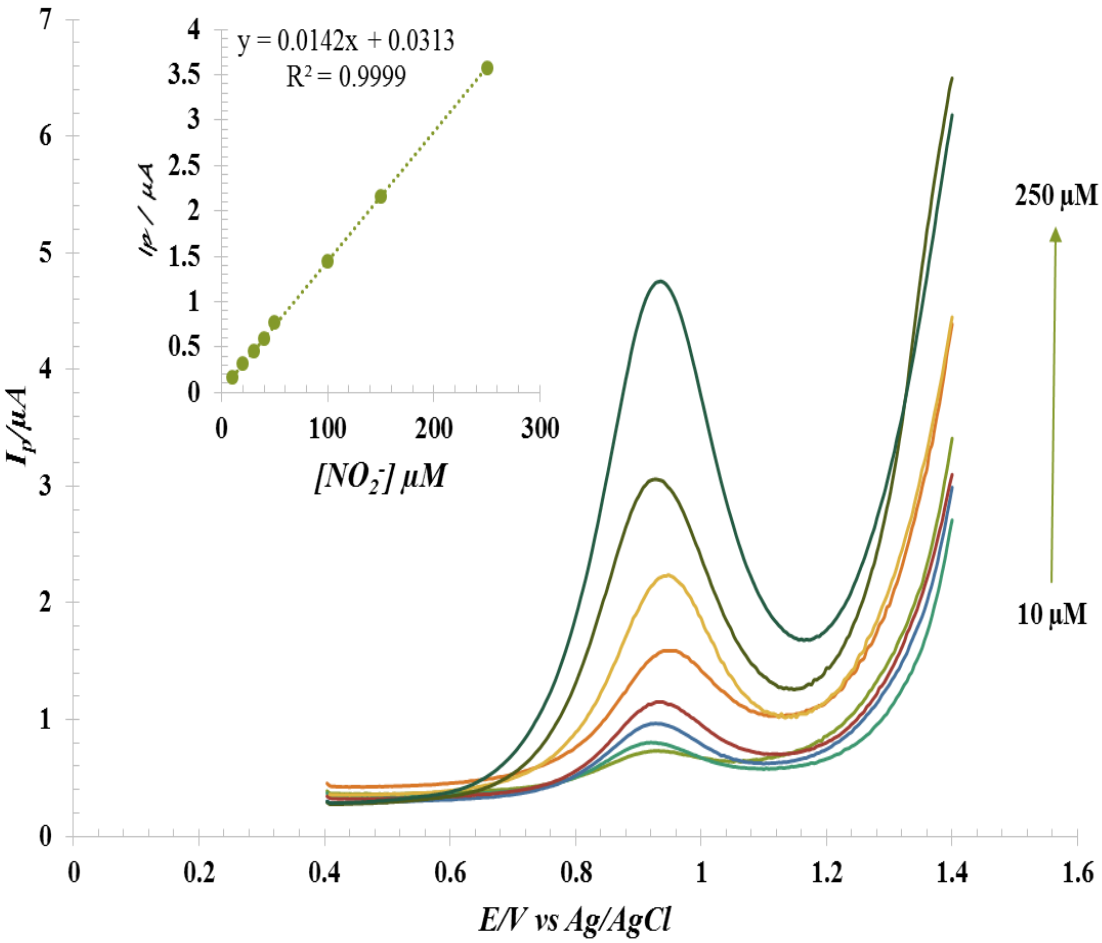

Fig. 4. 30 SWV showing dependence of the peak current on NO_2^- ion concentration. Inset is the relationship of peak current with concentration

4.6 Conclusion

Phosphate has been successfully imparted on mordenite framework. NMR and FT-iR have evinced the formation of aluminum phosphate interface on the mordenite. The continuous dealumination of the mordenite with increasing phosphoric acid concentration was notably observed by the EDX. The FE-SEM images show that crystal size increase with increasing gel Na/Si ratio. The cationic phosphate surface SiOAl–$(POH)_4^+$ was the sole agent for the catalytic oxidation of nitrite and framework Si/Al ratio in phosphate mordenite has great effect on nitrite detection. Phosphate buffer was the best buffer pH is the best electrolytic condition for nitrite oxidation. The calibration plot for nitrite oxidation at the electrode 15-0.75-P-MCPE-25 (i.e. **S** composite**)** showed an excellent linearity. The reproducibility of the electrode was determined by computing the RSD, which was found to be 3.3 %.

Chapter Five

5.1 Conclusions

The effective gel composition for Organic Structure Directing Agent (OSDA) free hydrothermal crystallization of pure mordenite with Si/Al molar ratio of 15, 20 and 25 was established. Purity of the crystals depends greatly on the alkalinity ratio. Synthesizing with different Si/Al ratios depends on the Na/Si ratios correspondingly. Size and morphology of the crystal also rely on silica source, Na/Si ratio, crystallization temperature and time. Phosphate was successfully imparted on mordenite via post synthesis impregnation. Different phosphate mordenite carbon paste electrodes were prepared. In catalytic amount phosphate mordenite enhanced the electrochemical oxidation of thiocyanate to cyanate. The pH has a significant effect on the activity of electrode. Framework Si/Al ratios of phosphate mordenite and p-loading on mordenite with different Si/Al ratio have affected the current intensity in nitrite oxidation. A more hydrophobic phosphate mordenite of Si/Al of 25 showed superior activity in nitrite detection. A strong linearity was obtained in the calibrations of composite electrode 15-0.75-P-MCPE-25 (i.e. **S** composite) in thiocyanate and nitrite stock solutions with R^2 values of 0.998 and 0.9999, respectively.

5.2 Recommendations

The mordenite used in this research is in micro meter size, its surface area would have been better if the nano sized is used which in turn would provide more electrocatalytic activity. Although it is very challenging, as we experienced, we recommend that more effort is required to investigate the exact gel condition and synthesis parameters that could give nanomordenite. The exact composition of the carbon

paste electrode containing mordenite can be further investigated as the content of the oil binder was unaltered in this work. Glassy carbon electrode and platinum electrode can be used as the working electrode after casting the composite materials onto their surfaces. Their performances can then be compared with different carbon paste electrodes based on phosphate zeolites

References

1. Weitkamp, J., *Zeolites and catalysis.* Solid State Ionics, 2000. **131**(1–2): p. 175-188.
2. Rhodes, C.J., *Zeolites: physical aspects and environmental applications.* Annual Reports Section "C" (Physical Chemistry), 2007. **103**(0): p. 287-325.
3. Busca, G., *Chapter 7 - Zeolites and Other Structurally Microporous Solids as Acid–Base Materials*, in *Heterogeneous Catalytic Materials*, G. Busca, Editor. 2014, Elsevier: Amsterdam. p. 197-249.
4. Hoelderich, W.F. and D. Heinz, *Research and development of zeolite catalysis in the 80ties and in the 90ties as well as forthcoming trends.* Research on Chemical Intermediates, 1998. **24**(3): p. 337-348.
5. Lukyanov, D.B., et al., *Insights into Brønsted Acid Sites in the Zeolite Mordenite.* The Journal of Physical Chemistry C, 2014. **118**(41): p. 23918-23929.
6. Xu, X., J. Wang, and Y. Long, *Zeolite-based materials for gas sensors.* Sensors, 2006. **6**(12): p. 1751-1764.
7. Tago, T. and T. Masuda, *Zeolite nanocrystals-synthesis and applications*. 2010: INTECH Open Access Publisher.
8. Chen, N.Y., *Hydrophobic properties of zeolites.* The Journal of Physical Chemistry, 1976. **80**(1): p. 60-64.
9. F., D., *A New Method for Characterization of Natural Zeolites and Organic Nanostructure Using Atomic Force Microscopy.* Nanomaterials 2(1), 79-91, 2012. **2(1)**: p. 79-91.

10. Vjunov, A., et al., *Quantitatively Probing the Al Distribution in Zeolites.* Journal of the American Chemical Society, 2014. **136**(23): p. 8296-8306.

11. Vjunov, A., et al., *Impact of Aqueous Medium on Zeolite Framework Integrity.* Chemistry of Materials, 2015.

12. Chumbhale, V.R., *Characterization of Aluminosilicates (Zeolites) by Laboratory Screening Tests for Selective Synthesis of Value Added Products: Case Studies.* Research Journal of Chemical Sciences, 2013. **3(8)**: p. 10-17.

13. Busca, G., *Chapter 1 - Heterogeneous Catalysts*, in *Heterogeneous Catalytic Materials*, G. Busca, Editor. 2014, Elsevier: Amsterdam. p. 1-7.

14. Larsen, S.C., *Nanocrystalline Zeolites and Zeolite Structures: Synthesis, Characterization, and Applications.* The Journal of Physical Chemistry C, 2007. **111**(50): p. 18464-18474.

15. Chen, B., et al., *Zeolitic imidazolate framework materials: recent progress in synthesis and applications.* Journal of Materials Chemistry A, 2014. **2**(40): p. 16811-16831.

16. Xu, L., et al., *Bifunctional Tandem Catalysis on Multilamellar Organic–Inorganic Hybrid Zeolites.* ACS Catalysis, 2014. **4**(9): p. 2959-2968.

17. Ledesma, C., et al., *Recent Approaches in Mechanistic and Kinetic Studies of Catalytic Reactions Using SSITKA Technique.* ACS Catalysis, 2014. **4**(12): p. 4527-4547.

18. Bakker, E. and Y. Qin, *Electrochemical Sensors.* Analytical Chemistry, 2006. **78**(12): p. 3965-3984.

19. Wu, Q., et al., *Sustainable Synthesis of Zeolites without Addition of Both Organotemplates and Solvents.* Journal of the American Chemical Society, 2014. **136**(10): p. 4019-4025.

20. Ren, L., et al., *Solvent-Free Synthesis of Zeolites from Solid Raw Materials.* Journal of the American Chemical Society, 2012. **134**(37): p. 15173-15176.

21. Bontempelli, G. and R. Toniolo, *MEASUREMENT METHODS | Electrochemical: Linear Sweep and Cyclic Voltammetry*, in *Encyclopedia of Electrochemical Power Sources*, J. Garche, Editor. 2009, Elsevier: Amsterdam. p. 643-654.

22. Cambridge, U.o., *Linear Sweep and Cyclic Voltametry: The Principles.* Department of Chemical Engineering and Biotechnology, 2014.

23. Prodromidis, M.I., et al., *The importance of surface coverage in the electrochemical study of chemically modified electrodes.* Electroanalysis, 2000. **12**(18): p. 1498-1501.

24. Elqudaby, H., et al., *Validated voltammetric method for the determination of some antiprotozoa drugs based on the reduction at an activated glassy carbon electrode.* Arabian Journal of Chemistry, 2013. **6**(3): p. 327-333.

25. Osteryoung, J.G. and R.A. Osteryoung, *Square wave voltammetry.* Analytical Chemistry, 1985. **57**(1): p. 101A-110A.

26. Hincapie, B.O., et al., *Synthesis of mordenite nanocrystals.* Microporous and Mesoporous Materials, 2004. **67**(1): p. 19-26.

27. Lu, B., et al., *Direct synthesis of high-silica mordenite using seed crystals.* Microporous and mesoporous materials, 2004. **76**(1): p. 1-7.

28. Al-Shammari, A.A., et al., *Catalytic cracking of heavy naphtha-range hydrocarbons over different zeolites structures.* Fuel Processing Technology, 2014. **122**: p. 12-22.

29. Zhao, G.-L., et al., *Catalytic cracking reactions of C 4-olefin over zeolites H-ZSM-5, H-mordenite and H-SAPO-34.* Studies in Surface Science and Catalysis, 2007. **170**: p. 1307-1312.

30. Mohamed, M.M., et al., *Synthesis of high silica mordenite nanocrystals using o-phenylenediamine template.* Microporous and mesoporous materials, 2005. **84**(1): p. 84-96.

31. Chumbhale, V., A. Chandwadkar, and B. Rao, *Characterization of siliceous mordenite obtained by direct synthesis or by dealumination.* Zeolites, 1992. **12**(1): p. 63-69.

32. Lv, A., et al., *Hydrothermal synthesis of high-silica mordenite by dual-templating method.* Microporous and Mesoporous Materials, 2011. **145**(1): p. 80-86.

33. Aguado, J., et al., *Catalytic cracking of polyethylene over zeolite mordenite with enhanced textural properties.* Journal of Analytical and Applied Pyrolysis, 2009. **85**(1): p. 352-358.

34. Wang, J., et al., *High-silica MOR type zeolite self-transformed from dry aluminosilicate gel in OSAs-free and fluoride-free reactant system.* Microporous and Mesoporous Materials, 2006. **96**(1–3): p. 307-313.

35. Patwardhan, S., *Zeolites: Synthesis, Characterization and Applications.* Academic Press, Boston, 2001.

36. Al-Shammari, A.A., et al., *Catalytic cracking of heavy naphtha-range hydrocarbons over different zeolites structures.* Fuel Processing Technology, 2014. **122**(0): p. 12-22.

37. Zhao, G.L., et al., *Catalytic cracking reactions of C4-olefin over zeolites H-ZSM-5, H-mordenite and H-SAPO-34,* in *Studies in Surface Science and Catalysis*, Z.G.J.C. Ruren Xu and Y. Wenfu, Editors. 2007, Elsevier. p. 1307-1312.

38. Chumbhale, V.R., A.J. Chandwadkar, and B.S. Rao, *Characterization of siliceous mordenite obtained by direct synthesis or by dealumination.* Zeolites, 1992. **12**(1): p. 63-69.

39. Shao, C., et al., *Synthesis of high-silica-content mordenite with different SiO2/Al2O3 ratios by using benzene-1,2-diol as additives.* Materials Letters, 2002. **56**(1–2): p. 24-29.

40. Jongkind, H., et al., *Synthesis and characterisation of zeolites using saturated cyclic amines as structure-directing agents.* Microporous Materials, 1997. **10**(4–6): p. 149-161.

41. Aguado, J., et al., *Catalytic cracking of polyethylene over zeolite mordenite with enhanced textural properties.* Journal of Analytical and Applied Pyrolysis, 2009. **85**(1-2): p. 352-358.

42. Jyoti Bhadauria, B.K.S., Avinash Tomar and Radha Tomar, *Synthesis and characterization of analogue of mordenite and its role as a catalyst for Friedel-Crafts acylation of anisole.* Journal of Chemical and Pharmaceutical Research 2011. **3(2)**: p. 245-257

43. Aly, H.M., M.E. Moustafa, and E.A. Abdelrahman, *Synthesis of mordenite zeolite in absence of organic template.* Advanced Powder Technology, 2012. **23**(6): p. 757-760.

44. Zhang, L., et al., *Crystallization and morphology of mordenite zeolite influenced by various parameters in organic-free synthesis.* Materials Research Bulletin, 2011. **46**(6): p. 894-900.

45. Zhang, L., et al., *Synthesis of large mordenite crystals with different aspect ratios.* Microporous and Mesoporous Materials, 2009. **126**(1–2): p. 115-124.

46. Moreno-Piraján, J., V. Garcia-Cuello, and L. Giraldo, *Synthesis of HMOR and HZSM-5 and their Behaviour in the Catalytic Conversion of Methanol to Propylene (MTP). J Thermodyn Catal 1: 101. doi: 10.4172/2157-7544.1000101*. 2010, OMICS Publishing Group J Thermodyn Catal ISSN.

47. Mignoni, M.L., et al., *Synthesis of mordenite using kaolin as Si and Al source.* Applied Clay Science, 2008. **41**(1–2): p. 99-104.

48. Chen, N., T.F. Degnan Jr, and C.M. Smith, *Molecular transport and reaction in zeolites: design and application of shape selective catalysis*. 1994: John Wiley & Sons.

49. Dykeman, R.R., et al., *Cover Picture: Rational Design of a Molecular Nanocatalyst-Stabilizer that Enhances both Catalytic Activity and Nanoparticle Stability (ChemCatChem 12/2012).* ChemCatChem, 2012. **4**(12): p. 1865-1865.

50. Blasco, T., A. Corma, and J. Martínez-Triguero, *Hydrothermal stabilization of ZSM-5 catalytic-cracking additives by phosphorus addition.* Journal of Catalysis, 2006. **237**(2): p. 267-277.

51. Panneerselvam, P., et al., *Phosphoric acid modified-Y zeolites: A novel, efficient and versatile ion exchanger.* Journal of Hazardous Materials, 2008. **159**(2–3): p. 427-434.

52. Zaiku Xie , Z.L., Yangdong Wang, Qihua Yang, Longya Xu and Weiping Ding *An Overview of Recent Development in Composite Catalysts from Porous Materials for Various Reactions and Processes* Int. J. Mol. Sci., 2010. **11(5)**: p. 2152-2187.

53. Huang, Y., et al., *Density Functional Theory study of the structural and electronic properties of H 3 PO 4/ZSM-5.* RSC Advances, 2014. **4**(28): p. 14573-14581.

54. Kaeding, W.W. and S.A. Butter, *Production of chemicals from methanol: I. Low molecular weight olefins.* Journal of Catalysis, 1980. **61**(1): p. 155-164.

55. Coudurier, G., C. Naccache, and J.C. Vedrine, J. Chem. Soc., Chem. Commun., 1982: p. 1413.

56. Lercher, J. and G. Rumplmayr, *Controlled decrease of acid strength by orthophosphoric acid on ZSM5.* Applied catalysis, 1986. **25**(1): p. 215-222.

57. Blasco, T., A. Corma, and J. Martineztriguero, *Hydrothermal stabilization of ZSM-5 catalytic-cracking additives by phosphorus addition.* Journal of Catalysis, 2006. **237**(2): p. 267-277.

58. Caro, J., et al., *NMR and IR studies of zeolite H-ZSM-5 modified with orthophosphoric acid.* Journal of Catalysis, 1990. **124**(2): p. 367-375.

59. Giudici, R., H.W. Kouwenhoven, and R. Prins, *Comparison of nitric and oxalic acid in the dealumination of mordenite.* Applied Catalysis A: General, 2000. **203**(1): p. 101-110.

60. Zhuang, J., et al., *Solid-state MAS NMR studies on the hydrothermal stability of the zeolite catalysts for residual oil selective catalytic cracking.* Journal of Catalysis, 2004. **228**(1): p. 234-242.

61. van der Bij, H.E., et al., *Phosphatation of Zeolite H-ZSM-5: A Combined Microscopy and Spectroscopy Study*. ChemPhysChem, 2014. **15**(2): p. 283-292.

62. van Donk, S., et al. *Probing the micropore accessibility in mordenite crystals using diffusion and coking studies*. in *NAM-18*. 2003.

63. Corma, A., J. Mengual, and P.J. Miguel, *Stabilization of ZSM-5 zeolite catalysts for steam catalytic cracking of naphtha for production of propene and ethene.* Applied Catalysis A: General, 2012. **421–422**(0): p. 121-134.

64. Li, J., et al., *Catalytic Cracking of Butene to Propylene over Modified HZSM-5 Zeolites.*

65. van der Bij, H.E., et al., *Hexane Cracking over Steamed Phosphated Zeolite H-ZSM-5: Promotional Effect on Catalyst Performance and Stability.* Chemistry – A European Journal, 2014. **20**(51): p. 16922-16932.

66. Dyballa, M., et al., *Effect of Phosphate Modification on the Brønsted Acidity and Methanol-to-Olefin Conversion Activity of Zeolite ZSM-5.* Chemie Ingenieur Technik, 2013. **85**(11): p. 1719-1725.

67. Corma, A., J. Mengual, and P.J. Miguel, *Stabilization of ZSM-5 zeolite catalysts for steam catalytic cracking of naphtha for production of propene and ethene.* Applied Catalysis A: General, 2012. **421-422**: p. 121-134.

68. Liu, J., et al., *Methanol to propylene: Effect of phosphorus on a high silica HZSM-5 catalyst.* Catalysis Communications, 2009. **10**(11): p. 1506-1509.

69. Li, P., et al., *Conversion of Methanol to Hydrocarbons over Phosphorus-modified ZSM-5/ZSM-11 Intergrowth Zeolites.* Catalysis Letters, 2009. **134**(1-2): p. 124-130.

70. Zhao, G., et al., *Effect of phosphorus on HZSM-5 catalyst for C4-olefin cracking reactions to produce propylene.* Journal of Catalysis, 2007. **248**(1): p. 29-37.

71. Z. Nawaz, X.T.a.F.W., *Hexene Catalytic Cracking Over 30% Sapo-34 Catalyst For Propylene Maximization: Influence Of Reaction Conditions And Reaction Pathway Exploration* Brazilian Journal of Chemical Engineering 2009. **vol. 26 N0. 04**: p. pp. 705 - 712.

72. Wang, X., et al., *Phosphorus modified HMCM-22: Characterization and catalytic application in methanol-to-hydrocarbons conversion.* Microporous and Mesoporous Materials, 2012. **151**(0): p. 99-106.

73. Jiang, G., et al., *Highly effective P-modified HZSM-5 catalyst for the cracking of C4 alkanes to produce light olefins.* Applied Catalysis A: General, 2008. **340**(2): p. 176-182.

74. Butter, W.W.K.a.s.A., *Production of Chemicals from Methanol.* Journal of Catalysis, 1980. **61**: p. 155-164.

75. Jacques c. Vẽdrine, A.A., Pierre Dejaifve, Valentin Ducarme, and a.S.Z. Hanna Hoser, *Catalytic and Physical Properties of Phosphorus-Modified ZSM-5 Zeolite.* Journal of Catalysis, 1982. **73**: p. 147-160.

76. Xue, N., et al., *Synergistic effects of tungsten and phosphorus on catalytic cracking of butene to propene over HZSM-5.* Applied Catalysis A: General, 2009. **352**(1-2): p. 87-94.

77. Xue, N., et al., *Understanding the enhancement of catalytic performance for olefin cracking: Hydrothermally stable acids in P/HZSM-5.* Journal of Catalysis, 2007. **248**(1): p. 20-28.

78. Wang, X., et al., *Phosphorus modified HMCM-22: Characterization and catalytic application in methanol-to-hydrocarbons conversion.* Microporous and Mesoporous Materials, 2012. **151**: p. 99-106.

79. Z. Nawaz*, X.T.a.F.W., *Hexene catalytic cracking over 30% SAPO-34 Catalyst for Propylrnr maximization: influence of Reaction conditions and Reaction Pathway exploration.* Brazilian Jouranal of Chemical Engineering, October-December, 2009. **26, 4**: p. 702-712.

80. Jianwen Li, H.M., Haitao Zhang, Qiwen Sun, Weiyong Ying, *Catalytic Cracking of Butene to Propylene over Modified HZSM-5 Zeolites.* International Journal of Chemical, Nuclear, Metallurgical and Materials Engineering, 2014. **8**: p. 604-608.

81. Lee, J., et al., *Catalytic cracking of C5 raffinate to light olefins over lanthanum-containing phosphorous-modified porous ZSM-5: Effect of lanthanum content.* Fuel Processing Technology, 2013. **109**(0): p. 189-195.

82. Epelde, E., et al., *Modified HZSM-5 zeolites for intensifying propylene production in the transformation of 1-butene.* Chemical Engineering Journal, 2014. **251**(0): p. 80-91.

83. Zeng, P., et al., *Preparation of phosphorus-modified PITQ-13 catalysts and their performance in 1-butene catalytic cracking.* Journal of Energy Chemistry, 2014. **23**(2): p. 193-200.

84. Walcarius, A., T. Barbaise, and J. Bessiere, *Factors affecting the analytical applications of zeolite-modified electrodes preconcentration of electroactive species.* Analytica Chimica Acta, 1997. **340**(1–3): p. 61-76.

85. Walcarius, A., *Zeolite-modified electrodes in electroanalytical chemistry.* Analytica Chimica Acta, 1999. **384**(1): p. 1-16.

86. Nezamzadeh-Ejhieh, A. and Z. Nematollahi, *Surfactant modified zeolite carbon paste electrode (SMZ-CPE) as a nitrate selective electrode.* Electrochimica Acta, 2011. **56**(24): p. 8334-8341.

87. Shaw, B.R. and K.E. Creasy, *Carbon composite electrodes containing alumina, layered double hydroxides, and zeolites.* Journal of Electroanalytical Chemistry and Interfacial Electrochemistry, 1988. **243**(1): p. 209-217.

88. Ardakani, M.M., et al., *Accumulation and voltammetric determination of cobalt at zeolite-modified electrodes.* Journal of Analytical Chemistry, 2008. **63**(2): p. 184-191.

89. Ardakani, M.M., et al., *Accumulation and voltammetric determination of cobalt at zeolite-modified electrodes.* Journal of Analytical Chemistry, 2008. **63**(2): p. 184-191.

90. Arvand, M., et al., *Electrochemical study of methylene blue incorporated into mordenite type zeolite and its application for amperometric determination of ascorbic acid in real samples.* Analytica Chimica Acta, 2003. **491**(2): p. 193-201.

91. Samadi-Maybodi, A., et al., *Application of nickel phosphate nanoparticles and VSB-5 in the modification of carbon paste electrode for electrocatalytic oxidation of methanol.* Journal of Solid State Electrochemistry, 2013. **17**(7): p. 2043-2048.

92. Nezamzadeh, A., M.K. Amini, and H. Faghihian, *Square-wave voltammetric determination of ascorbic acid based on its electrocatalytic oxidation at zeolite-modified carbon-paste electrodes.* Int j Electrochem Sci, 2007. **2**: p. 583-594.

93. Senthilkumar, S. and R. Saraswathi, *Electrochemical sensing of cadmium and lead ions at zeolite-modified electrodes: Optimization and field measurements.* Sensors and Actuators B: Chemical, 2009. **141**(1): p. 65-75.

94. Hassaninejad-Darzi, S.K. and M. Rahimnejad, *Electrocatalytic oxidation of methanol by ZSM-5 nanozeolite-modified carbon paste electrode in alkaline medium.* Journal of the Iranian Chemical Society: p. 1-10.

95. Manea, F., et al., *Simultaneous electrochemical determination of nitrate and nitrite in aqueous solution using Ag-doped zeolite-expanded graphite-epoxy electrode.* Talanta, 2010. **83**(1): p. 66-71.

96. Ojani, R., et al., *Electrochemical behavior of Ni (II) incorporated in zeolite Y-modified carbon electrode: application for electrocatalytic oxidation of methanol in alkaline solution.* Journal of Solid State Electrochemistry, 2011. **15**(9): p. 1935-1941.

97. Cundy, C.S. and P.A. Cox, *The hydrothermal synthesis of zeolites: Precursors, intermediates and reaction mechanism.* Microporous and Mesoporous Materials, 2005. **82**(1–2): p. 1-78.

98. Sharma, P., P. Rajaram, and R. Tomar, *Synthesis and morphological studies of nanocrystalline MOR type zeolite material.* Journal of Colloid and Interface Science, 2008. **325**(2): p. 547-557.

99. Sano, T., et al., *Synthesis of large mordenite crystals in the presence of aliphatic alcohol.* Microporous and Mesoporous Materials, 2001. **46**(1): p. 67-74.

100. Li, X., R. Prins, and J.A. van Bokhoven, *Synthesis and characterization of mesoporous mordenite.* Journal of Catalysis, 2009. **262**(2): p. 257-265.

101. Fernandes, L.D., et al., *Ethylbenzene hydroisomerization over bifunctional zeolite based catalysts: The influence of framework and extraframework composition and zeolite structure.* Journal of Catalysis, 1998. **177**(2): p. 363-377.

102. Sanhoob, M., et al., *Synthesis of ZSM-12 (MTW) with different Al-source: Towards understanding the effects of crystallization parameters.* Microporous and Mesoporous Materials, 2014. **194**(0): p. 31-37.

103. Ahmed, M.H.M., O. Muraza, and A.M. Al Amer, *Effect of synthesis parameters and ion exchange on crystallinity and morphology of EU-1 zeolite.* Journal of Alloys and Compounds, 2014. **617**(0): p. 408-412.

104. Seronu, U., H. Munarn, and M. KoIzuMI, *Crystallization of mordenite from aqueous solutions.*

105. Ma, Y., et al., *Large-pore mesoporous silica spheres: synthesis and application in HPLC.* Colloids and Surfaces A: Physicochemical and Engineering Aspects, 2003. **229**(1): p. 1-8.

106. Wang, J., et al., Microporous Mesoporous Mater., 2009. **117**: p. 561.

107. Mao, Y., et al., *Morphology-controlled synthesis of large mordenite crystals.* New Journal of Chemistry, 2014.

108. Zhang, X., D. Tang, and G. Jiang, *Synthesis of zeolite NaA at room temperature: The effect of synthesis parameters on crystal size and its size distribution.* Advanced Powder Technology, 2013. **24**(3): p. 689-696.

109. Ramsay, J.D.F. and S. Kallus, *Zeolite Membranes*, in *Membrane Science and Technology*, N.K. Kanellopoulos, Editor. 2000, Elsevier. p. 373-395.

110. Simoncic, P. and T. Armbruster, *Cationic methylene blue incorporated into zeolite mordenite-Na: a single crystal X-ray study.* Microporous and mesoporous materials, 2005. **81**(1): p. 87-95.

111. Meier, W.M., *The Crystal Structure of Mordenite (ptilolite).* Z. Kristallogr., 1961. **115**: p. 439-450.

112. O. J. Whittemore JR., *Synthesis of Siliceous Mordenite.* American Minerologist, 1972. **57**: p. 1146-1151.

113. Mohamed, M.M., A.K. Nohman, and M.I. Zaki, *Development of catalytic properties of mordenite zeolite via chemical modification.* ChemInform, 2006. **37**(38).

114. N. Y. Chen, T.F.D., Jr., C. Morris Smith., , *Molecular Transport and Reaction in Zeolites: Design and Application of Shape Selective Catalysis.* Catalyst, wiley, 1994. **94**.

115. Caeiro, G., et al., *Stabilization effect of phosphorus on steamed H-MFI zeolites.* Applied Catalysis A: General, 2006. **314**(2): p. 160-171.

116. Song, Z., et al., *Phosphorus-modified ZSM-5 for conversion of ethanol to propylene.* Applied Catalysis A: General, 2010. **384**(1–2): p. 201-205.

117. Takahashi, A., et al., *Effects of added phosphorus on conversion of ethanol to propylene over ZSM-5 catalysts.* Applied Catalysis A: General, 2012. **423–424**(0): p. 162-167.

118. Walcarius, A., *Zeolite-modified electrodes: Analytical applications and prospects.* Electroanalysis, 1996. **8**(11): p. 971-986.

119. Ndlovu, T., et al., *Reactivities of modified and unmodified exfoliated graphite electrodes in selected redox systems.* International Journal of Electrochemical Science, 2012. **7**(10): p. 9441-9453.

120. Gaoquan, S., et al., *Electrochemical behavior of MOR zeolite in poly(ethylene oxide) oligomer.* Journal of Electroanalytical Chemistry, 1993. **344**(1–2): p. 363-366.

121. Nezamzadeh-Ejhieh, A. and A. Badri, *Surfactant modified ZSM-5 zeolite as an active component of membrane electrode towards thiocyanate.* Desalination, 2011. **281**(0): p. 248-256.

122. Ghiaci, M., B. Rezaei, and R.J. Kalbasi, *High selective SiO2–Al2O3 mixed-oxide modified carbon paste electrode for anodic stripping voltammetric determination of Pb(II).* Talanta, 2007. **73**(1): p. 37-45.

123. Arvand, M., M. Vaziri, and M. Vejdani, *Electrochemical study of atenolol at a carbon paste electrode modified with mordenite type zeolite.* Materials Science and Engineering: C, 2010. **30**(5): p. 709-714.

124. Dehbi, S., H. Massai, and A. Chtaini, *Phosphate modified copper electrodes for methanol fuel cell.* Portugaliae Electrochimica Acta, 2010. **28**(4): p. 241-252.

125. Chung, J. and J.L. Wood, *Oxidation of thiocyanate to cyanide catalyzed by hemoglobin.* Journal of Biological Chemistry, 1971. **246**(3): p. 555-560.

126. Mohammed Zidane, T.W., Elyas Sadeq Algabhbari, Mansor Ahmad, Kamyar Shameli, *Voltammetric oxidation of potassium thiocyanate using ErBa2Cu3O7 modified glassy carbon electrode.* Int. J. Electrochem. Sci., 2013. **8**: p. 4818-4826.

127. Badri, A. and P. Pouladsaz, *Highly selective and sensitive thiocyanate PVC membrane electrodes based on modified Zeolite ZSM-5.* Int. J. Electrochem. Sci, 2011. **6**: p. 3178-3195.

128. Donk, S.v., *Adsorption, diffusion and reaction studies of hydrocarbons on zeolite catalysts.* 2002.

129. Marlinda, A., et al., *Electrochemical sensing of nitrite using a glassy carbon electrode modified with reduced functionalized graphene oxide decorated with flower-like zinc oxide.* Microchimica Acta, 2015. **182**(5-6): p. 1113-1122.

130. van der Bij, H.E. and B.M. Weckhuysen, *Local silico-aluminophosphate interfaces within phosphated H-ZSM-5 zeolites.* Physical Chemistry Chemical Physics, 2014. **16**(21): p. 9892-9903.

131. Wachter, A., *Sodium Nitrite as Corrosion Inhibitor for Water.* Industrial & Engineering Chemistry, 1945. **37**(8): p. 749-751.

132. Rahim, A., et al., *Electrochemical Detection of Nitrite in Meat and Water Samples Using a Mesoporous Carbon Ceramic SiO2/C Electrode Modified with In Situ Generated Manganese(II) Phthalocyanine.* Electroanalysis, 2014. **26**(3): p. 541-547.

133. Fan, K. and J. Wu, *Construction of a carbon paste electrode based on ionic liquid for trace electrochemical detection of nitrite in food samples.* Analytical Methods, 2013. **5**(19): p. 5146-5153.

134. Ianoul, A., T. Coleman, and S.A. Asher, *UV Resonance Raman Spectroscopic Detection of Nitrate and Nitrite in Wastewater Treatment Processes.* Analytical Chemistry, 2002. **74**(6): p. 1458-1461.

135. Siu, D.C. and A. Henshall, *Ion chromatographic determination of nitrate and nitrite in meat products.* Journal of Chromatography A, 1998. **804**(1–2): p. 157-160.

136. Martínková, E., T. Křžek, and P. Coufal, *Determination of nitrites and nitrates in drinking water using capillary electrophoresis.* Chemical Papers, 2014. **68**(8): p. 1008-1014.

137. Nagababu, E. and J. Rifkind, *Measurement of Plasma Nitrite by Chemiluminescence*, in *Free Radicals and Antioxidant Protocols*, R.M. Uppu, et al., Editors. 2010, Humana Press. p. 41-49.

138. Cui, Y., et al., *Electrochemical determination of nitrite using a gold nanoparticles-modified glassy carbon electrode prepared by the seed-mediated growth technique.* Analytical Sciences, 2007. **23**(12): p. 1421-1425.

139. Walcarius, A., et al., *Amperometric Detection of Nonelectroactive Cations in Electrolyte-Free Flow Systems at Zeolite Modified Electrodes.* Electroanalysis, 1999. **11**(6): p. 393-400.

140. Xiong, W. and M.D. Baker, *Electrochemistry of Zeolites on Thickness Shear Mode Oscillators.* The Journal of Physical Chemistry B, 2005. **109**(28): p. 13590-13596.

141. Muresan, L.M., *Zeolite-modified electrodes with analytical applications.* Pure and Applied Chemistry, 2010. **83**(2): p. 325-343.

142. Senaratne, C., et al., *Zeolite-modified electrodes: intra-versus extrazeolite electron transfer.* The Journal of Physical Chemistry, 1996. **100**(14): p. 5849-5862.

143. Zheng, Y., X. Li, and P.K. Dutta, *Exploitation of Unique Properties of Zeolites in the Development of Gas Sensors.* Sensors (Basel, Switzerland), 2012. **12**(4): p. 5170-5194.

144. Patwardhan, S., *Sol-Gel Synthesis of Zeolites: Effect of Process Parameters.*

145. Sol-Gel, Z., *Chemistry of silicates and aluminosilicates.* Ceramics− Silikáty, 2005. **49**(4): p. 287-298.

146. Ahlers, C.B. and J.B. Talbot, *Voltammetric behavior of zeolite-modified electrodes fabricated by electrophoretic deposition.* Electrochimica Acta, 2000. **45**(20): p. 3379-3387.

147. van der Bij, H.E., et al., *Aluminum-Phosphate Binder Formation in Zeolites as Probed with X-ray Absorption Microscopy.* Journal of the American Chemical Society, 2014. **136**(51): p. 17774-17787.

148. Li, G., *FT-IR studies of zeolite materials: characterization and environmental applications.* 2005.

149. Boveri, M., et al., *Steam and acid dealumination of mordenite: characterization and influence on the catalytic performance in linear alkylbenzene synthesis.* Catalysis today, 2006. **114**(2): p. 217-225.

150. Rebenstorf, B., T. Lindblad, and S.L.T. Andersson, *Amorphous AIPO4 as catalyst support 2. Characterization of amorphous aluminum phosphates.* Journal of Catalysis, 1991. **128**(2): p. 293-302.

151. Peng, X.D., et al., *Use of aluminum phosphate as the dehydration catalyst in single step dimethyl ether process*. 1998, Google Patents.

152. Bertotti, M. and D. Pletcher, *A study of nitrite oxidation at platinum microelectrodes.* Journal of the Brazilian Chemical Society, 1997. **8**(4): p. 391-395.

153. Broder, T.L., et al., *Electrochemical oxidation of nitrite and the oxidation and reduction of NO2 in the room temperature ionic liquid [C2mim][NTf2]*. The Journal of Physical Chemistry B, 2007. **111**(27): p. 7778-7785.

154. Vaughan-Jones, R.D., *Regulation of chloride in quiescent sheep-heart Purkinje fibres studied using intracellular chloride and pH-sensitive micro-electrodes.* The Journal of Physiology, 1979. **295**(1): p. 111-137.

155. Kamyabi, M.A. and F. Aghajanloo, *Electrocatalytic oxidation and determination of nitrite on carbon paste electrode modified with oxovanadium (IV)-4-methyl salophen.* Journal of Electroanalytical Chemistry, 2008. **614**(1): p. 157-165.

Vitae

Name: **Adamu Aminu Idris**

Nationality: **Nigerian**

Date of Birth: **10/20/1983**

E-mail: **marvelchm@gmail.com**

Academic Background: **B Tech Industrial Chemistry**

Awards: **Rapid Hospital and Educational Prize Limited and Dean School of Science Prize, Abubakar Tafawa Balewa University, Bauchi**

Experience: **Graduate Assistant @ Bayero University, Kano. 2012 – Date**

Conferences/symposium: **3rd Saudi International Technology Conference, KACST, Riyadh December, 2014**

Saudi – Japan Symposium on "Catalyst in Refining and Petrochemicals" KFUPM December, 2013